

**INOMANS²HIP****DELIVERABLE D3.1**
Energy Characteristics Modelling*WP3 “Interfaces and Network Design”*

Author(s):	Peter RAMPEN Cees MEIJER Stuart GUNPUT Manuel PELAEZ-CARUS Tom BRADLEY Hans VAN VUGT Adrian HIGGINBOTTOM
Reviewer(s):	Edward SCIBERRAS Lisa SMEATON Tony ROSKILLY
Identifier:	D3.1_INOMANS ² HIP_M30_V2
Dissemination level:	PU
Contractual Date:	M30
Number of pages:	110

Summary	In this deliverable is a description of activities during Task 3.1. The deliverable describes the first stage of development of mathematical models for energy recovery, renewable energy production and energy storage technologies, which could be implemented on-board a commercial cargo vessel. The report discusses the assumptions and decisions made about the technologies being investigated. The deliverable also explores the different ship power production and distribution architecture currently and being proposed on-board a vessel.
----------------	---

Approved by the Coordinator <input checked="" type="checkbox"/>	Date: 06/11/2013
--	-------------------------

* Dissemination Levels	
PU	Public
PP	Restricted to other programme participants (including the Commission Services).
RE	Restricted to a group specified by the consortium (including the Commission Services).
CO	Confidential, only for members of the consortium (including the Commission Services).

Document History

Revision	Date	Author	Comments
Draft V1.1	01/11/2011	Jean-Loup TRILLAT Abdollah MIRZAIAN Catherine JEAND'HEUR	Document Plan & Layout
Draft V1.2	16/11/2011	Adrian HIGGENBOTTOM Bill PAGE Hans VAN VUGT	Chapter 3 & 4
Draft V1.3	12/12/2011	Jean-Loup TRILLAT Abdollah MIRZAIAN Catherine JEAND'HEUR Manuel PELAEZ-CARUS	Chapters 1, 2, 5, 6, 9 & 10
Draft V1.4	21/12/2011	Tom BRABLEY Alex COLE	Chapters 7 & 8
V1 (Final)	28/12/2011	Lisa SMEATON Tony ROSKILLY	Final Review & Edit
Draft V2.1	16/09/2013	Peter RAMPEN Cees MEIJER Stuart GUNPUT	Document Review
Draft V2.2	04/10/2013	Tom BRADLEY	Chapter 6
Draft V2.3	27/10/2013	Peter RAMPEN Cees MEIJER Stuart GUNPUT	Rewrite of Chapter 5, 9 & Final Revisions (all other chapters)
Draft V2.4	29/10/2013	Edward SCIBERRAS	Edited
V2 (Final)	06/11/2013	Lisa SMEATON Tony ROSKILLY	Final Review

Partners' acronym list

Beneficiary Number*	Beneficiary name	Beneficiary short name	Country
1	University of Newcastle Upon Tyne	UNEW	United Kingdom
3	Nederlandse organisatie voor Toegepast Natuurwetenschappelijk Onderzoek -TNO	TNO	Netherlands
4	Goupement des Industries de Construction et Activités Navales	GICAN	France
6	Wärtsilä Finland Oy	WARTSILA	Finland
7	Novamen	NOVAMEN	France
8	National Renewable Energy Centre Limited	NAREC	United Kingdom
9	Germanischer Lloyd SE	GL	Germany
12	Imtech Marine	IMTECH	Netherlands

Table of Contents

1	INTRODUCTION	8
2	OVERVIEW OF THE GLOBAL ON-BOARD COMPONENTS INTERFACING	9
3	MARINE ENGINES.....	11
3.1	DESCRIPTION OF THE FUNCTION OF EACH ENGINE AND POSSIBLE TECHNOLOGICAL CHOICES	11
3.2	TECHNICAL SPECIFICATIONS OF THE CHOSEN DIESEL ENGINES	12
3.2.1	<i>W6L32 Engine.....</i>	12
3.2.2	<i>12V46F Engine</i>	12
3.2.3	<i>RT-flex68-D 7-Cylinder Engine.....</i>	12
3.2.4	<i>Waste Heat Recovery System.....</i>	13
3.3	PTO, PTI, PTH MODES PRESENTATION	14
3.3.1	<i>PTO: Power-Take-Out as an Electric Power Generation System.....</i>	14
3.3.2	<i>PTI: Power-Take-In with Booster Mode</i>	15
3.3.3	<i>PTH: Power-Take-Home run in Emergency Mode.....</i>	16
3.4	MATHEMATICAL ENGINE MODELS.....	17
3.4.1	<i>Specific Fuel Consumption and Management Laws.....</i>	17
3.4.2	<i>Dynamic characteristics of diesel engines.....</i>	18
3.4.3	<i>Engine Models in GES Software.....</i>	19
3.5	ALTERNATIVE SIMULINK MODEL	22
4	ELECTRICAL MACHINES.....	23
4.1	ASYNCHRONOUS MACHINES	23
4.2	INDUCTION VERSUS PERMANENT MAGNET MACHINES	24
4.3	ELECTRIC MACHINE MODELS.....	24
5	ENERGY STORAGE.....	26
5.1	OVERVIEW OF BATTERIES.....	26
5.1.1	<i>Lead Acid Batteries</i>	27
5.1.2	<i>Ni-Cd Batteries.....</i>	27
5.1.3	<i>Ni-Mh Batteries</i>	28
5.1.4	<i>Lithium Batteries.....</i>	28
5.2	SUPERCAPACITORS.....	30
5.2.1	<i>General Description.....</i>	30
5.2.2	<i>Arrangement of Supercapacitors Modules</i>	31
5.2.3	<i>Sizing of the Supercapacitors.....</i>	32
5.2.4	<i>Actual Solutions and Perspectives.....</i>	32
5.3	FLYWHEELS.....	32
5.3.1	<i>Physical Principle and Technologies.....</i>	33
5.3.2	<i>Economical View and Security.....</i>	35
5.4	TECHNICAL CHOICE	36
5.5	ENERGY STORAGE SYSTEM MODEL	37
5.6	CONCLUSION ON THE ENERGY STORAGE	37
6	FUEL CELLS.....	39
6.1	INTRODUCTION.....	39

6.2	TYPES OF FUEL CELL	40
6.2.1	<i>Polymer Electrolyte or Proton Exchange Membrane Fuel cells (PEMFC)</i>	40
6.2.2	<i>Direct Methanol Fuel Cell (DMFC)</i>	40
6.2.3	<i>Alkaline (AFC)</i>	41
6.2.4	<i>Phosphoric Acid Fuel Cell (PAFC)</i>	41
6.2.5	<i>Molten Carbonate (MCFC)</i>	41
6.2.6	<i>Solid Oxide (SOFC)</i>	41
6.2.7	<i>Overview</i>	41
6.3	TECHNOLOGY SUMMARY.....	41
6.4	LIFETIMES.....	42
6.5	HYDROGEN SYSTEMS HIERARCHY OF LEGISLATION.....	43
6.6	FUTURE POSSIBILITIES	43
6.7	CONCLUSION.....	43
7	SOLAR POWER GENERATION	44
7.1	INTRODUCTION.....	44
7.2	DEFINING THE PHOTOVOLTAIC MODEL	44
7.2.1	<i>Irradiance Model</i>	45
7.2.2	<i>Shading Model</i>	45
7.3	ELECTRICAL MODEL	46
7.3.1	<i>Simple Model</i>	48
7.3.2	<i>Simulink/Matlab Models</i>	49
7.4	SOLAR POWER GENERATION CONCLUSIONS	51
8	WIND POWER GENERATION	53
8.1	INTRODUCTION.....	53
8.2	WIND TURBINE MODELLING OVERVIEW	53
8.3	NAREC'S WIND TURBINE MODEL.....	55
8.3.1	<i>Introduction</i>	55
8.3.2	<i>Aerodynamic Block</i>	55
8.3.3	<i>Gearbox</i>	64
8.3.4	<i>Moment of Inertia</i>	70
8.3.5	<i>Generator</i>	71
8.4	CONCLUSION.....	77
9	DISTRIBUTION	78
9.1	TRANSFORMERS	78
9.1.1	<i>Power Rating</i>	78
9.1.2	<i>Power Density</i>	78
9.1.3	<i>Efficiency</i>	79
9.2	STATIC CONVERTERS FOR DISTRIBUTION	80
9.2.1	<i>AC/DC and DC/AC converters</i>	80
9.2.2	<i>DC/DC Converters (choppers)</i>	82
9.3	COLD IRONING	82
9.3.1	<i>Model of Cold Ironing</i>	82
10	GENERAL CONCLUSION	83
	APPENDIX A: SOLAR POWER GENERATION	84
	APPENDIX B: FLETTNER ROTOR PHYSICS.....	94

APPENDIX C FUEL CELL PAST AND CURRENT PROJECTS.....	101
APPENDIX D FUEL CELL LEGISLATION	106
REFERENCES.....	108

List of Figures

Figure 1: Multi-source mapping of ship on-board power systems.....	9
Figure 2: First global architecture approach.....	10
Figure 3: Waste heat recovery system integration into Wärtsilä.....	13
Figure 4: Waste heat recovery system diagram.....	13
Figure 5: Diagram of efficiency gain by adding waste heat recovery system.....	14
Figure 6: Ship PTO diagram.....	15
Figure 7: Ship PTI diagram.....	16
Figure 8: Ship PTH diagram.....	17
Figure 9: Basic diesel engine specific consumption mapping.....	18
Figure 10: 6L32 Maximum recommended load increase rates for engines operating at nominal speed.....	19
Figure 11: General diesel engine model in GES.....	19
Figure 12: Specific fuel and emission map for a diesel engine.....	20
Figure 13: Operational diagram for a diesel engines.....	20
Figure 14: Dual fuel diesel engine model in GES software.....	21
Figure 15: Dual fuel diesel engine model specific fuel consumption mapping.....	21
Figure 16: Specific fuel consumption mapping from the ISUZU diesel engine.....	22
Figure 17: Lookup table for Isuzu simulation.....	22
Figure 18: Asynchronous machine efficiencies.....	23
Figure 19: An IE classification of asynchronous machines.....	24
Figure 20 : Power and energy comparison of different storage devices.....	26
Figure 21 Lithium battery impedance.....	29
Figure 22 Lithium battery efficiency.....	30
Figure 23: Supercapacitor schematics (<i>source venturebeat.com</i>).....	30
Figure 24: Maxwell active balancing circuit.....	31
Figure 25: G3 Satellite flywheel energy storage prototype (<i>source "Conical bearingless motor-generators"</i>).....	35
Figure 26: The PNGV model.....	37
Figure 27: Basic diagram of a fuel cell.....	39
Figure 28: Fuel cell system scheme according to IEC 62281-1.....	40
Figure 29: Types of equivalent circuit for a photovoltaic cell from.....	46
Figure 30: Power output from NAREC's excel based PV simulator.....	48
Figure 31: IV curve from NAREC's excel based PV simulator.....	49
Figure 32: Model produced by the University of Colorado (5).....	49
Figure 33: Model produced by Risø National Laboratory(3).....	50
Figure 34: Model produced in (1).....	50
Figure 35: NAREC IV model of a photovoltaic cell.....	51
Figure 36: Photocurrent subsystem.....	51
Figure 37: Cell Saturation Dark Current Subsystem.....	51
Figure 38: Simplified diagram of the workings of a wind turbine.....	54
Figure 39: Three blocks of the Simulink wind turbine.....	55
Figure 40: C_P value selection if loop.....	60
Figure 41: Tip speed ratio for a wind turbine with a fixed pitch of 0 degrees.....	60
Figure 42: Tip speed ratio for a wind turbine with a variable pitch angle.....	61
Figure 43: Wind speed and hub height blocks, linked together with switches to allow the blocks to be deactivated when surplus to requirements.....	62
Figure 44.: Wind profile impacting a wind turbine, showing the effects of wind shear.....	63
Figure 45: Tower shadow and wind shear block.....	64
Figure 46: Simplification of two mass model.....	65
Figure 47: Two mass model of a wind turbine gearbox.....	66
Figure 48: step one of creating a model of Equation 30.....	68
Figure 49: step two of creating a model of Equation 30.....	68
Figure 50: step three of creating a model of Equation 31.....	68
Figure 51: One mass model of a wind turbine.....	69
Figure 52: One mass model of gearbox.....	70
Figure 53: Asynchronous machine with a constant voltage supply.....	72
Figure 54: Torque produced by asynchronous machine when used with continuous integration blocks.....	72

Figure 55: Torque produced by asynchronous machine when used in discrete mode.	72
Figure 56: Simulink representation of equations.....	74
Figure 57: Simulink representation of slip calculation.....	75
Figure 58: Varying levels of pitch angle alter the position a value of the peak C_p	76
Figure 59: Pitch controller block	77
Figure 60: Wild heat and purchase costs for three phase transformers as a function of the power density	79
Figure 61: Transformer efficiency for varying load factors.....	80
Figure 62: Single phase Switch-mode converter for bidirectional power flow.....	81
Figure 63: Example of a motor variable frequency drive with a switch-mode converter. The equipment in the red box is the actual power electronics.....	81

List of Tables

Table 1: Engines choices	11
Table 2: W6L32 engine specifications.....	12
Table 3: 12V46F engine specifications.....	12
Table 4: RT-flex68-D 7-cylinder engine specifications.....	12
Table 5: Batteries comparison.....	27
Table 6: Supercapacitor technologies comparison.....	31
Table 7: Flywheels shapes.....	33
Table 8: Flywheels materials	34
Table 9: Examples of types of flywheels used in different applications	35
Table 10: Fuel cell data from the US Department of Energy (US Department of Energy, 2011).....	42
Table 11: Example of model input data.....	56
Table 12: Coefficients for C_p calculations as given in Sloopweg et al.	58

Abbreviations

AC	Alternating Current
APM	Advanced Propulsion Motors
BMS	Battery Management System
CA	Consortium Agreement
DC	Direct Current
DOD	Deep Of Discharge
DoW	Description of Work (i.e. the Annex 1 of the Grant Agreement)
EC	European Commission
EMS	Energy Management System
GES	TNO Software for mathematical simulations
GTO	Gate Turn-Off thyristor
HTS	High Temperature Superconductor
IGBT	Insulated Gate Bipolar Transistor
IPC	Intellectual Property Committee
LCI	Load Commutated Inverters
LNG	Liquefied Natural Gas
MPPT	Maximum Power Point Tracking
OCV	Open Circuit Voltage
PEFC	Polymer Electrolyte Fuel Cell
PNGV	Partnership for a New Generation of Vehicles
PTH	Power Take Home
PTI	Power Take In

PTO	Power Take Out
PV	Photovoltaic
PWM	Pulse Width Modulation
SAB	Scientific Advisory Board
SOC	State Of Charge
WHRS	Waste Heat Recovery System
WP	Work Package
WPL	Work Package Leader
WT	Wind Turbine

1 INTRODUCTION

The aim of task 3.1 was to focus on the different power elements of a cargo ship. Studies of the different energy sources, storage devices and principal consumers were carried out to determine the on-board energy needs of a vessel.

The on-board systems of a ship were defined by the technical consortium partners of the project as precisely as possible. The final goal of the task was to determine the extent and nature of the mathematical models for the proposed on-board elements. The models allowed for the simulation to define the interaction of the different components and systems in order to develop the energy management requirements based on existing management laws defined in this task.

General operational profiles for each of the proposed renewable and energy recovery technologies are discussed in this document. Applying real-time physical variables of the operational profiles gives a precise idea of the reaction of on-board power requirements for a vessel. The operational profiles of each technology used as input variables to the mathematical model of the ship electrical arrangement.

2 OVERVIEW OF THE GLOBAL ON-BOARD COMPONENTS INTERFACING

The INOMANS²HIP project will explore many on-board ship's architectures and component solutions. The ship's propulsion system will also be considered, as this can be fully electric or include a connection from the diesel propulsion engine to an alternator/motor for Power-Take-Off (PTO), Power-Take-In (PTI) and Power-Take-Home (PTH) systems.

Figure 1 shows the mapping of the most important components, found on Cargo ships.

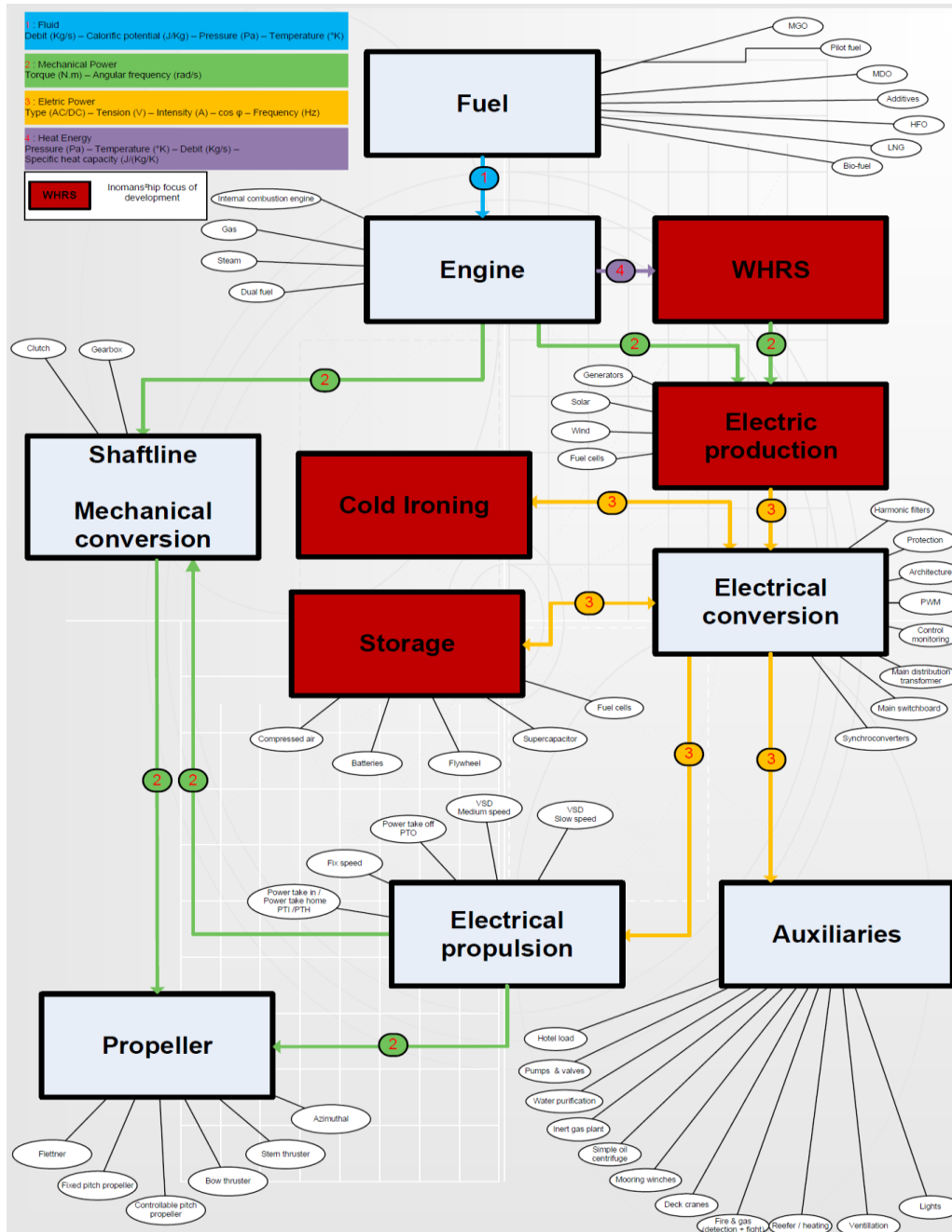


Figure 1: Multi-source mapping of ship on-board power systems

The first global approach takes into account the loads, sources and energy storage systems to better understanding the problem.

This global architecture is just a first approach and not a final solution in the development of the on-board energy systems, which is to be completed in Task 3.3 and reported in Deliverable D3.3.

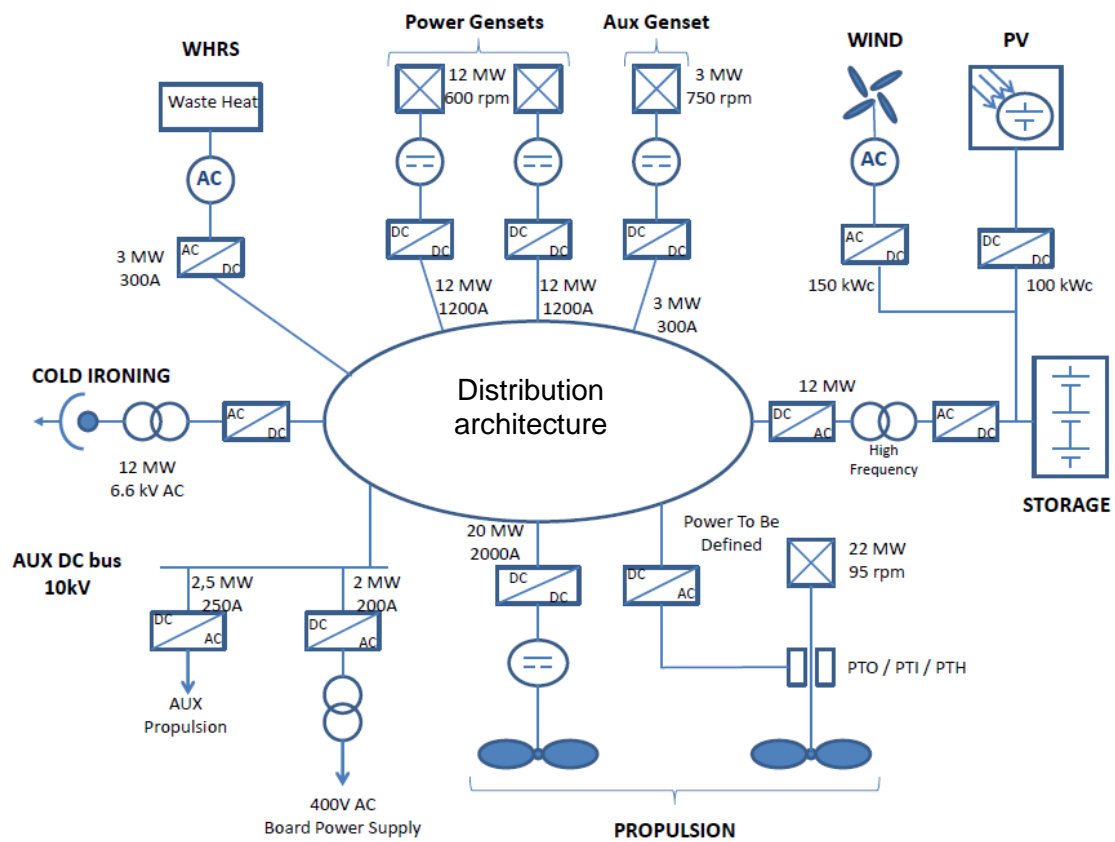


Figure 2: First global architecture approach

Figure 2 shows the different power renewable and energy recovery systems that can be implemented on-board a ship. Note:- it is easier to follow the defining protocols of each component.

3 MARINE ENGINES

Marine engines use the combustion of fuel to generate mechanical rotational power. This fuel, namely marine diesel oil (MDO) and heavy fuel oil (HFO), is the real energy source of the ship. In INOMANS²HIP, we consider using other energy sources like solar and wind, but the power generated by these means is limited and fuel powered engines will still meet the majority of the ship's energy needs.

Optimizing the fuel consumption of the engines has a great impact on the ship global energy consumption. One of most substantial points concerning the marine industry today is to reduce the overall on-board energy consumption and, thus, save fuel. The hydrodynamics of the ship and its propeller are not considered as part of the INOMANS²HIP project.

The energy management system (EMS) will have a global view of the engines to control them, optimizing their specific consumption point. The importance of the mapping of specific power consumption and consumers will be explained in further detail in the following pages.

On ships, different types of engines can be used, such as gas turbines, diesel 2-strokes engines, diesel 4-strokes engines and dual fuel diesel engines.

In INOMANS²HIP, 2-stroke- and 4-stroke diesel engines will be considered, as well as dual fuel diesel engines, using both marine fuel oil (MFO) and liquefied natural gas (LNG). The type of diesel engine and the fuel used is important to develop the energy management laws of the EMS. Furthermore, it is needed to choose the best specific fuel consumption point of the engine and optimize its operation to be as close as possible to the most efficient running point.

3.1 Description of the Function of each Engine and Possible Technological Choices

For a generic ship model, three types of engines were considered and defined from information provided from Wärtsilä:

- Main propulsion engine (around 22MW and 95 rpm)
- Diesel power generator engine (around 14.4 MW and 600 rpm)
- The auxiliary generator engine (around 3 MW and 750 rpm)

The chosen engines are convenient for a first approach to start the modelling process. Any future improvement will be integrated into the project's models.

	Engine Reference	Speed	Power (MW)
Propulsion engine	7-cylinder, RT-flex68	low speed 95 rpm	21,91
Power generator	12V46F	Medium speed 600 rpm	14,4
Auxiliary generator	W6L32	Medium speed 750 rpm	3

Table 1: Engines choices

A waste heat recovery system (WHR) can be incorporated into the hot exhaust of the 7-cylinder RT-flex68 engine main propulsion engine to produce steam to drive additional power generation systems or required on-board for heating. With some improvement, the WHR system could be adapted also to recover heat from the diesel generators as well.

3.2 Technical Specifications of the Chosen Diesel Engines

3.2.1 W6L32 Engine

Specification description	Values
Engine type	4-stroke, non-reversible, turbocharged and intercooled diesel engine with direct fuel injection
Piston displacement	32.2 L/cylinder
Number of valves	2 inlet valves, 2 exhaust valves
Cylinder configuration	6 in-line
Speed	750 rpm
Mean piston speed	10.0 m/s
Power	3,000 kW
Weight	33.5 tones
Exhaust gas flow at 85% load	5.1 kg/s
Temp. after turbocharger at 85% load	330 °C
Fuel consumption at 85% load	180 g/kWh
Approx. oil consumption at 100% load	0.5 g/kWh

Table 2: W6L32 engine specifications

3.2.2 12V46F Engine

Specification description	Values
Engine type	4-stroke, non-reversible, turbocharged and intercooled diesel engine with direct fuel injection
Piston displacement	96.4 L/cylinder
Number of valves	2 inlet valves, 2 exhaust valves
Cylinder configuration	12 in V-form
Speed	600 rpm
Mean piston speed	11.6 m/s
Power	14,400 kW
Weight	201 tones
Exhaust gas flow at 85% load	22.8 kg/s
Temp. after turbocharger at 85% load	320 °C
Fuel consumption at 85% load	170 g/kWh
Approx. oil consumption at 100% load	0.7 g/kWh

Table 3: 12V46F engine specifications

3.2.3 RT-flex68-D 7-Cylinder Engine

Specification description	Values
Engine type	Camshaftless low-speed, direct-reversible, 2-stroke engine, fully electronically controlled, 2 turbochargers
Piston displacement	987.82 L/cylinder
Cylinder configuration	7 in-line
Speed	95 rpm
Mean piston speed	8,6 m/s
Power	21,910 kW
Weight	533 tones
Exhaust gas flow at 85% load	45.3 kg/s
Temp. after turbine	294 °C
Fuel consumption at 100% load	169 g/kWh
Approx. oil consumption at 100% load	0.7 g/kWh

Table 4: RT-flex68-D 7-cylinder engine specifications

3.2.4 Waste Heat Recovery System

Wärtsilä have developed designs for incorporating a WHR system into the exhaust conjugate of their engines. By recovering energy from the engine exhaust gases, the overall fuel consumption is reduced, as shown in Figure 3, 4 and 5.

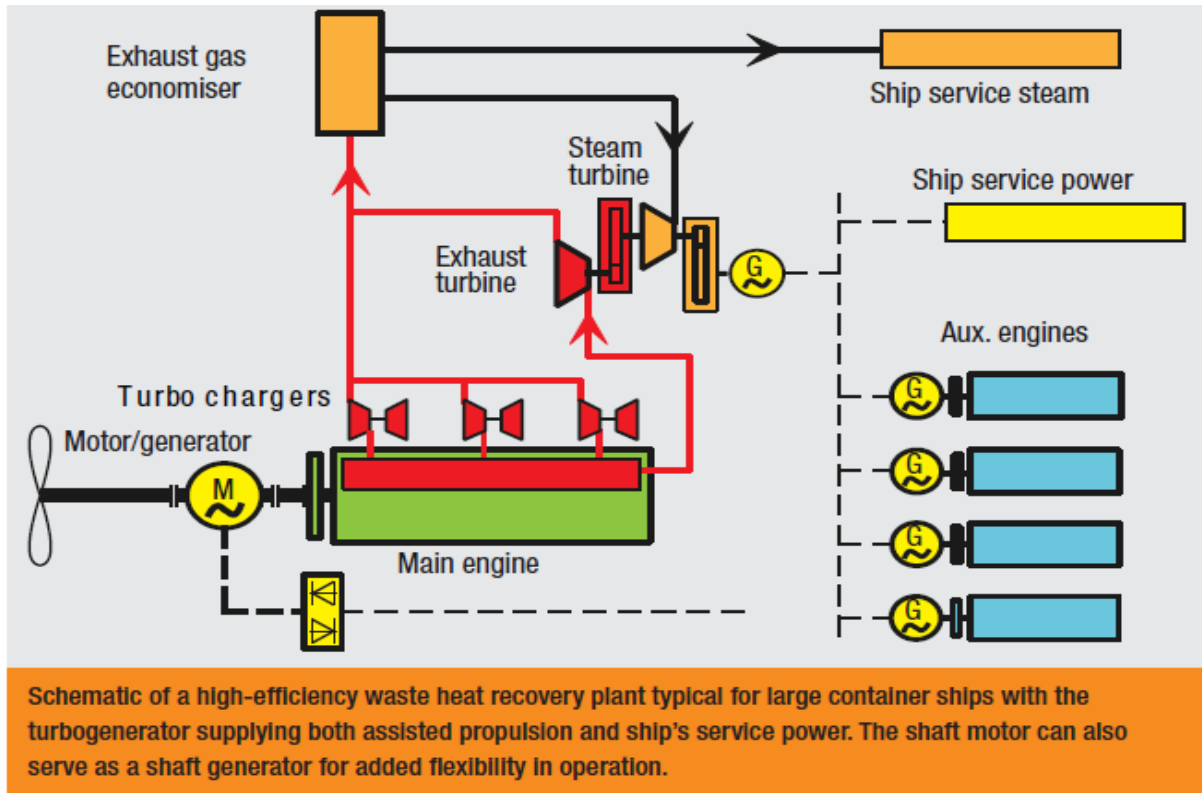


Figure 3: Waste heat recovery system integration into Wärtsilä

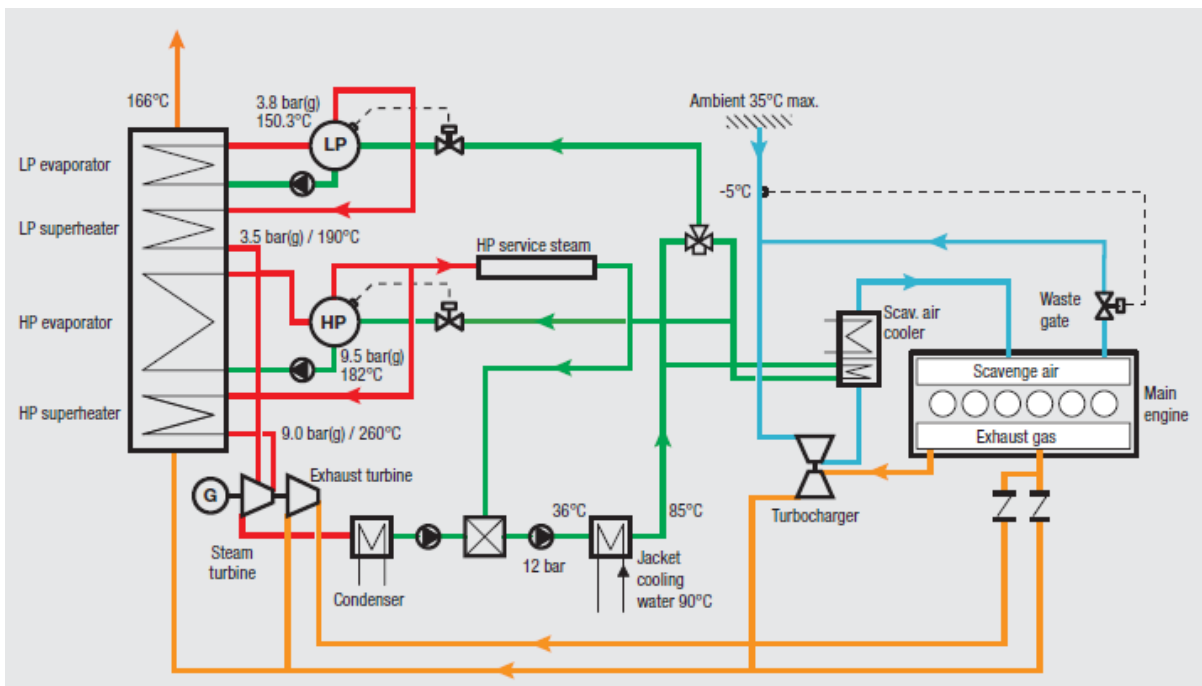


Figure 4: Waste heat recovery system diagram

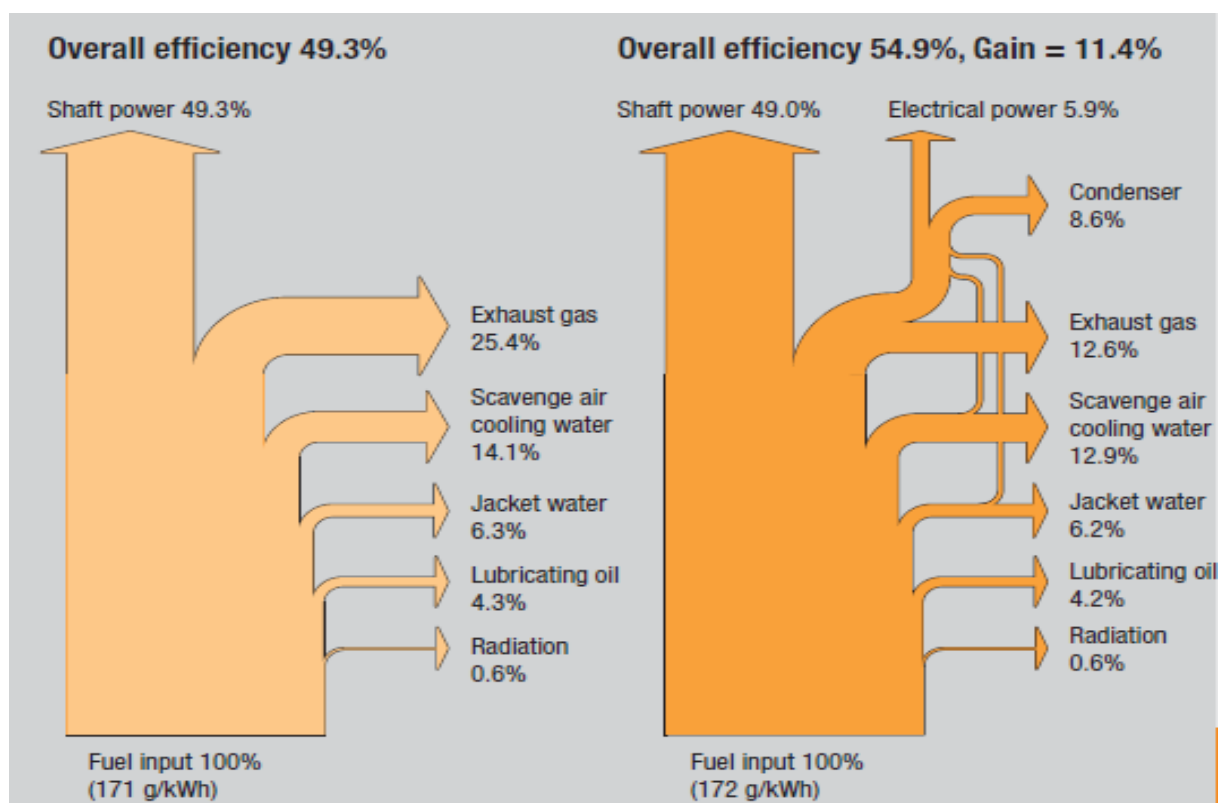


Figure 5: Diagram of efficiency gain by adding waste heat recovery system

As can be seen, the fuel consumption gain in using a WHR system is substantial. The investment cost is not negligible, but the return time on this initial investment is between 5 and 10 years.

3.3 PTO, PTI, PTH modes presentation

This section will discuss the Power-Take-Out (PTO), Power-Take-In (PTI) and Power-Take-Home (PTH) modes. Firstly, every mode will be explained with a mathematical model of the power systems be given at the end of the section.

3.3.1 PTO: Power-Take-Out as an Electric Power Generation System

The growing number of installed PTO systems, mainly on container carriers, is revealing an increase in the electrical power needed on-board vessels. The PTO generation system has the advantage of producing an economic power coming from the main engine using heavy fuel at a better efficiency point.

In the PTO mode the main engine is used to drive the shaft generator. The converter converts the generated electricity into the main service voltage. The diesel generator sets are not in operation.

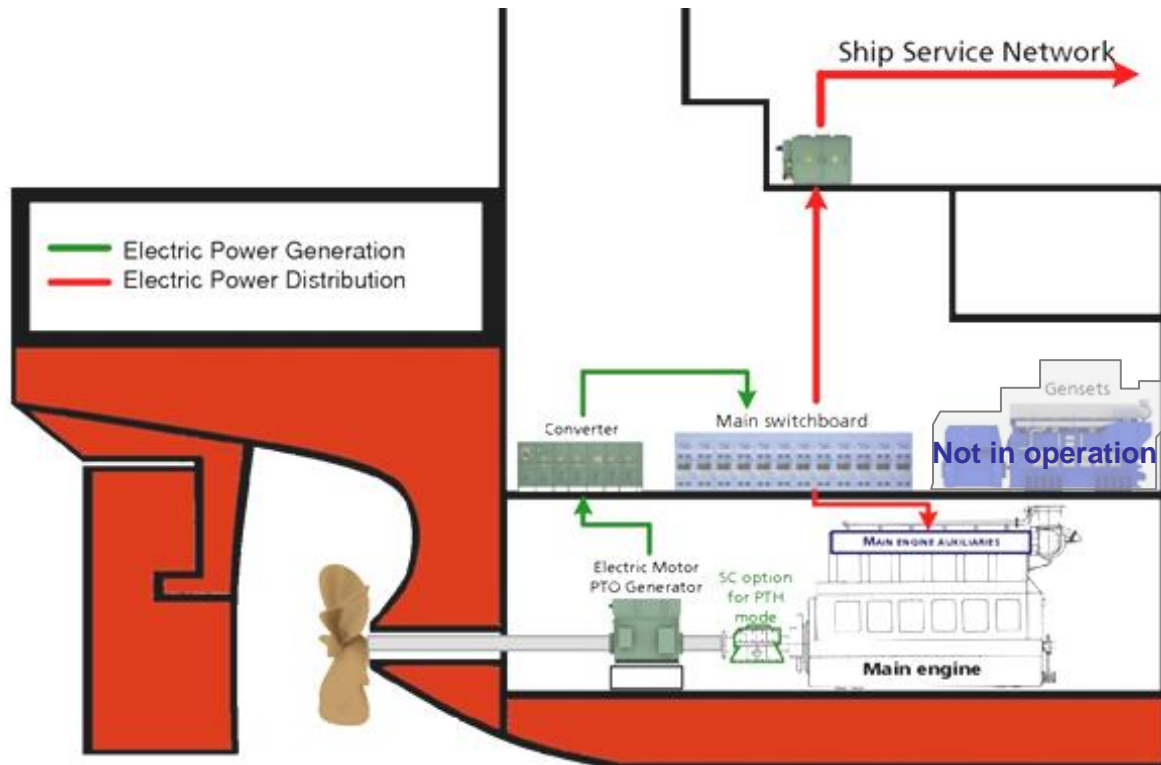


Figure 6: Ship PTO diagram

The main advantages of the PTO mode are:

- **Economic electric power generation:**
 - **Redundancy of electric power sources** (Electric power is supplied by PTO generators and/or generators of the Main generators)
 - **Independence of main engine with regard to generators** (no need of generators to supply main engine auxiliaries)
- **Improved Generator integration:**
 - **Less generators needed on-board** (a part of electric power generation comes from PTO generators)
 - **Less maintenance on generators** (Generators are not used during free sailing)
 - **Less noise, vibrations and losses in engine control room** (generators are not used during free sailing)

3.3.2 PTI: Power-Take-In with Booster Mode

PTI mode - Booster mode - is an economical solution to increase the power and the efficiency of the propulsion of any kind of vessels, converting energy coming from exhaust gases of main engine into free of charge electric power.

In the PTI mode the main engine is online and drives the main propeller. The heat recovery system is used, which in turn drives a generator. This free of charge electric power is distributed via the main switchboard to the ships service network. In addition remaining power is distributed to the converter and drives the shaft generator for extra power to the propeller when needed.

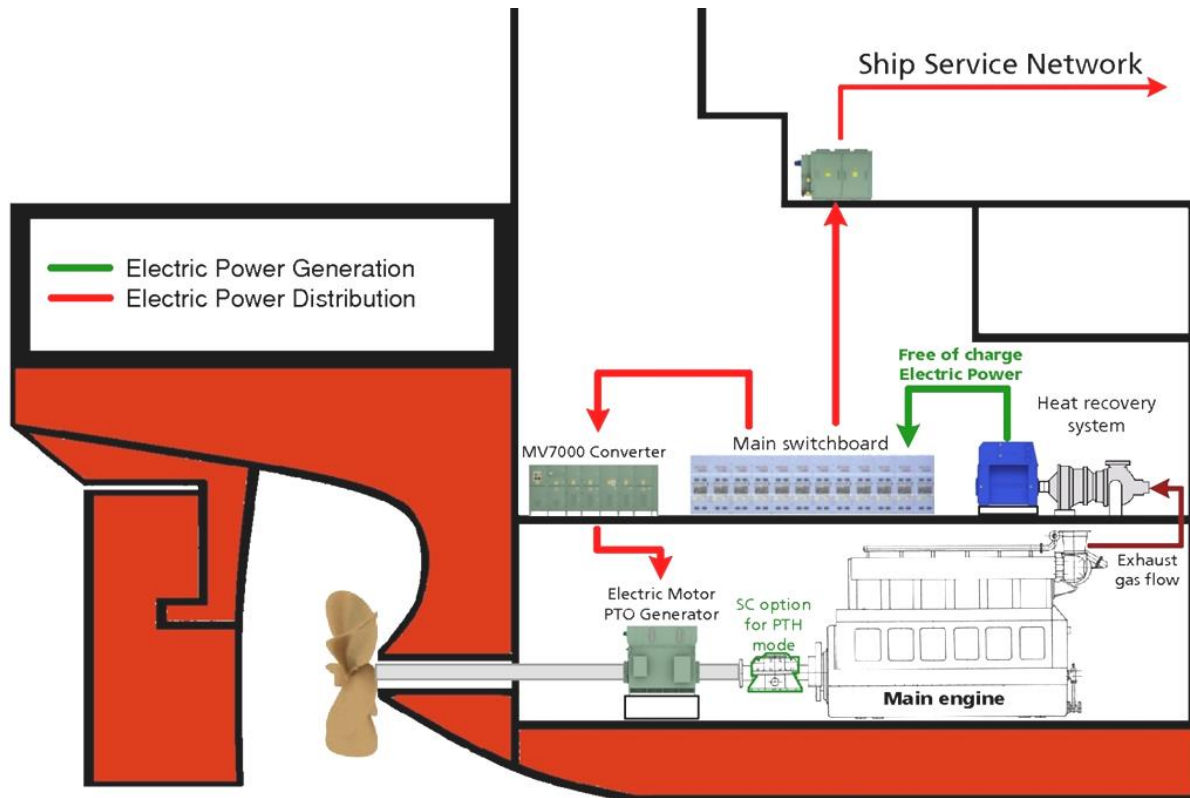


Figure 7: Ship PTI diagram

The main advantages of the PTI mode are:

- **Free of charge electric power:**
 - **Increased propulsion power:** for shipbuilding of new heavy tankers, classical main engine propulsion power is not sufficient, in order to keep only one shaft line. Electric Booster is the simplest solution to maintain competitive operational vessel speed.
 - **For the same vessel speed, main engine can be smaller:** the global thrust power is supplied by main engine and PTI electric motor.
 - For the same main engine, **vessel has a better overall efficiency**, represented by an increase of free sailing speed.
 - **Allows fuel cost savings**

3.3.3 PTH: Power-Take-Home run in Emergency Mode

PTH are similar to a PTI, as both have an alternator/motor which can be used to either provide electrical power to the ship or used to provide power to the propeller. While a PTI system will be used to boost the power of the main engine, a PTH system can disconnect the main engine from the propeller shaft to allow the ship's propulsion to be driven by the electric motor/alternator only. This is generally used at slow sailing speeds or to boost a smaller main engine when required.

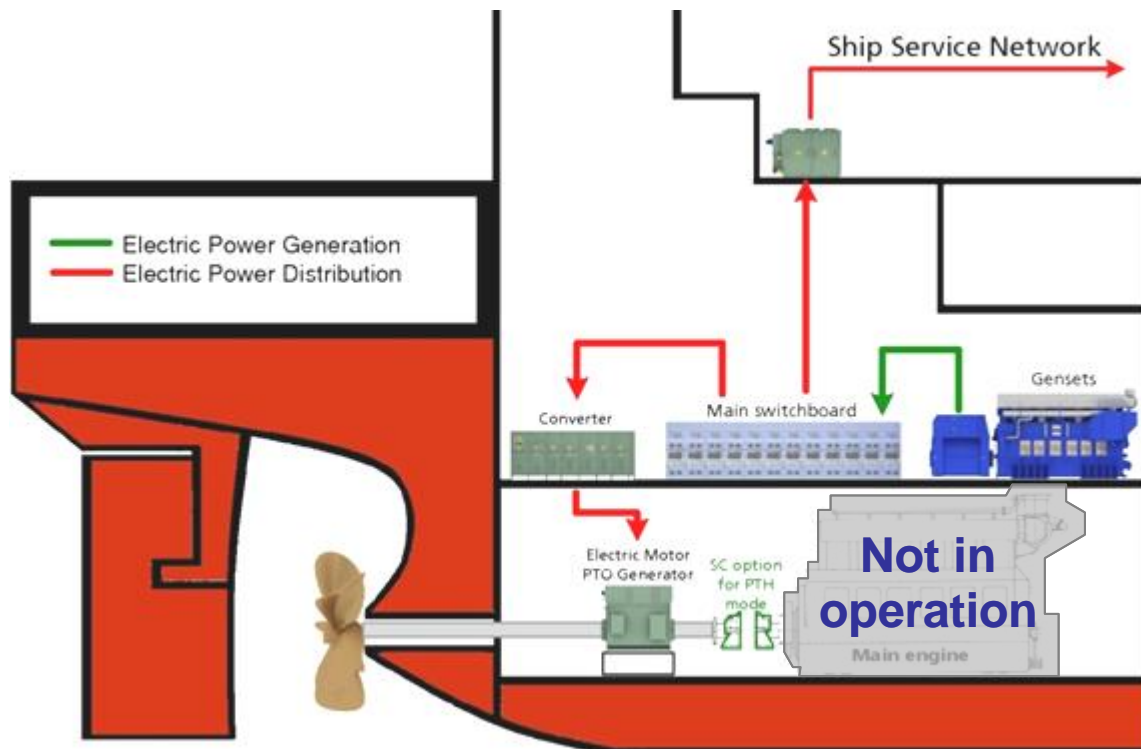


Figure 8: Ship PTH diagram

The main advantages of the PTH mode are:

- **Fully redundant propulsion system:**
 - **Fully independent propulsion system in case of main engine failures:** in case of emergency, vessels fitted with PTH drive are able to maintain manoeuvrability and reach harbour.
 - **Fully compliant with redundancy class specified by classification societies** for the minimization of cargo loss which can lead to ecological disasters.
 - **Electric propulsion is available in short order:** vessels can start quickly in case of emergency.
- **Economic benefits:**
 - **Main propulsion system only used during free sailing:** With PTH drive, main engine are only used during optimum load conditions so less engine maintenance is needed.
 - **Ship-owner can benefit of electrical propulsion advantages during slow speed manoeuvres:** During harbour manoeuvres and slow speed transit, electric propulsion can be used. Electric propulsion main advantages are:
 - **Fuel savings** (better overall efficiency)
 - **Environmental friendliness** (fully compliant with harbour regulations)
 - **Easy ship operation** (less tug and less harbour fees are needed)

3.4 Mathematical Engine Models

3.4.1 Specific Fuel Consumption and Management Laws

The specific fuel consumption (SFC) is the fuel mass consumed to generate one kWh of mechanical energy, expressed in g/kWh. The fuel mass is related to the chemical energy of

combustion, so the SFC is an image of efficiency. Instead of expressing the engine's efficiency as a percentage of energy out compared to energy in, it is expressed in g/kWh for practical reasons.

It is important to understand that the SFC of an engine changes as a function of its output torque and speed. Engines run at maximum efficiency at a particular torque and speed, for example the efficiency decreases significantly when the engine is under loaded.

SFC can be represented as a 2dimensional diagram (i.e. torque/speed, pressure/speed or power/speed). Figure 14 shows an efficiency mapping of a diesel engine.

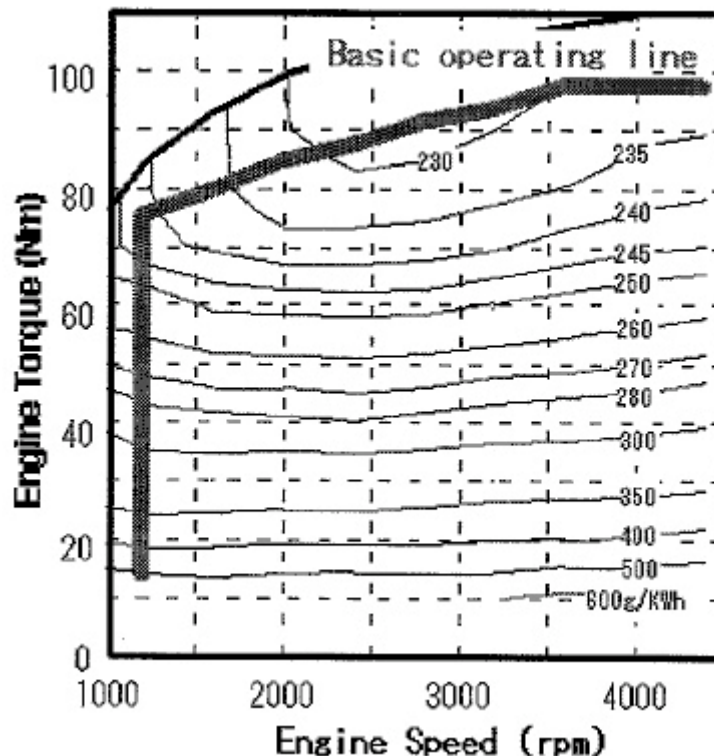


Figure 9: Basic diesel engine specific consumption mapping

In a diesel propulsion system with an electrical machine connected to the propulsion shaft, the power from the shaft is shared between the main propeller and the electrical machine operating as a generator. Alternatively, the electrical machine can also be used to provide additional power to the propeller by acting as a motor. This allows the possibility to optimise the operating point of the diesel engine.

3.4.2 Dynamic characteristics of diesel engines

Another point to consider when managing the engines in order to reduce its overall fuel consumption is to take into account their loading and unloading rates. Changing the loading on an engine is not instantaneous and is dependent on time, as shown in Figure 10.

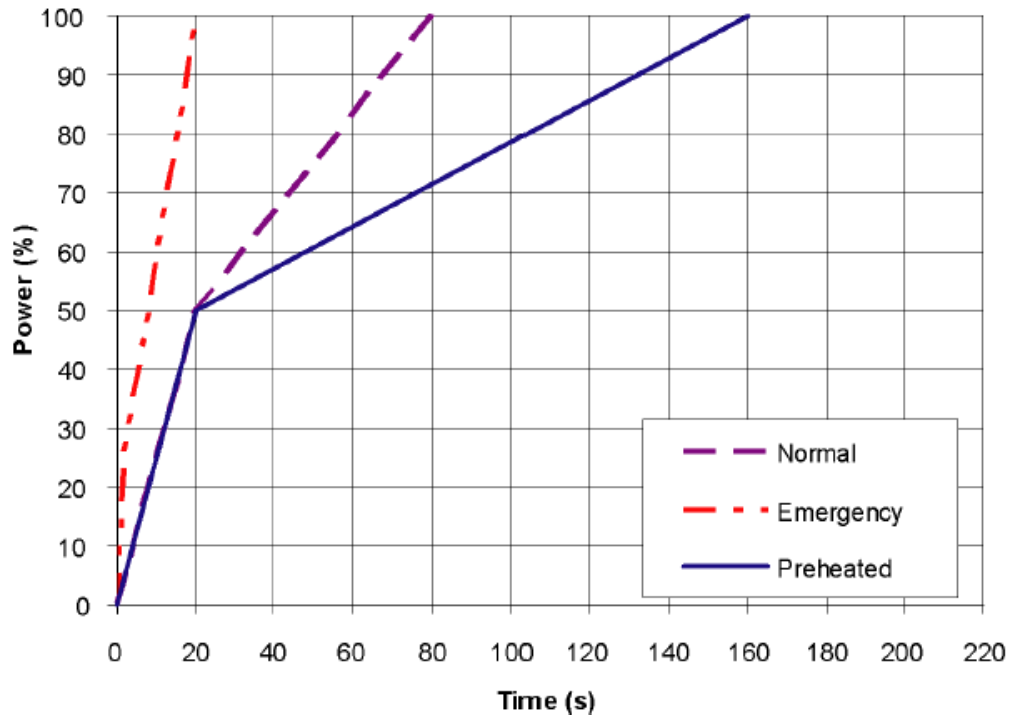


Figure 10: 6L32 Maximum recommended load increase rates for engines operating at nominal speed

3.4.3 Engine Models in GES Software

3.4.3.1 General Diesel Engine Model

TNO has already developed diesel engines models in the General Energy Software (GES). These models are based on combustion models of the fuel inside the engine. The only necessary parameters needed for this model are the specific engine area map of SFC, specific hydrocarbon emissions (SHC), specific nitrogen emissions (SNOx) and specific carbonates emissions (SCO). It is also important to know the specific fuel properties, such as the percentage carbon (C), the percentage hydrogen (H) and the percentage sulphur (S) in the fuel. If some particulate matter (PM) information is available, then the model can be used to calculate all PM quantities.

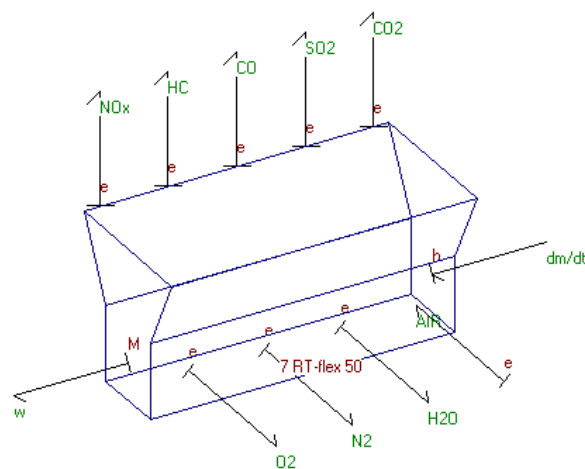


Figure 11: General diesel engine model in GES.

Standardised maps are available in the models for all of the aforementioned combustion properties. The model uses these maps if no specific information for a given diesel engine is

available. Figure 12 shows examples of standardised specific engine maps for the combustion process used in the GES engine models:

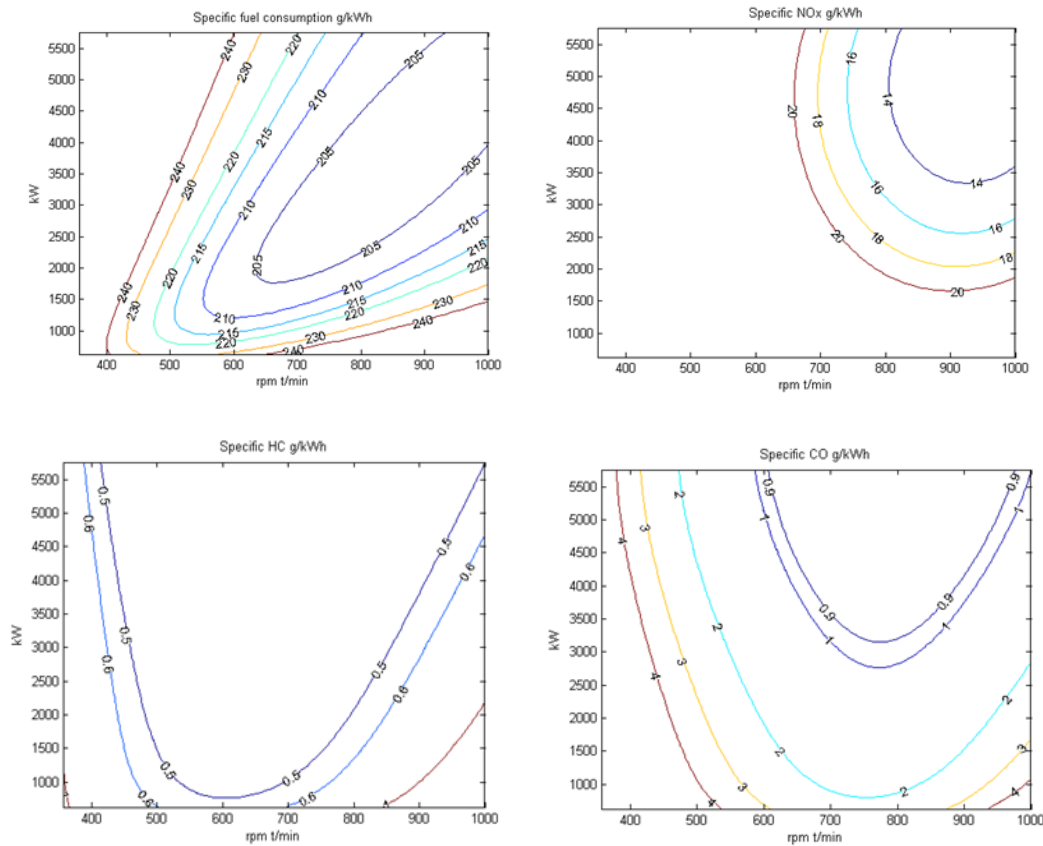


Figure 12 Specific fuel and emission map for a diesel engine

When running the engine model a controller can be opened and remains open in the operation area, as shown in Figure 13. This tracks in real-time the operation of the engine model over its operational range.

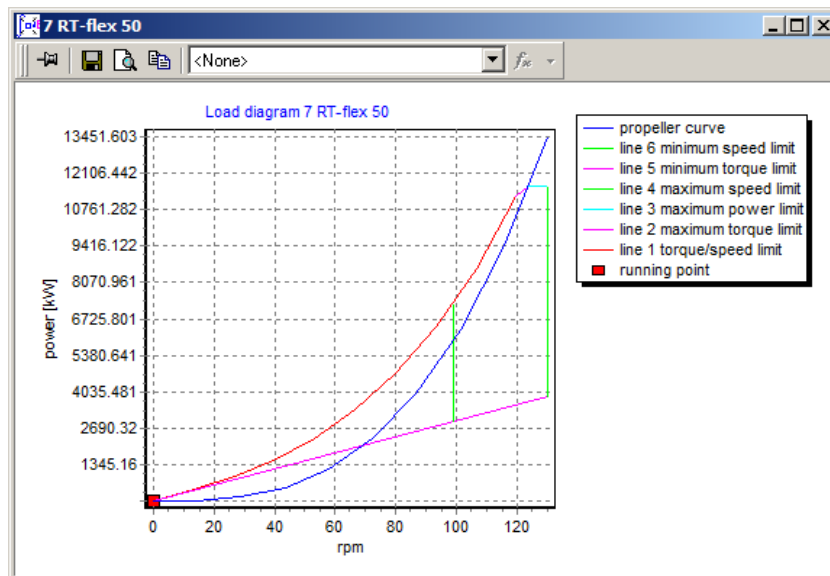


Figure 13: Operational diagram for a diesel engines.

3.4.3.2 Dual Fuel Engine Model

A simulated dual fuel diesel engine is also available in the GES software, as shown in Figure 14.

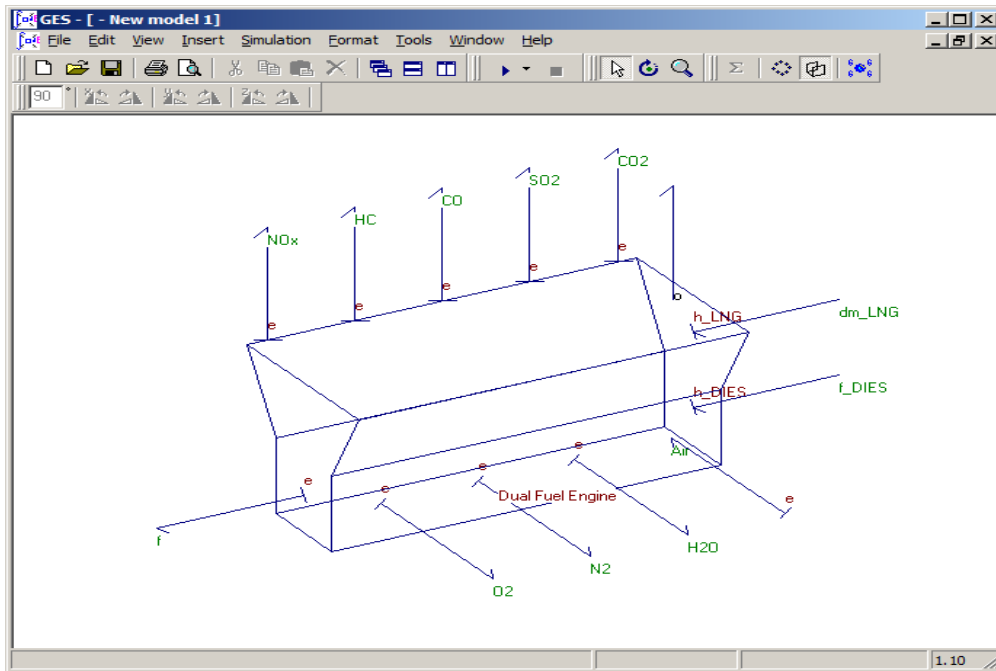


Figure 14: Dual fuel diesel engine model in GES software

In this model, the physical inputs are LNG fuel, marine fuel and the airflow rates. The outputs are the mechanical power generated and the different exhaust gases produced.

The SFC map for the dual fuel engine is shown in Figure 15.

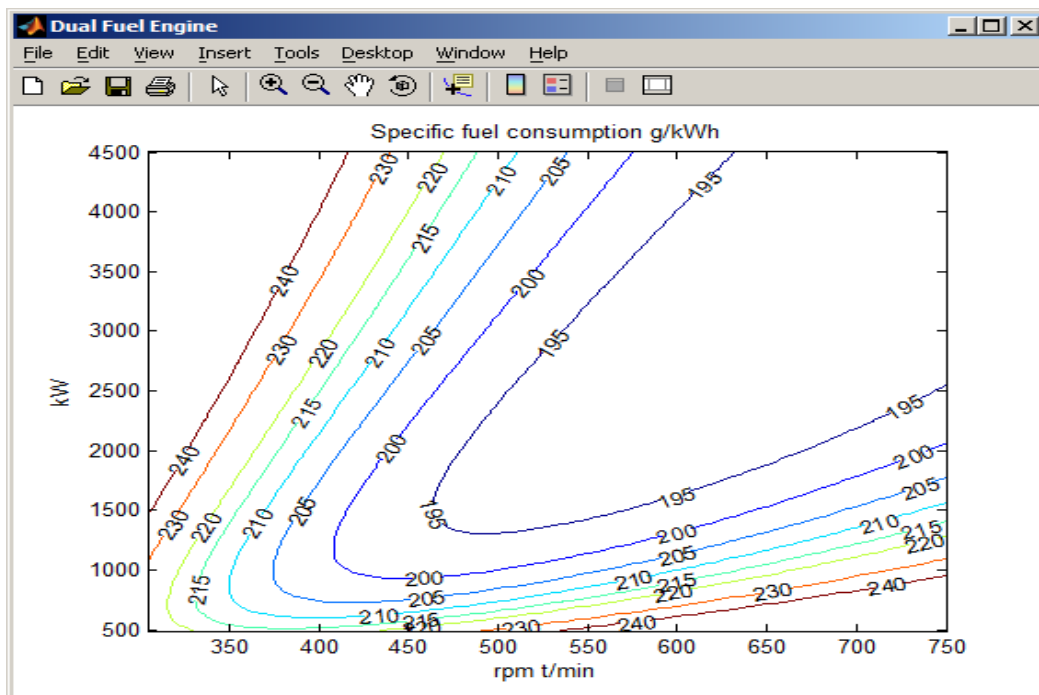


Figure 15: Dual fuel diesel engine model specific fuel consumption mapping

This physical model will be used for the ship simulation, to explore the different power generation and operational profiles of on-board systems.

3.5 Alternative Simulink Model

However, if the model produced is incompatible with Matlab or if the simulation time is too long, a two-dimension SFC graph can be generated in Matlab/Simulink using the ISUZU engine model, as shown in Figure 16:

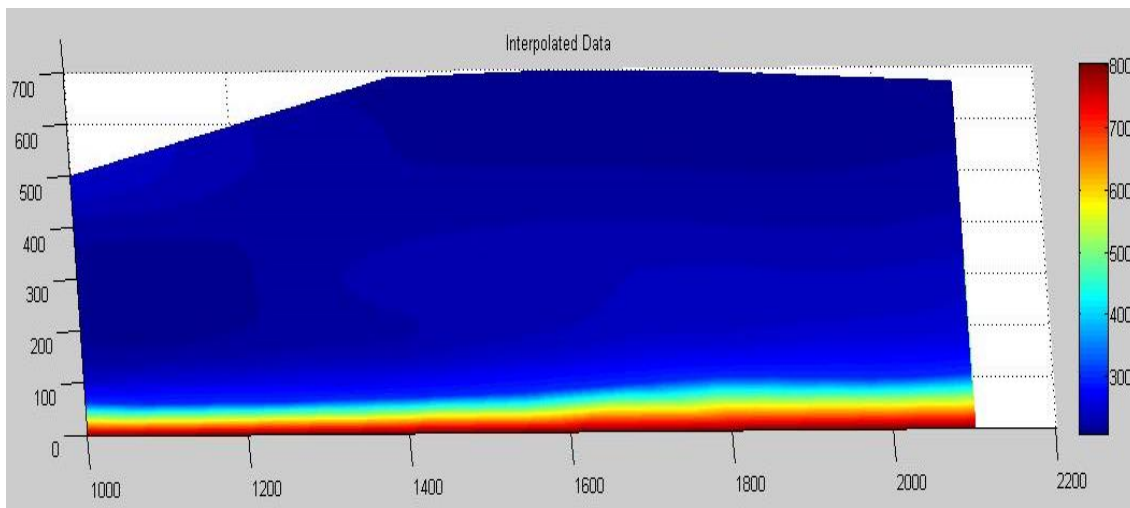


Figure 16: Specific fuel consumption mapping from the ISUZU diesel engine

Along the X-axis is plotted the engine speed, in rpm, and along the Y-axis is plotted the torque of the engine, in Nm. The coloured scale gives the SFC, in g/kWh for the engine.

The advantage of this solution is that it can simulate an engine in Matlab/Simulink using the SFC mapping directly from a lookup table.

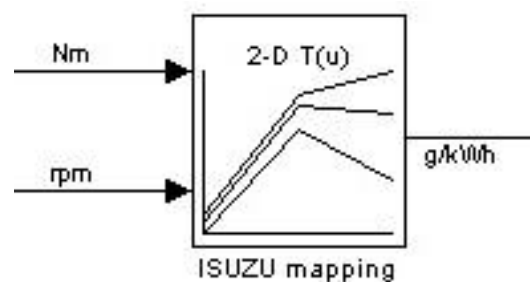


Figure 17: Lookup table for Isuzu simulation

This solution has been proven as a reliable modelling block in Simulink, able to simulate several different engines types. To simulate different engines, the SFC map is needed from the manufacturer.

4 ELECTRICAL MACHINES

The overall goal of this project is to reduce the CO₂ footprint of cargo ships. The basic way to achieve this with respect to electrical machines is by using components in the drive train with the highest possible efficiency.

Electrical machines in the drive train are the generators and the propulsion motors. At this moment the machines with high efficiency are of the permanent magnet (PM) type. Efficiencies can be found in brochures varying from 81% at low speed (127 rpm) and at low power (17kW), up to 98.2% at high speed (600 rpm) and at high power e.g. 2594kW.

4.1 Asynchronous machines

Selection of an asynchronous machine results in the following possible efficiencies:

Minimum efficiency values defined in IEC 60034-30:2008 standard (based on test methods specified in IEC 60034-2-1:2007)

Out-put kw	IE1 Standard efficiency			IE2 High efficiency			IE3 Premium efficiency		
	2 pole	4 pole	6 pole	2 pole	4 pole	6 pole	2 pole	4 pole	6 pole
0.75	72.1	72.1	70.0	77.4	79.6	75.9	80.7	82.5	78.9
1.1	75.0	75.0	72.9	79.6	81.4	78.1	82.7	84.1	81.0
1.5	77.2	77.2	75.2	81.3	82.8	79.8	84.2	85.3	82.5
2.2	79.7	79.7	77.7	83.2	84.3	81.8	85.9	86.7	84.3
3	81.5	81.5	79.7	84.6	85.5	83.3	87.1	87.7	85.6
4	83.1	83.1	81.4	85.8	86.6	84.6	88.1	88.6	86.8
5.5	84.7	84.7	83.1	87.0	87.7	86.0	89.2	89.6	88.0
7.5	86.0	86.0	84.7	88.1	88.7	87.2	90.1	90.4	89.1
11	87.6	87.6	86.4	89.4	89.8	88.7	91.2	91.4	90.3
15	88.7	88.7	87.7	90.3	90.6	89.7	91.9	92.1	91.2
18.5	89.3	89.3	88.6	90.9	91.2	90.4	92.4	92.6	91.7
22	89.9	89.9	89.2	91.3	91.6	90.9	92.7	93.0	92.2
30	90.7	90.7	90.2	92.0	92.3	91.7	93.3	93.6	92.9
37	91.2	91.2	90.8	92.5	92.7	92.2	93.7	93.9	93.3
45	91.7	91.7	91.4	92.9	93.1	92.7	94.0	94.2	93.7
55	92.1	92.1	91.9	93.2	93.5	93.1	94.3	94.6	94.1
75	92.7	92.7	92.6	93.8	94.0	93.7	94.7	95.0	94.6
90	93.0	93.0	92.9	94.1	94.2	94.0	95.0	95.2	94.9
110	93.3	93.3	93.3	94.3	94.5	94.3	95.2	95.4	95.1
132	93.5	93.5	93.5	94.6	94.7	94.6	95.4	95.6	95.4
160	93.7	93.8	93.8	94.8	94.9	94.8	95.6	95.8	95.6
200	94.0	94.0	94.0	95.0	95.1	95.0	95.8	96.0	95.8
250	94.0	94.0	94.0	95.0	95.1	95.0	95.8	96.0	95.8
315	94.0	94.0	94.0	95.0	95.1	95.0	95.8	96.0	95.8
355	94.0	94.0	94.0	95.0	95.1	95.0	95.8	96.0	95.8
375	94.0	94.0	94.0	95.0	95.1	95.0	95.8	96.0	95.8

Figure 18: Asynchronous machine efficiencies

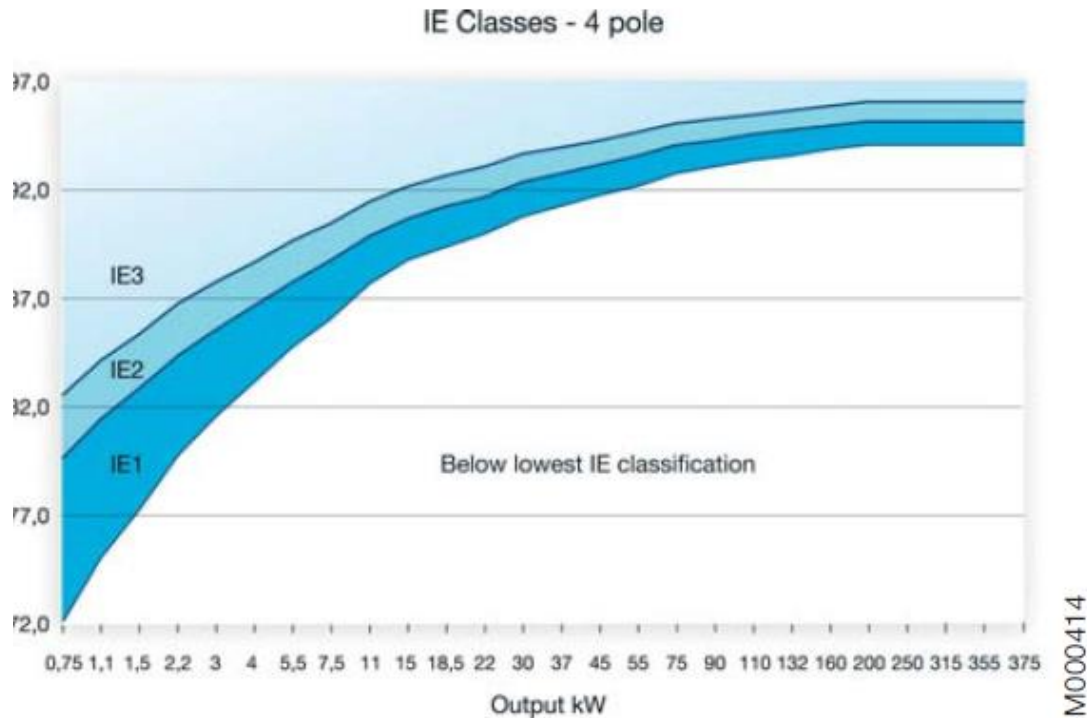


Figure 19: An IE classification of asynchronous machines

4.2 Induction versus permanent magnet machines

Comparison of drive trains realized with PM machines with respect to induction machines reveals a 4% gain absolute and 4.5% relatively.

		Chosen solution	
		Induction Machine	Permanent Magnet Machine
Efficiency	Generator	96%	98%
	Propulsion Motor	96%	98%
	Overall	92.2%	96.4%

4.3 Electric machine models

Suitably realistic models for the simulation of induction machines and permanent magnet machines can be found in literature readily available on the internet.

Induction machines:

<http://www.google.nl/url?sa=t&rct=j&q=&esrc=s&frm=1&source=web&cd=1&ved=0CDkQFjAA&url=http%3A%2F%2Fwww.springer.com%2Fcontent%2Fdocument%2Fdocument%2Fdownloaddocument%2F9780857299000-c2.pdf%3FSGWID%3D0-0-45-1293539-p174129069&ei=pr5OUsgaKu-B7Qat2IBQ&usq=AFQjCNGwNfNhtDpNUI0G58kvlfVFBRuOVw&bvm=bv.53537100,d.bGE>

<http://www.tdx.cat/bitstream/handle/10803/6317/06Chapter1.PDF;jsessionid=C6769CCFDD5DC230AC76B96A7090A4A0.tdx2?sequence=6>

Permanent magnet machines:

http://cdn.intechopen.com/pdfs/12288/InTech-Magnetically_nonlinear_dynamic_models_of_synchronous_machines_their_derivation_parameters_and_applications.pdf

http://www.google.nl/url?sa=t&rct=j&q=&esrc=s&frm=1&source=web&cd=1&ved=0CDQQFjAA&url=http%3A%2F%2Fwww.ipst.org%2FTechPapers%2F2005%2FIPST05_Paper159.pdf&ei=4h1NUoj6F5TY4QSHmIGQBw&usg=AFQjCNEI9dKriF4SK4V9C-c3mNsg5QOQPg

http://www.google.nl/url?sa=t&rct=j&q=&esrc=s&frm=1&source=web&cd=3&ved=0CEcQFjAC&url=http%3A%2F%2Frepository.tudelft.nl%2Fassets%2Fuuid%3A855bc4-6254-4f1f-8218-f0fa4ec5fcd8%2F211583.pdf&ei=4h1NUoj6F5TY4QSHmIGQBw&usg=AFQjCNGdMTQ_OEsXymDxVIRXDX2JzwqOpg

5 ENERGY STORAGE

There are several storage devices that can be used on-board a ship, which will be explored in detail as part of this project. These include batteries, supercapacitors or flywheels. All of the storage devices have clearly different properties. Supercapacitors and flywheels can deliver high power, but they have a low specific energy (around 5 Wh/kg). Batteries have a much higher specific energy (more than 100 Wh/kg) with more or less power. This depends on their technologies (lead acid, nickel metal hydride, lithium based, etc...) and their construction to give either high specific energy or high specific power.

A short description of different storage devices is given in the following sections, with a brief overview of the technologies potentially of interest for the INOMANS²HIP project.

Figure 20 shows an overview of the specific energy and power ranges for the different energy storage technologies.

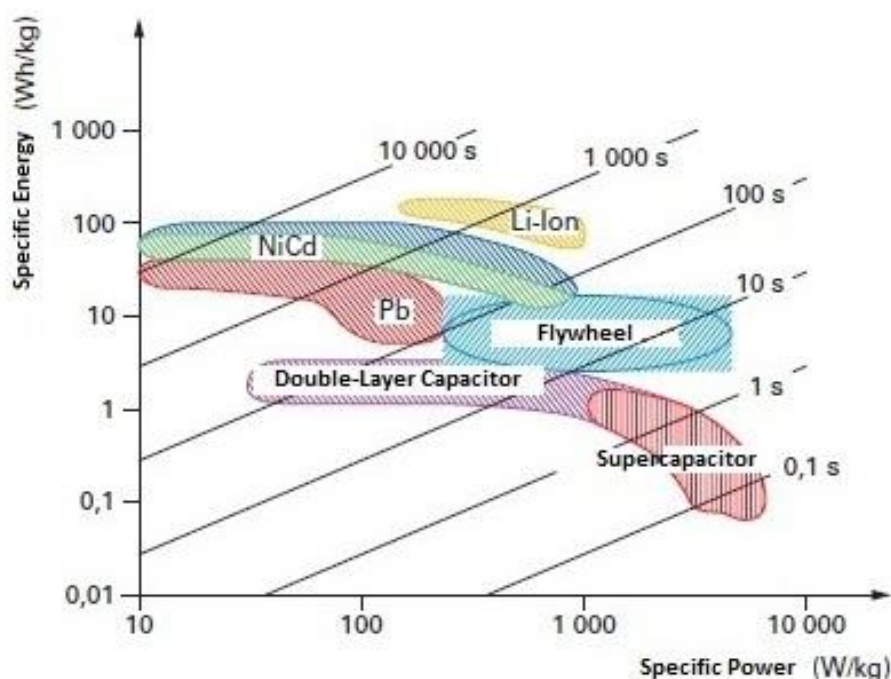


Figure 20 : Power and energy comparison of different storage devices

5.1 Overview of Batteries

There are many types of battery technologies, but only the most important were considered as part of this task of the project:

- Lead acid
- Nickel Cadmium (Ni-Cd)
- Nickel Metal Hydride (Ni-Mh)
- Lithium based (Li ion, LMP, LiFeO, etc...)
- Sodium based (Zebra)

Batteries consist of a combination of accumulators, which use chemical reactions, such as oxidation and reduction, to store and deliver electrical energy. The conversion from chemical to electrical and vice versa is not perfect; there are some losses dependent on the batteries types, i.e. the efficiency of a charge/discharge cycle is between 70% and 90% depending on the battery chosen.

In this overview, sodium based batteries will be excluded because of their high auto discharge of up to 50% daily. Sodium based batteries are more commonly known as hot battery technology because the electrochemical reactions during the charge and discharge cycle taking place at high temperatures, around 300°C. These batteries consume their stored energy to heat themselves and to maintain their operating temperature.

This rate of auto discharge is not acceptable for the selection of a suitable energy storage system for a ship. Also considered is that the energy storage has to be efficient in order to reduce the ship consumption.

Table 5 shows the main properties of the different battery types studied in this task.

Battery Technology	Lead	Ni-Cd	Ni-Mh	Lithium
Specific Energy Wh/kg	15 – 40	30 – 60	65 – 90	90 – 150
Power Density W/Kg	40 – 100	80 – 160	210 – 350	200 – 1000
No load cell Voltage	2.1 V	1.30 V	1.32 V	4.1 V
Op Temp (Charge)	10 to 40°C	0 to 45°C	0 to 40°C	0 to 45°C
Auto discharge	15%/month	25%/month	10%/month	2%/month
Life cycles (full charge/discharge)	400 cycles	1000 cycles	700 cycles	>3000 cycles
Cost in \$/kWh	150	300	200 - 350	800 – 1200

Table 5: Batteries comparison

5.1.1 Lead Acid Batteries

Gaston Planté invented lead acid batteries in 1859. A lead acid battery is reliable and relatively cheap, but performances are poor when compared to other battery types. The energy density is limited, but lead acid batteries allow high peak power.

Like every battery technology, the lifetime depends on the discharge depth. It is expected that a lifetime of 400 cycles at 80% depth of discharge (DoD) for lead acid batteries. To extend a battery life the DoD has to be as small as possible.

The most important risks with using lead acid batteries are short-circuiting, high heating in overload, loss of sulphuric acid and hydrogen release.

Lead acid batteries are relatively easy to recycle when compared to other battery technologies.

5.1.2 Ni-Cd Batteries

Ni-Cd (nickel–cadmium) batteries were discovered by Waldemar Jungner in 1899 and gave similar properties as lead acid batteries. However, in 1928 Schlecht and Ackermann upgraded the electrodes allowing fast charge and discharge of Ni-Cd batteries at high power.

The price of Nickel and Cadmium, and the complex production process make the price of Ni-Cd batteries much higher than lead acid batteries. The other problem is the toxicity of cadmium for the environment and health, which causes concern in disposal of the batteries.

The life of a Ni-Cd battery is approximately 1000 cycles. Extending the life expectancy of and limiting the depth of discharge must be done considering the memory effect of the battery. The memory effect is a phenomenon where battery appears to lose voltage capacity due to not fully discharging and then fully charging over several cycles. Under

these circumstances, a Ni-Cd battery loses the initial charge left on the battery after discharge, reducing its capacity. Temporary battery memory effects can be mitigated through overcharging the battery during the charging cycle, i.e. charging > 100% of battery capacity.

5.1.3 Ni-Mh Batteries

Ni-Mh (nickel–metal hydride) batteries were developed in the 1980's after research into alloys able to store hydrogen. Ni-Mh is the evolution of Ni-Cd with the negative Cadmium electrode replaced by an active material, i.e. hydrogen absorbed in a metallic alloy.

The gain in specific energy is around 80Wh/kg compared to the 35 or 55Wh/kg for Ni-Cd and the energy density is also higher reaching 350Wh/L. Ni-Mh allows charge and discharge power to be a little bit higher than Ni-Cd, but the life expectancy is around 700 cycles.

Low deep cycle is possible to extend the life of the batteries without suffering from the memory effects of the Ni-Cd batteries. Ni-Mh batteries are progressively being replaced by lithium batteries, except where high specific power is needed, such as for hybrid vehicles.

5.1.4 Lithium Batteries

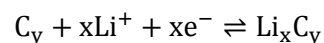
Lithium batteries were developed in 1970's with Sony putting the first industrial cells on the market in 1990. Lithium is a light metal, particularly well adapted to create high specific energy and power batteries. However, lithium reacts violently with water needing an adapted organic electrolyte to mitigate this effect.

During charging, the chemical reactions are:

On the positive electrode



On the negative electrode



Combining negative and positive electrode reactions gives,



Where x varies between 0 and 5; y/x corresponds to the composites of Li and C, where $n = x$ or $y = 24, 18, 12$ or 6 . In discharge phase, the chemical reactions are reversed.

Lithium battery cells can be classified in two categories, being the liquid electrolyte and the polymer electrolyte lithium cells.

The polymer electrolyte are all solid cells, the advantage being to allow more variety of cell shape with good shock and vibration resistance. In terms of performances, they are similar to liquid electrolyte cells.

Lithium batteries need to have a performance protection control to avoid any risk in terms of security and environment.

Lithium batteries are designed with:

- Devices avoiding the internal suppressions, over and under voltages chip inside the batteries
- Components used to limit high currents at high temperatures, such as thermostat or positive temperature coefficient (PTC) device

The internal electronics of the batteries can also provide data on their state at any given time. Modern batteries are designed to pass the UL-1642 standard of tests, aimed at testing the resilience of the battery to vibration, overcharging, forced discharge, short circuits, environmental conditions, and immersion, amongst other conditions.

Lithium-ion batteries don't use heavy metals so they don't represent an environmental risk. However, lithium cells must be recycled, as they can react with sodium and water to generate hydrofluoric acid and lithium hydroxide on the negative electrode, which are corrosive. In addition, lithium-ion batteries contain some flammable elements, which require proper disposal.

To conclude lithium batteries give the best performances of all the batteries discussed. The safe operation of the batteries has been resolved by implementing several internal elements, such as electronic management systems and secured battery design. In addition, the environmental risks are minimal, if the batteries are properly disposed of.

Figure 22 shows an unofficial graph from a Li-Ion battery manufacturer (EB) giving a typical value for efficiency of between 86-97.5% can be achieved depending on the discharge current. The impedance of a battery cell is given below as shown in Figure 21. At 45A load current and a cell voltage of 3.2V and an internal cell resistance of 3mΩ, therefore, a loss (heat) is generated in the cell of $3\text{m}\Omega \cdot (45\text{A})^2 = 6.08\text{W}$. Assuming that the cell is supplying 45A @ 3.2V, i.e. 144W an efficiency can be calculated of $(144-6)/144 = 95.8\%$. From literature it can be determined that the internal resistance of a Lithium ion cell is quite flat with respect to SOC.

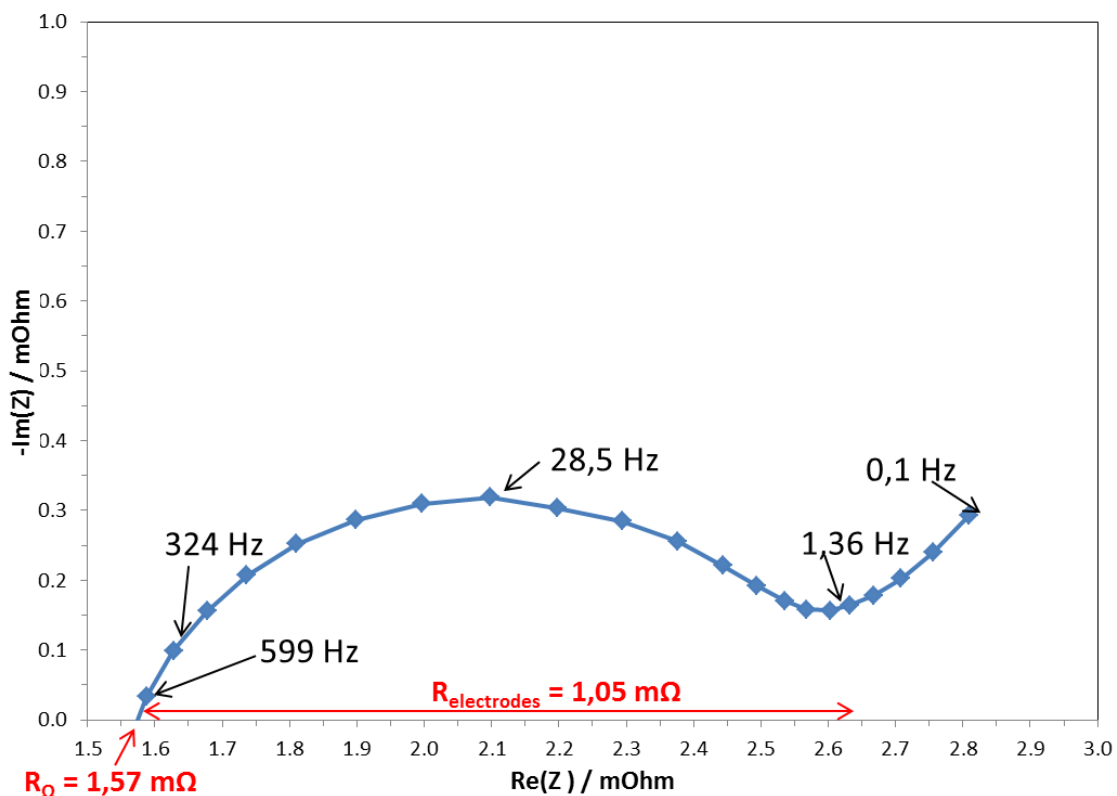


Figure 21 Lithium battery impedance

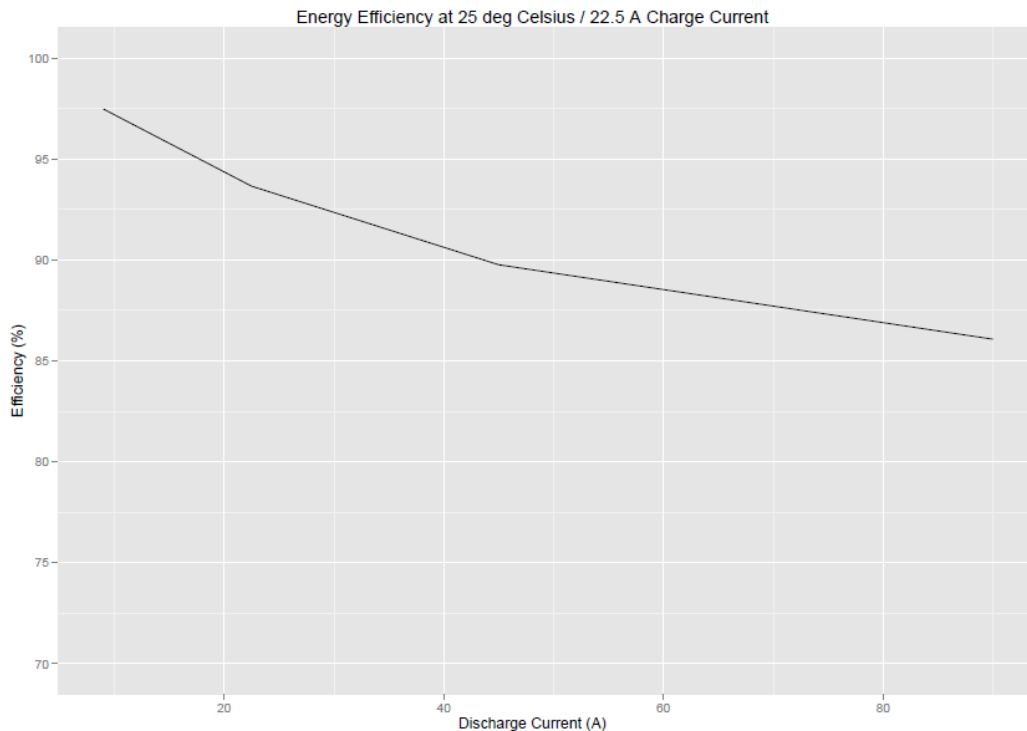


Figure 22 Lithium battery efficiency

5.2 Supercapacitors

5.2.1 General Description

Supercapacitors have a very high capacitance to store energy. They are used in application needing high power, but relatively low energy.

The principal advantages of supercapacitors are the relatively high power density, long lifecycles and the high charge/discharge efficiency, around 95%.

The operating principle of supercapacitors is the same as for a standard electrolytic capacitor, but with some optimisation. This mainly involves increasing the exchange surface of the electrodes by using porous materials and increasing the operational voltage using a high stability electrolyte, as shown in Figure 23.

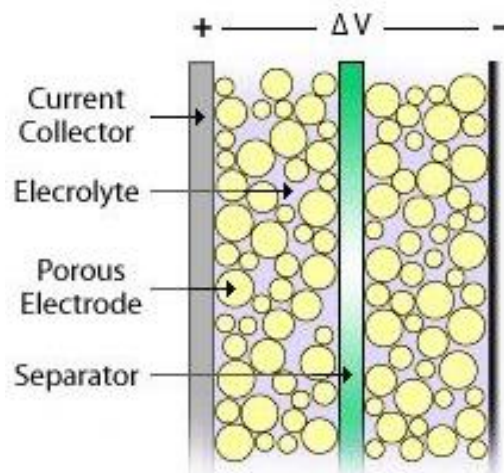


Figure 23: Supercapacitor schematics (source venturebeat.com)

There are different types of supercapacitors, the most common are shown in Table 6

	Active Coal Liquid Electrolyte	Active Coal Organic Electrolyte	Active Coal Solid Electrolyte	Metal Oxide Liquid Electrolyte	Conductive Polymer Organic Electrolyte
Energy density (Wh/kg)	0,2 to 2	1 to 5	1 to 5	2 to 10	2 to 10
Power density (kW/kg)	1 to 5	0,2 to 2	0,1 to 0,5	1 to 10	0,1 to 0,5
Voltage (V)	0,8 to 1,2	2 to 3	2 to 3	0,8 to 1,2	0,8 to 1,3
Cycles	>100 000	>100 000	>10 000	>50 000	>10 000
Relative cost	Low	Low	Medium	High	Medium

Table 6: Supercapacitor technologies comparison

The table compares the different supercapacitor technologies. Supercapacitors have to be assembled in modules to respond immediately to the voltage, the power and the energy demanded.

5.2.2 Arrangement of Supercapacitors Modules

Supercapacitors are connected in parallel and/or in series depending on the system requirements. Supercapacitors have an operating voltage and peak voltage that is reached for only a few hundred milliseconds before damage is caused. Studies have shown that a balancing circuit is necessary to have the same voltage on every cell. There are two kinds of balancing circuit;

Passive balancing: It's the simplest circuit, consisting of an added parallel resistor on every supercapacitor. This balancing resistor is sized by the nominal voltage of the supercapacitor and the current that needs to be deflected. Ideally, this current would be equal to the supercapacitor's charge current, generally very high, (>100A) and the resistor will significantly increase the current loss. A compromise must be reached between the size of the resistor, the cost and the deflected current.

Active balancing: An active balancing circuit is more complex than a passive balancing circuit. It consists of a power electronic circuit in parallel with the supercapacitors. The current is deflected when the voltage on a supercapacitor is near its maximum operating voltage. However, these circuits can be high in price, approximately the same cost of the supercapacitor. Figure 24 shows a lower cost alternative using a low current active balance circuit.

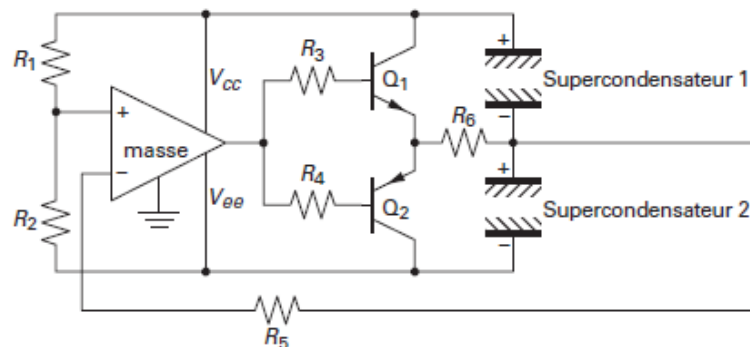


Figure 24: Maxwell active balancing circuit

However, a full current deflection circuit is expensive because the current is relatively high. Generally, the deflected current doesn't exceed a few amperes to minimise the balancing circuit cost.

5.2.3 Sizing of the Supercapacitors

A supercapacitor module is sized depending on power needed and time required to deliver this power. As a basic rule, sizing a supercapacitor is dependent on;

- The voltage level and the nominal current
- The total capacity of the supercapacitor module to use
- The number of elements to put in series (N_{series}) and in parallel ($N_{parallel}$).

The total capacity (C_t) and the internal resistance (R) of the module are expressed as,

$$C_t = (N_{parallel}/N_{series})C(N_{parallel}/N_{series})$$

$$R = ESR(N_{series}/N_{parallel})$$

Where ESR is the series resistance of one supercapacitor.

5.2.4 Actual Solutions and Perspectives

Actual supercapacitors can nominally reach 10Wh/kg with a theoretical limit up to 30Wh/kg. So replacing batteries by supercapacitors is not possible and will not be possible on the application needing important energy.

Supercapacitors have strengths where the batteries have weakness, such as life expectancy of 1000 times the number of cycles compared to batteries and higher power density, i.e. extremely fast charge and discharge. This is why using a hybrid storage system composed of batteries and supercapacitors is a good choice where batteries cannot be used alone due to the lack of instant power or to prolong their life.

Research on supercapacitors has led to an increasing of component performances and a decrease in production costs.

To summarise supercapacitors, the energy and the power density is not as high when they are packed in modules compared to batteries, with the best actual modules reaching 2Wh/kg to 10Wh/kg. The operating temperatures are between -40°C to 65°C allowing a good flexibility and supercapacitors can reach 1,000,000 cycles with a decrease of only 20% of capacitance and an increase of 100% of series resistance.

5.3 Flywheels

The flywheel was designed to smooth rotational movement and used on steam velocipedes.

A flywheel can also be used as an electric storage device to store mechanical energy, as kinetic energy of a rotating heavy disc. An electrical alternator, attached to the disc, can be used to convert this mechanical energy into useful electrical energy. Alternatively, an electric motor can be used to power the disc, converting electrical energy into mechanical energy of the rotating disc.

5.3.1 Physical Principle and Technologies

The kinetic energy stored by a flywheel is;

$$E_c = \frac{1}{2}J\omega^2 \quad \text{Equation 1}$$

Where J is the inertial moment and ω is the rotation frequency

The inertial moment is function of the mass and the shape of the rotation part.

The storable energy is limited by the maximum mechanical stress produced by the centrifugal force acting on the rotating disc. This stress, σ , is proportional to the density, ρ , of the material and the square of its tangential speed and is given by;

$$\sigma = k\rho V^2 \quad \text{Equation 2}$$

The total storable kinetic energy is given by the mass of the disc, m (in kg), and is;

$$E_k/m = A\sigma/\rho \quad \text{Equation 3}$$

The shape factor, A, is a dimensionless number, which is dependent on the shape of the rotating disc.

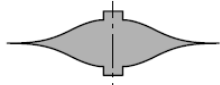
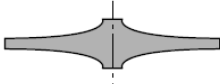
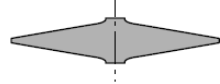
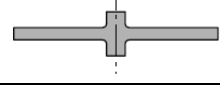
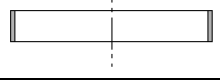
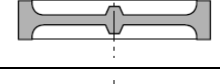
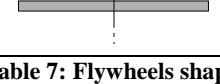
Flywheel type	Schematic	Shape factor A
Constant stress disc		1
Modified constant stress disc		0.931
Conic		0.806
Undrilled plate disc		0.606
Thin coronal		0.5
Full wheel		0.4
Drilled plate disc		0.305

Table 7: Flywheels shapes

The maximum storable energy in a flywheel is also a function of the material properties used, i.e. the density and maximum yield stress of the disc's material. Table 8 shows the maximum theoretical specific energy of different materials with a shape factor of 1.

Material	Maximum Yield Stress (MPa)	Density (kg/m ³)	Specific Energy (Wh/kg)
Steel(AISI 4330)	1,800	7,800	32
Aluminium	400	2,700	21
Titanium	850	4,500	26
Glass composite	1,800	2,100	120
Carbon composite	2,400	1,500	220

Table 8: Flywheels materials

The maximum specific energies shown in the table are purely theoretical as they consider only the flywheel, not the entire system, such as the electrical alternator/motor, vacuum pump, auxiliary control systems, surrounding wall, bearings, etc...

The entire system is much heavier and larger than the single flywheel.

Bearings are very important on flywheels because the rotational speed is very fast, up to 53,000 rpm depending on the application and design. Rotational speed is not only limited by the material stresses sustainable by the flywheel, but also by the type of bearings used. In addition, aerodynamic effects, air resistance and turbulence, also need to be considered. To reduce these effects most flywheel systems are run in a partial or nearly total vacuum. Some materials, like modern composites, and special bearings can be used to sustain very high rotation speeds in order to reduce losses and to limit the mechanical wear.

Mechanical bearings

Ball bearings are used on slow rotation flywheel, as they are simple to use, compact and inexpensive. However, friction losses became too important at high speeds, the heat generated cannot be evacuated and lubrication cannot be satisfactorily performed in a vacuum. The mechanical wear is also too fast at high speed, and thus, this type of bearing can only be used on low speed flywheels.

Passive magnetic bearings

A floating bearing is created by using the attraction and repulsion forces between permanent or variable reluctance magnetic materials. Since these bearings do not share a surface contact, there are no frictional losses and hence, no energy is lost. Passive magnetic bearings cannot be used alone because they are not stable. In this case, an associated mechanical system or an active magnetic device is needed to control the stability of the bearing.

Active magnetic bearings

Active magnetic bearings use an electric current to control the magnetic field of the bearing. A servo-controller varies the current to sustain the mobile part of the magnetic circuit in position. However, an active magnetic bearing needs a constant energetic power supply to enable it to work correctly. Active magnetic bearings are complex and large. For full suspension needs, an electronic control system with five degrees of freedom is required.

Superconductor magnetic bearings

Active magnetic bearings can be made to sustain a magnetic field without the need of an energy supply using superconductor materials. However, these types of bearings require a cryogenic unit to maintain the very cold operating temperatures, and the high material costs reduce the economic viability of this solution.

The type of bearings used depends of the application requirements (type of flywheel, rotation speed, etc...) and the desired level of performance. Examples of the application and different types of flywheel are shown in Table 9.

Applications	Peak power	Energy stored (kWh)	Max rotation speed (rpm)	Tangential speed (m/s)	Rotor material	Rotor mass (kg)
Satellite	2 kW	0,4	53,000	900	Composite	30
Power source	400 kW	1,3	10,000	400	Steel	1,400
Hybrid bus	150 kW	2	40,000	900	Composite	60
Space station	3.6 kW	3,7	53,000	900	Composite	75
Hybrid military vehicle	11 MW pulse - 350 kW continuous.	14	18,000	540	Composite /Steel	280
Electromagnetic starter	5 to 10 GW	14 to 42	10,000	450	Composite	4,000
Train	2 MW	130	15,000	950	Composite	2,500

Table 9: Examples of types of flywheels used in different applications

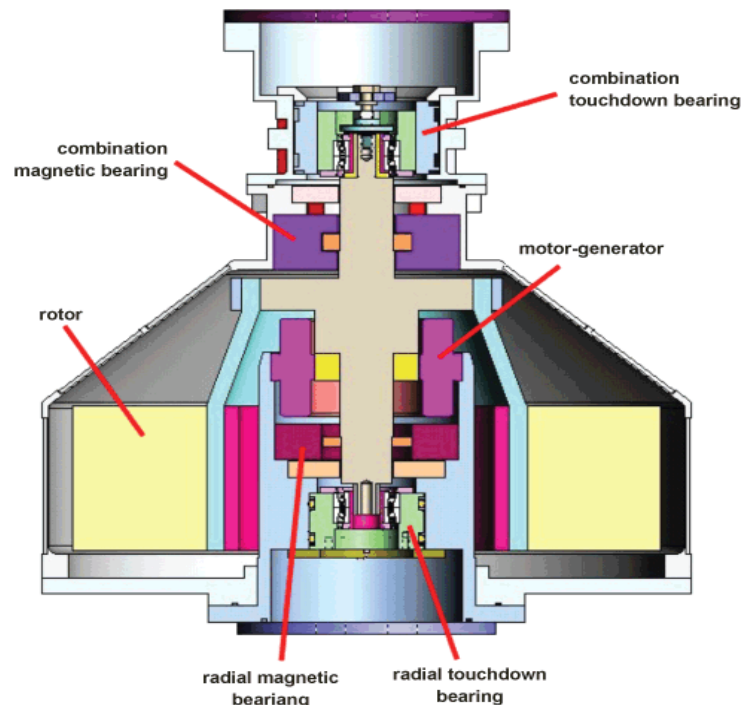


Figure 25: G3 Satellite flywheel energy storage prototype (source “Conical bearingless motor-generators”)

5.3.2 Economical View and Security

The cost of flywheel depends greatly on the technology chosen for the specific application. Slow speed flywheels for use in stationary application are of relatively low cost and a simpler technology, but they are heavy and large, and are not suitable for use in vehicles where space is limited.

High-speed flywheels offer good performance compared to supercapacitors with lower maintenance cost and long life expectancy, i.e. more than a billion cycles. Their high efficiency is up to 85 %, lower than supercapacitors energy storage devices. However, the complexity of high-speed flywheels are extremely high since the construction must be extremely precise with auxiliary controlled precision bearings, the vacuum being contained in

an airtight housing and a cooling system designed to operate in a vacuum. All this complexity dramatically increases the cost of high-speed flywheels, being much higher than supercapacitors.

The materials used in the construction of a flywheel are environmentally friendly and easy to recycle, but there is a danger from high rotation speeds and stresses which could lead to the dangerous disintegration requiring the housing to be designed to withstand any catastrophic failure.

5.4 Technical choice

In selecting a suitable energy storage system to be implemented on-board a ship, size is important, as well as the power and the energy capacity requirements. The energy capacity depends on the limits placed on the storage system operating in full electric mode, the autonomy time, the down time of the on-board generators, etc... In this case, full electric mode is considered when a ship sails into harbour and wishes to minimise exhaust emissions so runs the minimum number of diesel engines.

Storage devices are seen as one method that can be used to optimise the running of diesel generators. The aim of all thermo and electric hybridisation is to reduce the overall marine engines' fuel consumption through controlling the load. The efficiency of diesel engines varies greatly depending on the speed and the load at any given moment. To reduce the fuel consumption of an engine one has to optimise the operation to be as close as possible at all times to the most efficient working point of the engine. It is possible to control the load of an engine in order to optimise its running through the charging and discharging of energy storage systems. In this case, the load of the marine engine is not only a function of the power needs of the vessel, but also the control of the electric power generation and power consumers. Marine engines are rarely used at their best efficiency while manoeuvring or at slow speeds, which increases specific fuel consumption; however, if loading or unloading them with an electrical motor/generator at appropriate times can be implemented this will decrease the overall fuel consumption of the ship.

A good way to size the power of the energy storage system is to consider that the maximum power needed is equal to the maximum electrical power of an on-board generator. In this case, a 12MW generator was considered. A 12MW is enough to operate a ship at speed in full electric mode in harbours. To have an idea of the energy capacity of the storage system we need to make some assumptions.

- The highest energy constraint on the storage system will be in full electric mode while in harbour.
- The electric power requirements (electric propulsion, auxiliaries consumers, etc...) during this phase was considered to be around 4-5 MW for a time of one hour.
- Therefore, the energy capacity of the storage device would have to be around 5 MWh (18 GJ).

In this case, the storage should be able to deliver 12MW and to store 5MWh. This kind power/energy ratio is particularly adapted to the use of batteries, as flywheels and supercapacitors have high power densities, but relatively low energy density. They are able to store 5MWh in a flywheel system or supercapacitors, but would require a storage system of around 1,700 tonnes and the maximum power output would be extremely high.

It can be concluded that the most suitable energy storage solution would be to use lithium high-energy batteries. Their specific power is limited to 3 to 5 times their capacity, but this is not a problem in this case as the maximum power, 12MW, is about 3 times the batteries

capacity, 5MWh. Another advantage is that with these batteries the entire storage device would not exceed 50 tonnes.

In the second case to be studied, the full electric operating mode of the ship is not a requirement, thus, the energy capacity needs would be much lower. In this case, the minimum energy needs of the ship were approximated to about 500kWh, 10 times less than before. This would still require a 170 tones flywheel or supercapacitors system and was considered to be too high. However, using high specific power lithium batteries would weigh around 20 tonnes, which was considered much more acceptable.

The simple case studies and the assumptions just made give an order of the power and energy requirements, but this first approach initially shows that using lithium high specific energy batteries, depending on the power requirements of the ship are the most suitable option to be implemented and will be studied further in this project. Further simulations and case studies will allow the energy storage system specification to be defined more precisely.

5.5 Energy Storage System Model

For the simulation, an equivalent battery model will be used. Many different models of batteries already exist, with high or low levels of detail and precision. For this project, the Partnership for a New Generation of Vehicles (PNGV) model, developed by V.H Johnson, was considered as a suitable choice to base the initial models required for on-board ship applications.

Figure 26 show the PNGV model, which can be used to simulate the performances of Ni-Mh, lead and Li-ion batteries.

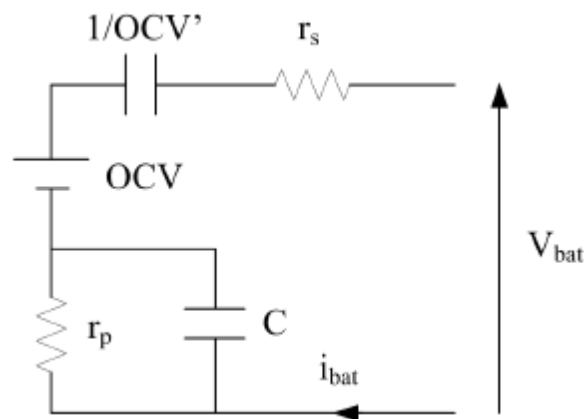


Figure 26: The PNGV model

The model is composed of a RC circuit in series with an open circuit voltage (OCV) and a series resistor (r_s). A second capacity allows the modelling of the open circuit voltage variation in the battery to simulate charging (SOC). The PNGV model has been implemented in Matlab/Simulink software with the value of the equivalent elements of the model being defined by the battery specification from the manufacturer.

5.6 Conclusion on the Energy Storage

At this initial stage of the project, the energy storage solution most suitable for on-board applications is to use lithium high specific energy batteries according to the case studies and modelling performed so far.

Having a high-energy capacity will allow the batteries to operate, most of the time, in low deep discharge at relatively low charge and discharge rates, increasing the life expectancy of the energy storage system.

Of course, the quantity of batteries to use is important, a special secured room would have to be designed with security system in case of fire (no water on lithium batteries) and a good cooling system.

The BMS uses sensors to monitor and control the batteries' states (cell voltage, current, temperature, etc) and will communicate with the global Energy Management System (EMS) of the ship. With the BMS information, the EMS will be able to take decisions on the different on-board energy sources and loads.

6 FUEL CELLS

6.1 Introduction

The fuel cell concept was first developed and demonstrated in 1839, but the technology has not been developed to its full potential due to the popularity of other competing technologies, such as combustion engines. However, with increased fuel costs and serious concerns about the dangers of climate change (Alexander, Allen, Bindoff, & Bréon, 2013) leading to tougher emission regulations, fuel cell development and commercialisation is increasingly popular. Fuel cell exports in 2011 were over 24,600 units (excluding toys and electronic kits), which was a 39% increase on the previous year (Fuel Cell Industry Review 2012, 2012).

The basis of a fuel cell is the conversion of chemical energy from a fuel and an oxidant into electricity and heat without the use of combustion. Various types of fuel are used, all of which are converted into hydrogen through a reformer. Some of the common fuels used for fuel cells are hydrogen, methanol, ethanol and liquid natural gas (LNG). A fuel cell involves an anode, where the hydrogen loses electrons, and a cathode, where the hydrogen ion recombines with the free electrons and oxygen to form water. This process is similar for all fuel cells, although with some differences to the structure and order of the chemical reactions.

The basic operation for a simple fuel cell is shown in Figure 27 and the equations in the cell are shown for the anode (Equation 4), cathode (Equation 5) and overall (Equation 6) (Barbir, 2012).

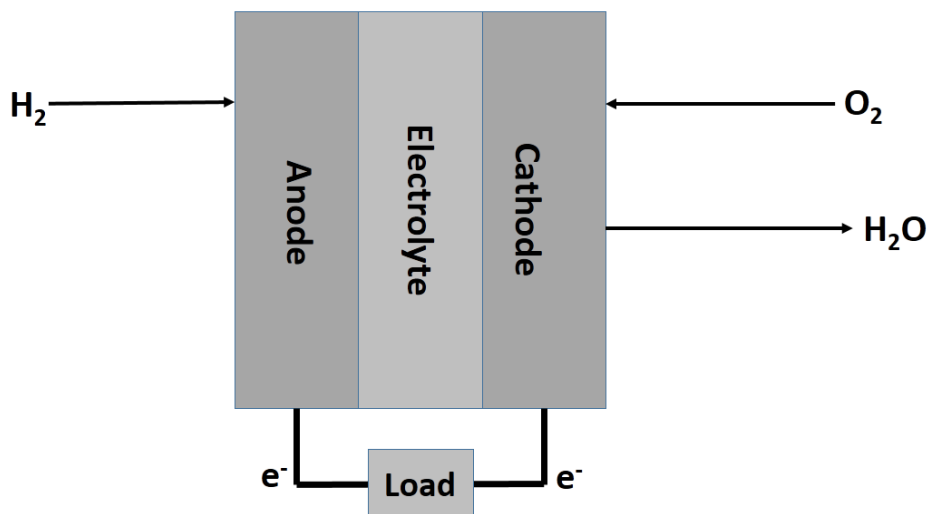
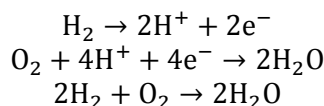


Figure 27: Basic diagram of a fuel cell



Equation 4

Equation 5

Equation 6

Although often referred to as a clean energy storage solution, this is only true if the hydrogen is produced from water by electrolysis using electricity from a renewable source. Although, a reduction in greenhouse gas emission is found when comparing fossil fuels to fuel cells running on hydrogen extracted using energy produced from fossil fuels. Looking at the full infrastructure around a fuel cell, the basic system for a hydrogen fuel cell system, according to IEC 62281-1, is given in Figure 28 (Krewitt, 2007).

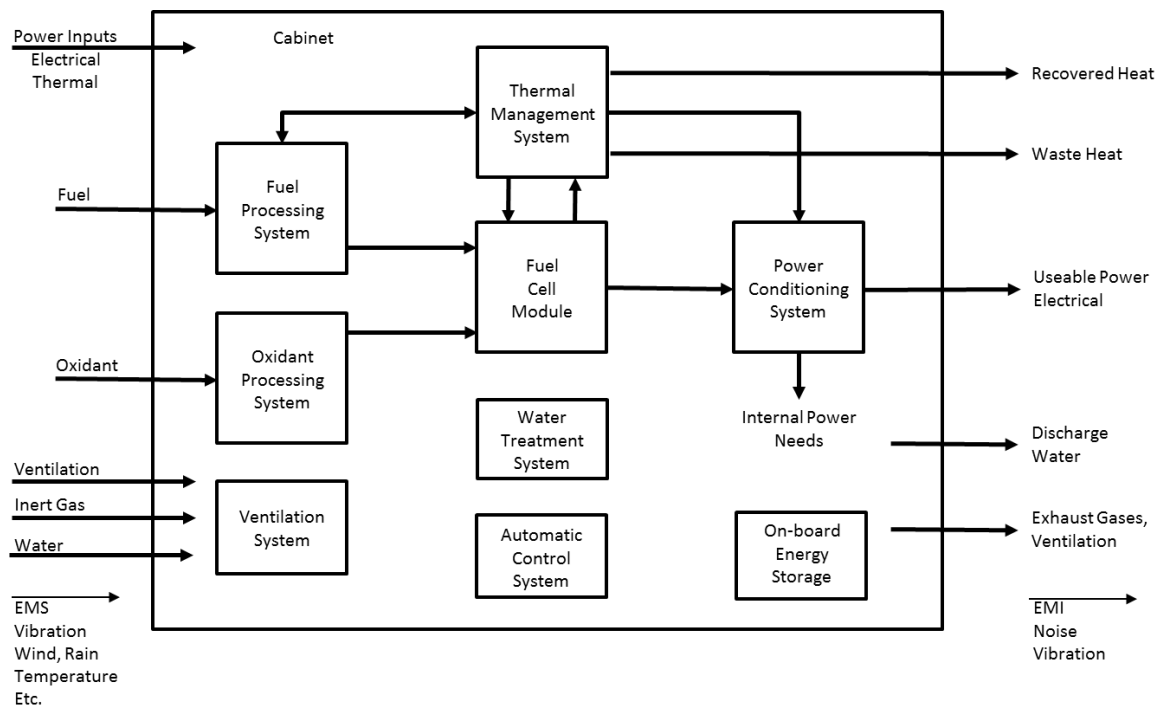


Figure 28: Fuel cell system scheme according to IEC 62281-1

6.2 Types of fuel cell

Fuel cells are defined by a range of different features, normally related to the type of electrolyte used. This can be aqueous, solid or molten, and can be acid, alkaline or pH neutral. The electrolyte could be made of a polymer, chemical substance or ceramic. The type of electrolyte determines the working temperature range of the fuel cell, which in turn determines the materials used in the fuel cell, and thus, the chemical reactions within the fuel cell (Behling, 2013).

6.2.1 Polymer Electrolyte or Proton Exchange Membrane Fuel cells (PEMFC)

These are the most well-known family of all fuel cells, which as their name suggest are based around using a polymer membrane. These are generally used for transport, but they are now being marketed for domestic energy use as well. The development of PEMFC has seen increasing attention from more academic and commercial R&D organisations than all other types of fuel cells combined. There are numerous advantages in using these systems, including high power density, quick start up times and minimal corrosion. When used as a domestic fuel cell in combined heat and power (CHP) systems, PEMFC's have efficiencies in the region of 28% electrical and 50-52% thermal. The lifetimes of the stacks are in the region of 40,000 hours, but require a strictly controlled operating temperature and humidity (Behling, 2013) (INVESTIRE Thematic Network, 2002).

6.2.2 Direct Methanol Fuel Cell (DMFC)

These essentially are PEMFCs where the fuel is methanol instead of hydrogen. The methanol delivers the hydrogen ions to the anode. Many small military, portable and off-the-grid systems use methanol for its easier transportation and storage due to its relatively stable liquid form (INVESTIRE Thematic Network, 2002). DMFC systems have a low efficiency compared to other fuel cells and operate over a working temperature range of 90-120°C.

6.2.3 Alkaline (AFC)

AFC, PAFC, MCFC and SOFC operate using similar electrochemical reactions, which involve the movement of oxide ions. AFCs were the first fuel cells to be used for space applications. As with PEM (PEMFC or DMFC), they run on pure hydrogen and the electrolyte uses potassium hydroxide (INVESTIRE Thematic Network, 2002). The operating efficiency is about 60% over a working temperature range of 90-100°C.

6.2.4 Phosphoric Acid Fuel Cell (PAFC)

PAFC are known as the most mature of the fuel cell technologies. For an electrolyte it uses 100% concentrated phosphoric acid. The operating temperature of these systems is approximately 150-200°C with an operating efficiency of around 40% (INVESTIRE Thematic Network, 2002).

6.2.5 Molten Carbonate (MCFC)

MCFCs operate at temperatures of approximately 650°C in order to keep the electrolyte (carbonated salt) molten. One advantage of this high temperature is that the system can carry out internal reforming of different fuel types without an external fuel processor. However, a major issue with MCFCs is the short service life and high costs (Behling, 2013).

6.2.6 Solid Oxide (SOFC)

SOFCs have the advantage that they are simpler in concept than most types of fuel cell. They are solid state devices with a ceramic electrolyte. With no liquid electrolyte, there are no issues with corrosion or water management. The systems operate at temperatures up to 1,000°C, which has multiple advantages, including high efficiency, internal reforming and high grade heat that can be recovered for other means. These systems range in capacities from 1kW to demonstration projects to the low MW range (Behling, 2013) (New Energy Externalities Developments for Sustainability, 2008).

6.2.7 Overview

PEM type fuel cells may be supplied directly with hydrogen, whereas others can be supplied with natural gas, alcohols or gasoline. It is worth noting that natural gas (called G20 in Europe) has a number of impurities unlike LPG. With G20 during the reforming process in a fuel cell ammonia condenses out and it ends up destroying the reformer unit over time.

6.3 Technology Summary

The following is based on data from the US Department of Energy (US Department of Energy, 2011), from 2011, but it is the most up to date technology summary found during a detailed literature review.

Fuel Cell Type	Common Electrolyte	Operating Temperature	Typical Stack Size	Efficiency	Advantages	Disadvantages
Polymer Electrolyte Membrane (PEM)	Perfluoro sulfonic acid	50-100°C	< 1kW–100kW	60% transportation 35% stationary	<ul style="list-style-type: none"> • Solid electrolyte reduces corrosion & electrolyte management problems • Low temperature • Quick start-up 	<ul style="list-style-type: none"> • Expensive catalysts • Sensitive to fuel impurities • Low temperature waste heat
Alkaline (AFC)	Aqueous solution of potassium hydroxide soaked in a matrix	90-100°C	10–100 kW	60%	<ul style="list-style-type: none"> • Cathode reaction faster in alkaline electrolyte, leads to high performance • Low cost components 	<ul style="list-style-type: none"> • Sensitive to CO₂ in fuel and air • Electrolyte management
Phosphoric Acid (PAFC)	Phosphoric acid soaked in a matrix	150-200°C	400 kW 100 kW module	40%	<ul style="list-style-type: none"> • Higher temperature enables CHP • Increased tolerance to fuel impurities 	<ul style="list-style-type: none"> • Pt catalyst • Long start up time • Low current and power
Molten Carbonate (MCFC)	Solution of lithium, sodium, and/or potassium carbonates, soaked in a matrix	600-700°C	300 kW-3 MW 300 kW module	45-50%	<ul style="list-style-type: none"> • High efficiency • Fuel flexibility • Can use a variety of catalysts • Suitable for CHP 	<ul style="list-style-type: none"> • High temperature corrosion and breakdown of cell components • Long start up time • Low power density
Solid Oxide (SOFC)	Yttria stabilized zirconia	700-1000°C	1 kW–2 MW	60%	<ul style="list-style-type: none"> • High efficiency • Fuel flexibility • Can use a variety of catalysts • Solid electrolyte • Suitable for CHP & CHHP • Hybrid/GT cycle 	<ul style="list-style-type: none"> • High temperature corrosion and breakdown of cell components • High temperature operation requires long start up time and limits

Table 10: Fuel cell data from the US Department of Energy (US Department of Energy, 2011)

6.4 Lifetimes

NAREC has carried out an extensive market study of small fuel cell systems, which are generally PEM based (PEMFC or DMFC). These usually have lifetimes in the region of 4,000 hours (as opposed to larger stationary systems which have lifetimes of 40,000 hours).

As described in the FellowSHIP (Fuel Cells for Ships) project, it demonstrated a marine application for an MCFC system which ran for 18,500 hours up to the end of Phase II of the project. Phase III has now begun.

SOFCs are known for their short lifetimes, with many research projects currently underway to increase longevity of systems.

The general approach for dealing with the short lifetime is to have a hybrid system. The fuel cell will run most efficiently when on full power for short periods, recharging a battery system connected to a fuel cell. The fuel cell will recharge the battery every so often, running at maximum power. The battery can then be used as a source of variable power, following the peaks and troughs in demand.

6.5 Hydrogen Systems Hierarchy of Legislation

A range of legislative documents are available providing guidelines for the operation, installation, maintenance and final disposal of fuel cells. One of the most relevant documents is "Rules for Classification and Construction VI Additional Rules and Guidelines: Guidelines for the Use of Fuel Cell Systems on Board of Ships and Boats" by Germanischer Lloyd Aktiengesellschaft. This is currently the only specific guide for the installation and operation of fuel cell systems on marine vessels. The majority of current fuel cell demonstration ships use this guide.

With regard to safety, it is important to consider the implications for fuel cell systems in standards related to explosive atmosphere, such as ATEX 137 (1999/92/EC), further safety conditions can be found in ISO standards such as ISO TR 15916:2004.

Finally, but most importantly, IEC 62282-2 should always be considered, which gives the minimum requirements for safety and performance of fuel cells.

6.6 Future possibilities

FP7 projects such as ORECCA (Off-shore Renewable Energy Conversion platforms - Coordination Action) have looked in detail at floating islands generating energy from multiple renewable sources (wind, wave and tidal). One possibility is the use of these offshore generating platforms to produce hydrogen through large hydrolysers to store the energy, which could then be used to refuel fuel cell based ships.

6.7 Conclusion

Fuel cell systems are being demonstrated on ships, with the FellowSHIP project as the largest example relevant to INOMANS²HIP. However, the systems are still comparatively small compared with the scale of a cargo ship engines. In order to extend the lifetime of a fuel cell, it is necessary to use a hybrid system with batteries, occasionally being charged from fuel cell.

Following the same logic as employed by the FellowSHIP project, it seems sensible to look in details at MCFC devices for part of the contribution to the energy system within INOMANS²HIP.

7 SOLAR POWER GENERATION

7.1 Introduction

Task 1.1 explored the various issues with photovoltaics (PV) on ships, as given in deliverable D1.1. It showed that there are numerous examples of PVs being used in the marine environment, including the Auriga Leader, Solar Sailor, Sun 21 and TuranorPlanetSolar. The largest PV array on an ocean going vessel is the 100kWp system on the TuranorPlanetSolar. Clearly, in the marine environment there are issues with corrosion, as well as the added complexity of having the PV on a moving object, so solar resource will be varying at a much higher rate than that for a stationary system.

This work package focuses on the electrical model, but, imperative for the work in WP2 and WP4, the exact energy yields along particular routes have to be considered. Therefore NAREC will also discuss the yield calculators. These will not be of any use until the type of ship and operational profile are defined for this project. At which point exact solar yields can be modelled.

From the work in WP1, it has been decided that standard silicon modules which have been tested to Level 6 of the IEC 61701 standard “Salt Mist Corrosion Testing of Photovoltaic (PV) Modules” will be used. Modules such as these are a well-established technology which has been used in numerous marine applications.

There are numerous existing models for photovoltaic systems which are used within academia and industry. These include software packages and online systems such as PSPICE, PVSyst or PVGIS. The issue is that these models are for stationary systems; this model must take account of the movement of a ship, with varying irradiance and very quickly moving shadows.

7.2 Defining the Photovoltaic Model

The full model NAREC intend to use, which will be fully developed in WP2 and WP4, has a detailed and complex yield calculator to take account the fact the ship is a moving object, both in its operational profile and the movement due to waves.

The model will be split into three distinct parts. These are:

1. **Irradiance model:** to calculate the levels of irradiance at a specific time and position of the ship
2. **Shading model:** to calculate the self-shading created by the ship at a particular time and position
3. **Electrical model:** to calculate the energy output and other factors from the PV system according to information from the shading and irradiance model.

Further models which would be “nice to have” would be:

- Pitch and role model
- Particulate data model

Additionally, there is the predicted change in global and local irradiance due to climate change, i.e. specific weather conditions.

The majority of modelling on INOMANS²HIP is based around Matlab/Simulink and GES models. However, the shading model will be written using Ruby script, to interface with the shading capabilities of Trimble SketchUp (formerly Google Sketchup).

The yield sides of the whole PV model will be discussed next.

7.2.1 Irradiance Model

There are numerous issues to consider with irradiance levels. These include:

- Weather cycles (El Nino, La Nina, etc...)
- Brightness of the sun (varies by 0.1% over a ~10.7 year period)
- Air mass
- Atmospheric Particulates
- Time of year
- Time of day

The data for irradiance is to be taken from Meteosat. This dataset covers a 20 year period, with the earth split into 0.03" x 0.03" grids, with irradiance levels for every hour. This is based on satellite data for irradiance at the edge of the Earth's atmosphere, collated with weather data.

For the model, an average year is to be created. This will take the average irradiance for each 0.03" x 0.03" square for each hour of the year, creating an average for each average of the base year.

It is important to note that irradiance levels are changing. For example, laws on particulates emissions in Europe have increased levels of irradiance, whereas the increasing industrialisation within Asia has led to lower irradiance levels. At the same time, climate change is causing changes in cloud and precipitation, and hence irradiance levels are also affected.

This model, which is to be written in Matlab, will use a look up table of this average year, to give the level of irradiance for whatever position and time the ship is at.

7.2.2 Shading Model

Shading will cause a lowering of the output of the system. As a module becomes shaded, bypass diodes will ensure the module is not used, so that it does not end up effectively consuming energy "dark current".

This model is to use the package "Trimble Sketchup" which is a free package originally created by *@Last Software*, and now owned by Trimble. This allows for shading analysis to be performed on geometrical models, with a time, longitude and latitude being defined. Sketchup can be programmed using the scripting language Ruby.

Sketchup can read models from other packages in a number of formats, including dxf,dwg, 3ds Collada and STL. For this work NAREC chose the open source format Collada to be used.

The essential idea for this package is that the shading will be calculated for the position of a ship to the centre of each 0.03" x 0.03" degree square for each hour. The surface of the ship will be divided into a grid of 0.1m x 0.1m squares. Each one will record if it is shaded or not.

If there is shading on >50% of a module, then the module will be turned off. The information on active and inactive modules will then be fed back into the electrical model.

The electrical part, which is the focus of WP3 will be explained in the next section.

7.3 Electrical Model

As with the next section discussing wind power options, it is important to have a quick basic model to try different solutions for the photovoltaic system, and a larger more complex model setup when various basic assumptions, such as the type of ship, have been finalised. Currently the ship is not known; hence a highly complex model has been designed by NAREC, which can be modified when the reference ship is known.

This model is to be built using Matlab/Simulink. The photovoltaic electrical model will interface with the two yield models. The irradiance model will inform how much energy each module can deliver, whilst the shading model will decide if a module is active, or if it is bypassed by a bypass diode.

Ultimately, a photovoltaic cell is simply a p-n semiconductor junction, which when exposed to light produces a current proportional to the exposed light intensity. Therefore, an equivalent circuit can be designed using resistors and diodes.

Within this basic model, the output current from the cell is proportional to the light falling on it, the photocurrent (I_{ph}). Assuming the system is not connected (due to the usage of a bypass diode) when shaded it will not be an active device, however, if connected to an external supply it will generate a current I_D known as the dark current.

There are numerous equivalent circuits of increasing complexity and accuracy, which can be used; these are the general model, the double exponential model, the appropriate model and the simplified model as shown in Figure 29.

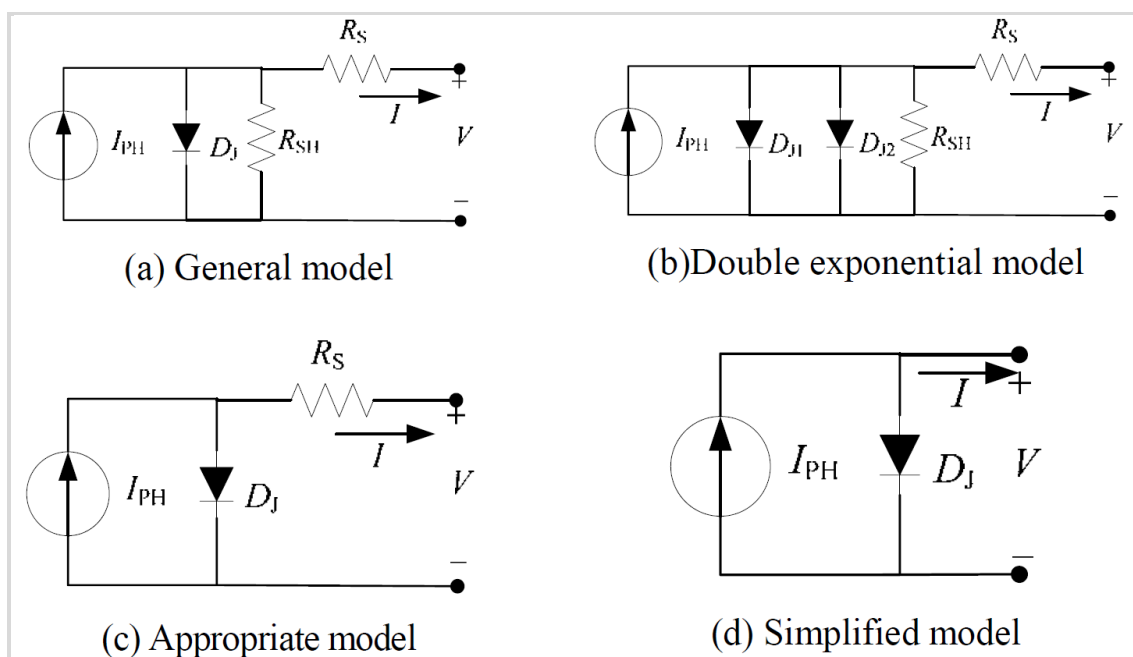


Figure 29: Types of equivalent circuit for a photovoltaic cell from

For model (a) the circuit can be represented by Equation 7

$$I = I_{PH} - I_S \left(e^{\frac{q(V+IR_S)}{AKT}} - 1 \right) - \frac{(V + IR_S)}{R_{SH}} \quad \text{Equation 7}$$

Where:

I_{PH} =Photocurrent ;

I_0 =Cell saturation Dark Current

q =electron charge ($1.6 \cdot 10^{-19} \text{C}$)

k =Boltzmann constant ($1.38 \cdot 10^{-23} \text{JK}^{-1}$)

T_C =Cell's working temperature

A =Ideality factor (1.2 for monocrystalline silicon and 1.3 for polycrystalline silicon)

R_{SH} =shunt resistance [Ω]

R_S =Series Resistance [Ω]

The photocurrent's main dependencies are on the solar irradiance and the temperature of the cell so can be calculated approximately;

$$I_{PH} = [I_{SC} + K_1(T_C - T_{Ref})]\lambda \quad \text{Equation 8}$$

Where;

I_{SC} =cell's short circuit current under standard test conditions (25°C and $1\text{kW}/\text{m}^2$)

K_1 =cell's short circuit current temperature

T_{Ref} =Cell's reference temperature

λ =irradiance [kWm^{-2}]

In turn, the saturation current varies with the cell temperature, which can be described by;

$$I_S = I_{RS} \left(\frac{T_C}{T_{Ref}} \right)^3 e^{\left[\frac{qE_G \left(\frac{1}{T_{Ref}} - \frac{1}{T_C} \right)}{kA} \right]} \quad \text{Equation 9}$$

Where;

I_{RS} =Cell's reverse saturation current at standard test conditions

E_G =Band gap energy of the semiconductor (in this case, silicon)

More detailed descriptions can be used for photovoltaic cells, such as the double exponential model. However, this model is far more complex to derive equations for an IV curve.

A simpler model as if the shunt resistance R_{SH} is removed, which has a negligible effect on the efficiency of a photovoltaic cell, especially compared against the series resistance R_S . This leaves the voltage current equation simplified from Equation 7 to;

$$I = I_{PH} - I_S \left(e^{\frac{q(V+IR_S)}{AKT}} - 1 \right) \quad \text{Equation 10}$$

The system can be simplified further as if the series resistance is zero. However, this is not realistic of the systems this project will be considering'

$$I = I_{PH} - I_S \left(e^{\frac{qV}{AKT}} - 1 \right) \quad \text{Equation 11}$$

For this work, the appropriate model (c) will be used. It is important to state that for this model, the typical values provided on an information sheet with any new PV system can be used to derive the appropriate parameters.

Maximum Power	(P _m)
Voltage at Maximum Power	(V _m)
Current at Maximum Power	(I _{sc})
Short circuit current	(V _{oc})
Open circuit current	(B)
Temperature coefficient of open circuit voltage	(α)
Temperature coefficient of short circuit current	
Temperature coefficient of power at normal operating cell temperature	

This means that by using readily available data numerous systems could be tested if it is deemed necessary by the project leader for INOMANS²HIP.

7.3.1 Simple Model

NAREC has created a simple MS Excel model to create IV curves based on the above equations. This can be used for quick calculations while the type of ship, and, thus, the photovoltaic configuration, are unknown. The Excel sheet model can be used to also find the effects of shadows on a module, with or without bypass diodes.

The two below screenshots are IV curves generated by the excel model.

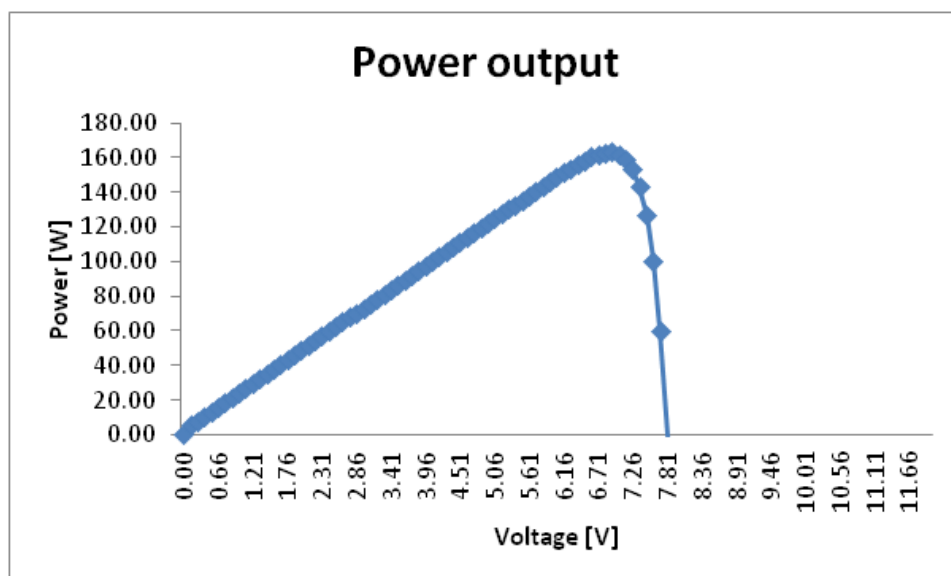


Figure 30: Power output from NAREC's excel based PV simulator

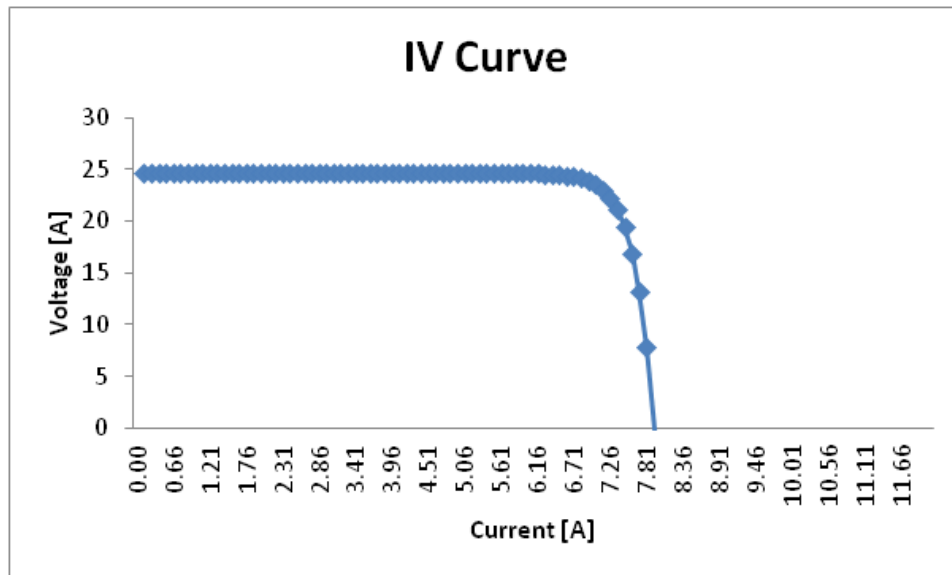


Figure 31: IV curve from NAREC's excel based PV simulator

7.3.2 Simulink/Matlab Models

NAREC have carried out work on a Simulink model which follows the same mathematical basis as the above models. However, this model could be interchanged with others in the peer reviewed literature without any great difference. Several models are shown below, including that produced by NAREC. The major parts that are innovative within this project with relation to PV will be the yield and shading calculators. If it is felt necessary, NAREC will expand their PV model to become more refined than that in the literature, especially if any issues are found with the interaction between the electrical and yield components.

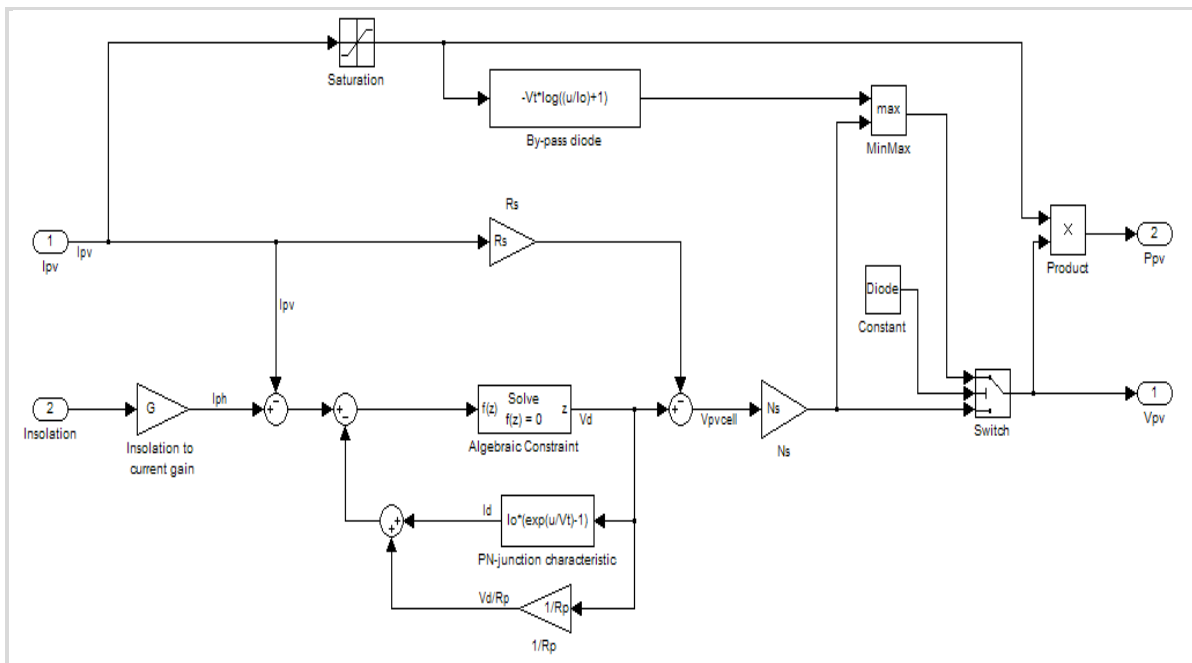


Figure 32: Model produced by the University of Colorado (5)

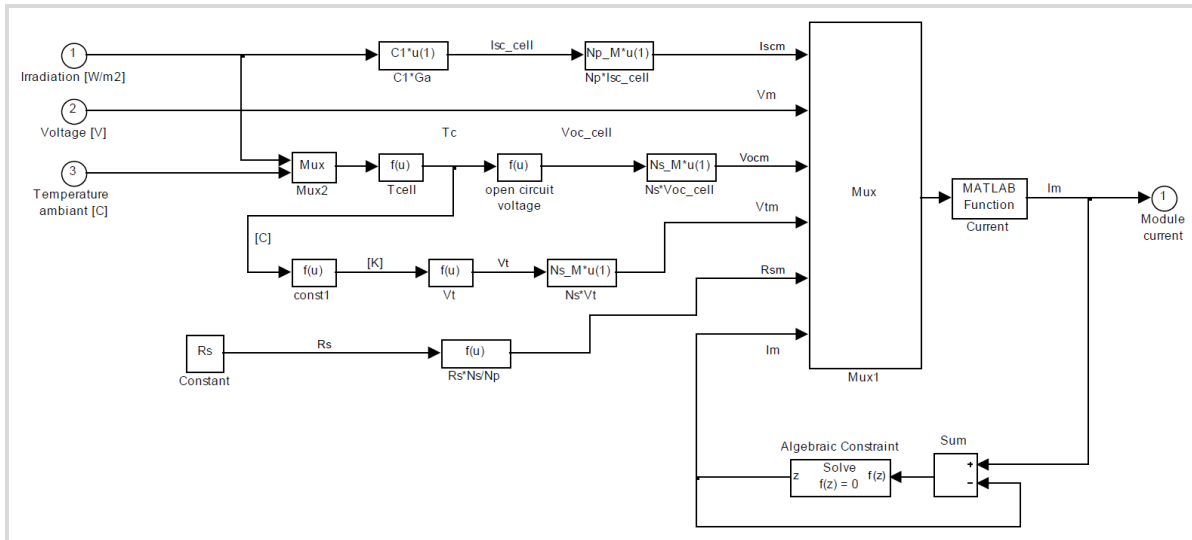


Figure 33: Model produced by Risø National Laboratory(3)

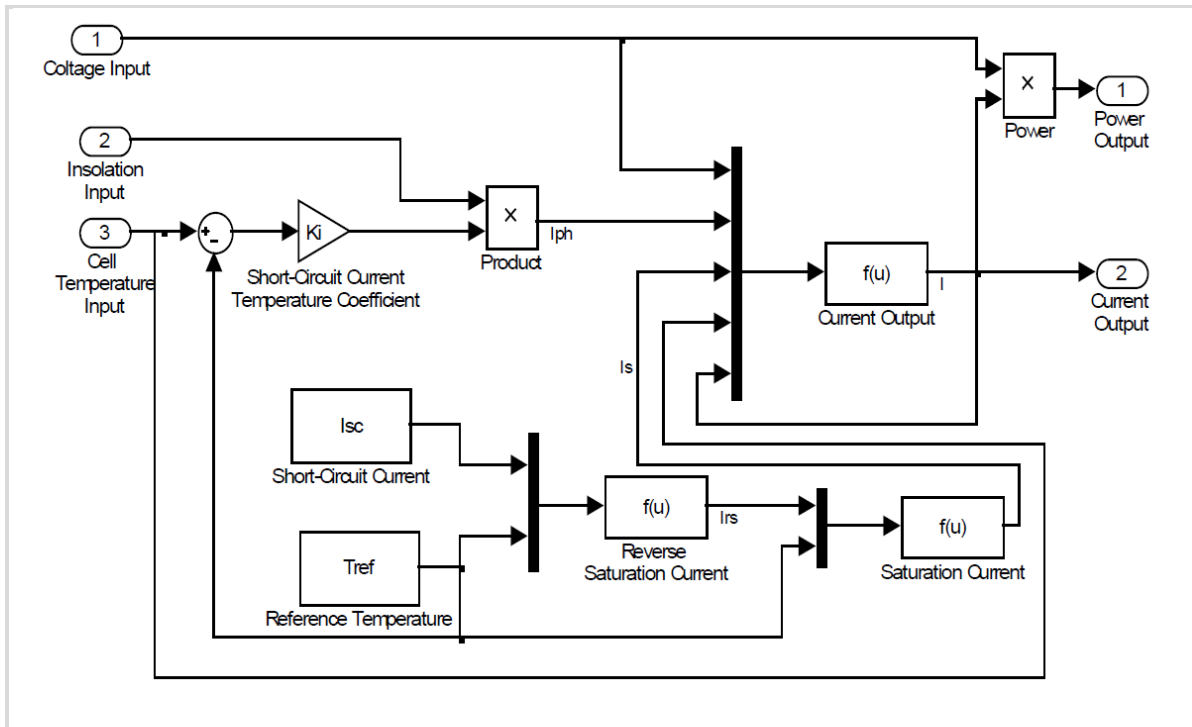


Figure 34: Model produced in (1)

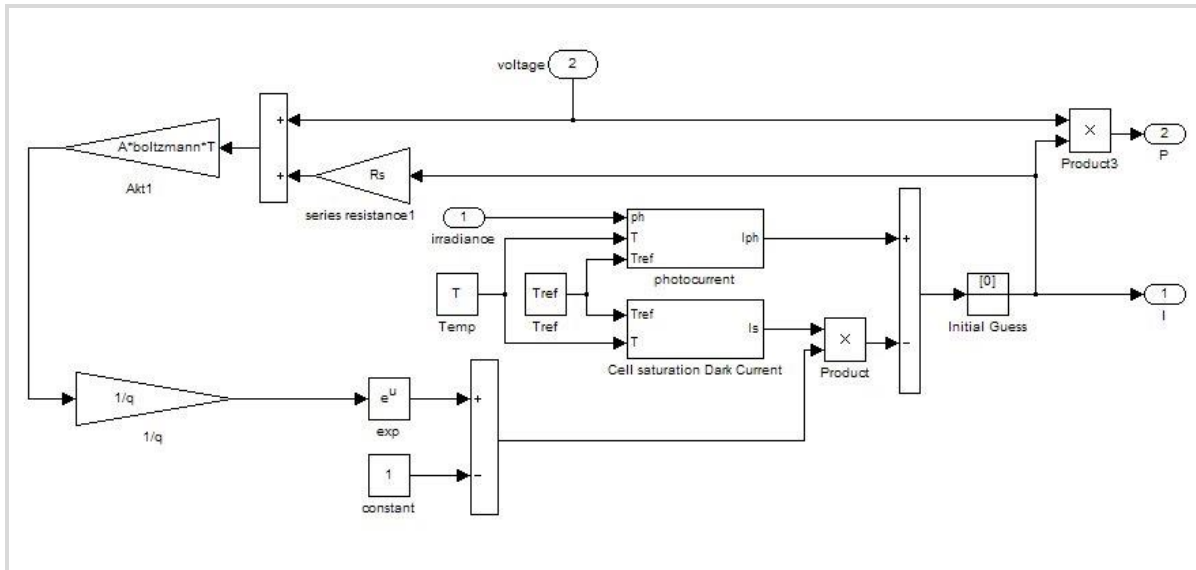


Figure 35: NAREC IV model of a photovoltaic cell

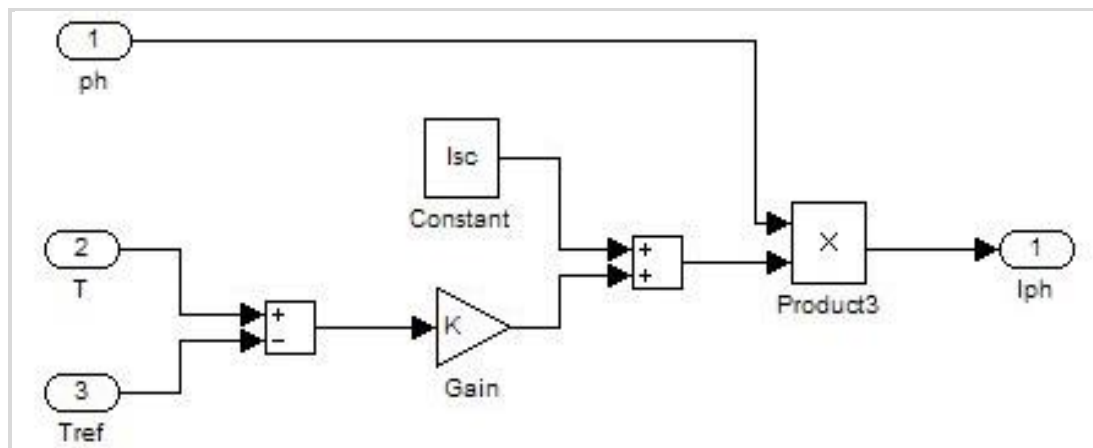


Figure 36: Photocurrent subsystem

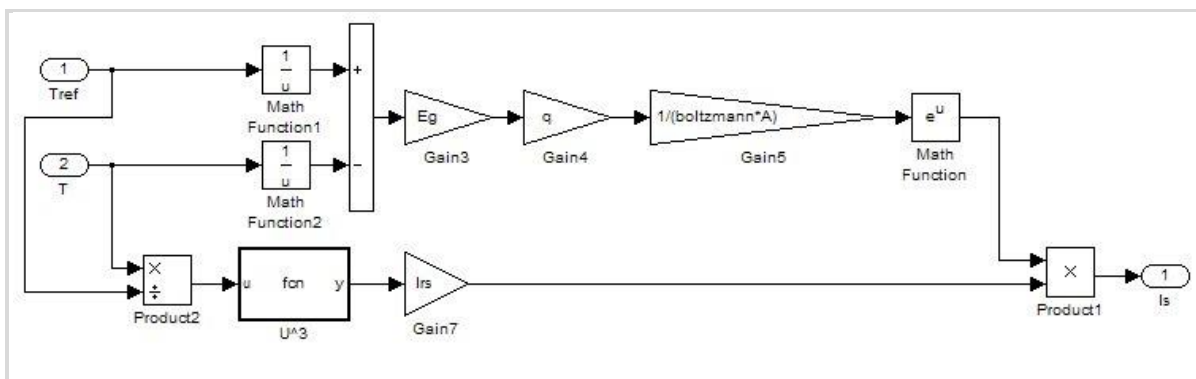


Figure 37: Cell Saturation Dark Current Subsystem

7.4 Solar Power Generation Conclusions

This part of the report has looked at the production of the photovoltaic part of the INOMANS²HIP simulation. This particular work package is focusing on the electrical side of the work, but is connected to the detailed plans for the yield calculator, which is currently under production. NAREC have produced a basic Excel calculator for photovoltaic cells, and a Matlab/Simulink based model. It was recognised that there are a number of Matlab/Simulink models of PV cells, which all work according to the same basic physics and

equivalent circuits. There is no preference at this present time for NAREC's model or any other that currently exists, the decision for this will be made after further investigation of the models to determine which works best with the varying output of the yield modules in the other work packages.

NAREC also recommends that crystalline silicon cells are used. The reasons for this are that crystalline silicon photovoltaic modules:

- Have a high efficiency against surface area
- Numerous commercial makes tested against saline conditions (ISO 61701)
- Do not degrade over time to the same level as thin film
- Reasonably priced commercial product
- Well developed and understood technology
- Already used on various marine PV applications

8 WIND POWER GENERATION

8.1 Introduction

WP1 looked in detail at the various issues with wind turbines on ships. To summarise the results of this Work Package, there are numerous issues with wind turbines on ships. From a physics point of view, the force diagram for a wind turbine on a ship is a complex problem, and a case must be avoided where the engines are doing extra work because of drag on a wind turbine, which will mean ultimately there is no real energy generation, just an illusion. This needs very careful consideration. Other issues, as specified before, are with the wind speed in the frame of reference of a ship being dependent on the ships movement and the wind direction. Ultimately, from a force diagram point of view, wind turbines on ships do not make sense in a situation where the ship is moving. However, they may be useful for times when the ship is stationary, such as when loading/unloading cargo. This means the wind turbine should be retractable in some way, so it does not create additional drag on the ship when it is moving.

This part of WP3 looks at the complexity of developing a wind turbine model for INOMANS²HIP. It looks at a turbine model developed by NAREC.

For the model, something needs to be created which is general enough to allow multiple wind turbine types to be tested. Anything too specific will mean trying out numerous turbine types would be time consuming, but anything too simple would mean the model would not be of any use for the energy management of the ship.

The model, developed by NAREC, is for a small synchronous generator based system rated at around 7.5kW output. The model uses the swept area, which means for the sake of simulation they can represent either horizontal or vertical axis. Vertical axis turbines will have the additional issue of start motors, which can be assessed through a detailed look through the results of Encraft wind study.

8.2 Wind Turbine Modelling Overview

A wind turbine is a complex device to model. This project has taken two approaches to modelling wind turbines, one very simple and easily configurable, the other more complex, but more difficult to configure.

In order to understand modelling of wind turbines, it is first important to consider the basic elements of a turbine. Figure 38 shows a cut away of a basic wind turbine. This can be divided into three discrete parts;

- Aerodynamic portion (transfer of the power in the wind to mechanical energy)
- Gearbox (transferring the mechanical energy from the turbine to the generator rotor)
- Generator (converts the mechanical energy of the rotor into electrical energy)

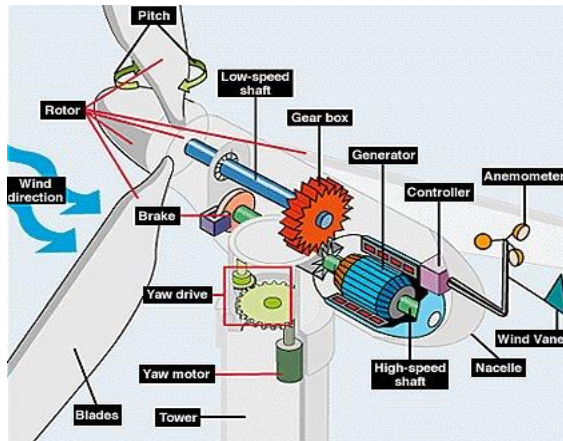


Figure 38: Simplified diagram of the workings of a wind turbine

For this work, the two models of the wind turbines have been created in Matlab/Simulink. This is partly due to the expertise of the partners in this project, and partly because this allows for feedback between different modules in the turbine model.

Various papers on Simulink/Matlab models of wind turbines exist. For example, a good explanation of wind turbine models given compares three different simulations of wind turbines, to find ways in which the processing speed can be improved upon. Other models in the literature included used a similar mathematical construct of S-functions to the

third model to simulate a doubly fed induction generator. Using S-functions requires the code to be written directly with real time C as opposed to the visual block method within Simulink. Although this does lead to a far more efficient piece of code, it does add an extra level of complexity to the construction of the model when compared with using Simulink blocks. Other papers focus on matrix transformations initially, to move into the natural coordinate system of the rotor and stator via a Clarke transformation, before manipulating the mathematics into the S-structure of C-MEX files to use within Matlab. Detailed explanations of the effects of generator inductances of a doubly fed induction generator's dynamic response when experiencing a fault can be found in several papers. Simulink/Matlab models also exist, whereby a single wind turbine is working in conjunction with either a fuel cell or a diesel generator.

The most detailed methodology found in the literature was that of the PhD thesis of Pedro Rosas from the Ørsted Institute in 2003. This model used Matlab/Simulink to simulate an aggregate wind farm model, and it goes into significant depth on the simulation of wind, with specific reference to the turbulence undergone from other wind turbines. As with other wind turbine models comparisons were made against real turbine systems, using real wind data in the model. This showed good agreement between the model and real turbines.

The above literature all use similar, but slightly different methods for the simulation of wind turbines. A further look through the literature shows many slightly different ways to simulate synchronous and induction generators, but the essential methodology of splitting the system into wind/turbine/grid components, and attempting most calculations in the natural reference frames of the rotor and stator, is constant. A detailed explanation of d-q reference frames as used in much of the above literature can be found.

The majority of the above examples also use the basic P_{mech} as given in Equation 17. Obvious differences do exist, for example, in how the wind component is calculated. Whilst used a three component method for the wind with a ramp and sinusoidal component on top of the base line, use a four component method made up of the baseline, ramp, gust and noise components. More complex methods of simulating the wind speeds are necessary when considering wind farms, in which the turbulence due to the proximity of other wind turbines must be considered.

$$P_{mech} = \frac{1}{2} \rho A C_P V_T^3 \quad \text{Equation 12}$$

Where;

P_{mech} = mechanic power [W]

ρ = air density [kg m^{-3}]
 A = area swept by turbine [m^2]
 C_p = power coefficient
 V_T = velocity of air [ms^{-1}]

8.3 NAREC's Wind turbine model

8.3.1 Introduction

Following a large portion of the literature, the basic structure for a simulation, is split into three separate interacting components. These are:

- 1 Aerodynamic
- 2 Gearbox
- 3 Generator

The interactions between these components are shown in Figure 48.

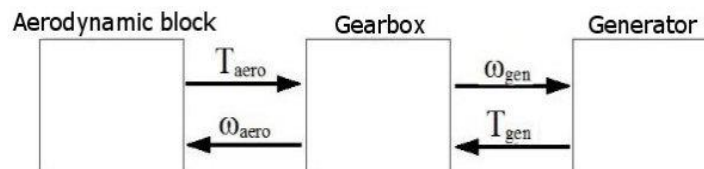


Figure 39: Three blocks of the Simulink wind turbine

A brief description of each block is given below:

- 1 **Aerodynamic:** Takes the wind speed data, alters it to take account of the differing height between the wind recorder and the turbine hub height, calculates the tip speed ratio and coefficient of performance, then from this calculates the mechanical power and thus, the mechanical torque. This also includes optional considerations of wind shear and tower shadow influences.
- 2 **Gearbox:** Uses the mechanical torque from the Aerodynamic block along with predetermined information on the damping, stiffness and moment of inertia of the device to calculate the angular velocity which the generator will receive. This also feeds back the new mechanical angular velocity into the Aerodynamic block.
- 3 **Generator:** Takes the angular velocity from the gearbox and translates this into an active and reactive power output. This block feeds electrical torque back into the gearbox. The generator has internal controls so that it activates when the gearbox is running above synchronous speed, and also has controls to cut out if the wind speeds are either too high or too low.

The advantage of setting out the model into discrete blocks is that various functions can be substituted for improved versions when developed, allowing for continuous improvement of the model once the basic structure is in place.

8.3.2 Aerodynamic Block

The aerodynamic block takes wind speed data from a spread sheet of wind speeds, which for tests NAREC used data derived from Met Office data, and translates these into torque via a basic aerodynamic model. This block takes account of the difference in height between the wind speed recorder and turbine hub, and the local terrain, to give an accurate wind speed

acting on the blades. Alternatively, there is an option to simply have a constant wind speed. Two options have been created for simulating the power coefficient, as have blocks offering the ability to read a manufacturers power curve fed into the turbine, additional options include having a variable or fixed blade pitch. The majority of advanced options can be turned off, hence allowing the model to simulate a turbine with the maximum available information.

8.3.2.1 Torque Calculation

To translate wind speeds into torque, first begin with the formula for kinetic energy;

$$KE = \frac{1}{2}mv^2 \quad \text{Equation 13}$$

Where; m =mass [kg] and v =velocity [ms^{-1}]

Now, consider the mass of air hitting the blades per second.

$$m_{sec} = A\rho v \quad \text{Equation 14}$$

Where; A =projected area [m^2], m_{sec} =mass of air hitting per second [kg s^{-1}] and ρ =density of air= 1025 kg m^{-3}

Substituting Equation 13 in Equation 12 gives the energy per second, i.e. the power;

$$P = \frac{1}{2}\rho Av^3 C_p(\beta, \lambda) \quad \text{Equation 15}$$

Where; C_p = power coefficient.

Within the model, there are two options for inputting wind speed. A constant wind speed can be selected for simple tests, or real data can be inputted into Matlab as an excel spreadsheet as shown in Table 11;

T	v
0.01	5.8
0.02	5.6
0.03	5.4
0.04	5.2
0.05	5.3
0.06	5.1

Table 11: Example of model input data

The T-column is interpreted as seconds, whilst the v-column the velocity of the wind as ms^{-1} . The model uses a 1D look up table to interpolate between data points, as wind speed data is unlikely to be of the time resolution required for a three phase current output.

The wind speed options are controlled by a small masked block centred on a switch. In order to prevent Simulink searching for a non-existent matrix when constant wind speed is selected, the following code was inserted into the mask;

```

maskStr = get_param(gcb, 'MaskValues');
% Check the "Data from spreadsheet" is selected in the pop-up
if strcmp(maskStr{1}(1), 'D'),
    % Set the disable the wind speed box
    set_param(gcb, 'MaskEnables', {'on'; 'off'; 'on'; 'on'; 'on'; 'off'}),
        set_param(gcb, 'MaskVisibilities', {'on'; 'on'; 'on'; 'on'; 'on'; 'off'
' })),
    % Put spreadsheet data into a matrix
    wind_data = data,
else
    % Enable the wind speed box
    set_param(gcb, 'MaskEnables', {'on'; 'on'; 'on'; 'on'; 'on'; 'off'}),
        set_param(gcb, 'MaskVisibilities', {'on'; 'on'; 'on'; 'on'; 'on'; 'off'
' })),
    %Create dummy wind speed matrix to avoid crashing Simulink
    wind_data = [1,2;3,99999],
end

```

In order to conserve memory, if a wind speed data matrix has been inputted into the model, it will be wiped when “constant wind speed” is selected. Note, that if there is no matrix of wind data uploaded into Simulink, then an error will be displayed by Simulink if the spread sheet option is selected in the mask.

8.3.2.2 Power Coefficient Calculation

The power coefficient (C_p) is a measure of how much energy is extracted from the wind, against that which is actually available. The maximum value of C_p , known as the Betz limit, is 0.5929. However, in practice this will be closer to 0.4. In the literature, there are two approaches taken to calculating C_p with regard to wind turbine simulations. The first option is to use the data from a manufacturer and simply read off the value of C_p against tip speed ratio, which if the turbine has been subjected to independent testing will be a perfectly reasonable approach to take. The other option is to simulate the curve. With this model, both approaches have been implemented.

Two different but similar simulation methods have been made for this model, which vary in complexity and the level of information about the turbine required.

Method 1:

This methodology is similar to the approach used in the non-real time wind turbine block within SimPowerSystems.

Initially, take the tip speed ratio λ ;

$$\lambda = \omega_T \frac{R_T}{u} \quad \text{Equation 16}$$

Where;

ω_T =angular velocity of wind turbine blades [rad s⁻¹]
 R_T =radius of wind turbine [m]
 u =wind velocity [ms⁻¹]

Both the tip speed ratio and pitch angle β together give the value of λ_i ;

$$\frac{1}{\lambda_i} = \frac{1}{\lambda + b_1\beta} - \frac{b_2}{\beta^3 + 1} \quad \text{Equation 17}$$

Where;

$b_1=0.008$
 $b_2=0.035$

This in turn is used to calculate the power coefficient;

$$C_p(\lambda_i, \beta) = c_1 \frac{c_2}{\lambda_1} - c_3\beta - c_4 e^{\frac{-c_5}{\lambda_i}} \quad \text{Equation 18}$$

Where;

$c_1=0.22$
 $c_2=116$
 $c_3=0.4$
 $c_4=5$
 $c_5=12.5$

Method 2:

A similar but extended version of the methodology above is used in, where the power coefficient and λ_i are given as;

$$C_p(\lambda_i, \beta) = c_1 \frac{c_2}{\lambda_i} - c_3\beta - c_4\beta^{c_5} - c_6 e^{\frac{-c_7}{\lambda_i}} \quad \text{Equation 19}$$

$$\frac{1}{\lambda_i} = \frac{1}{\lambda + b_1\beta} - \frac{b_2}{\beta^3 + 1} \quad \text{Equation 20}$$

The variables used for the coefficients c_1 to c_7 and b_1 to b_2 are given as follows for constant and variable speeds;

	c1	c2	c3	c4	c5	c6	c7	c8	c9
Constant Speed	0.44	125	0	0	0	6.94	16.5	0	-0.002
Variable Speed	0.73	151	0.58	0.002	2.14	13.2	18.4	-0.02	-0.003

Table 12: Coefficients for C_p calculations as given in Sloodweg et al.

8.3.2.3 Manufacturer's Data

Some wind turbines may come with the performance curve already calculated, in this case then there is the option for the model to read this from a table and use the manufacturer's data. The data has to be inputted into Matlab as a spread sheet. Manufacturer's data may be for either a constant blade pitch angle, or a varying one. To allow for this a nested "if"

loop was created to choose between the three options, with both a 1D and 2D look up table. Both lookup tables are capable of interpolating between points. The calculation as used in Method 1 is kept out of the actual IF block, as Simulink has issues with “From” and “Goto” blocks within “if” loops. As with the wind speeds, two small dummy matrices are created in the data mask so Simulink does not request a non-existent matrix. In order to conserve memory the mask wipes the matrix not currently in use. The two pieces of code are shown below;

```
maskStr = get_param(gcb, 'MaskValues');
if strcmp(maskStr{1}(1), 'C'),
    % If Calculate is selected, hide the 1D or 2D option
    set_param(gcb, 'MaskVisibilities', {'on'; 'off'; 'off'; 'off'});
    % Wipe the two data matrices of
    % Cp and replace with dummy matrices
    tip_speed_data_2D = [1,10,27;15,27,58;94,95,99];
    tip_speed_data_1D = [1,10;15,27];
else
    % Allow the second option to be visible
    set_param(gcb, 'MaskVisibilities', {'on'; 'on'; 'off'; 'off'});
end
- - - - -
maskStr = get_param(gcb, 'MaskValues');
if strcmp(maskStr{1}(1), 'Y'),
    % If a 2D matrix is selected, replace
    % the 1D matrix with a dummy matrix
    tip_speed_data_1D = [1,10;15,27];
else
    % If a 1D matrix is selected, replace
    % the 2D matrix with a dummy matrix
    tip_speed_data_2D = [1,10,27;15,27,58;94,95,99];
end
```

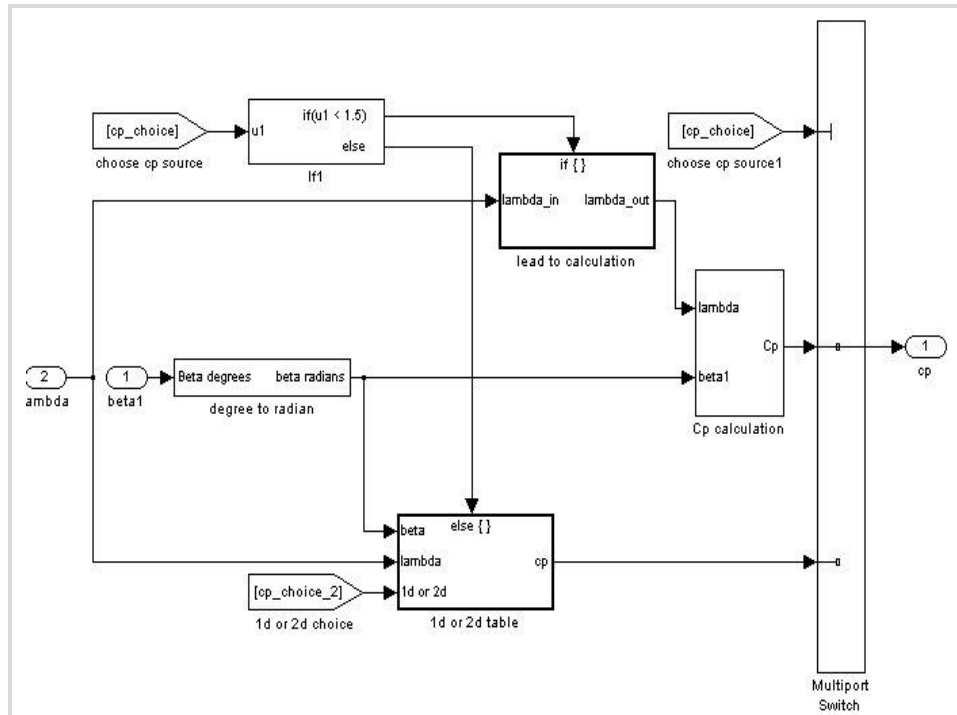


Figure 40: Cp value selection if loop.

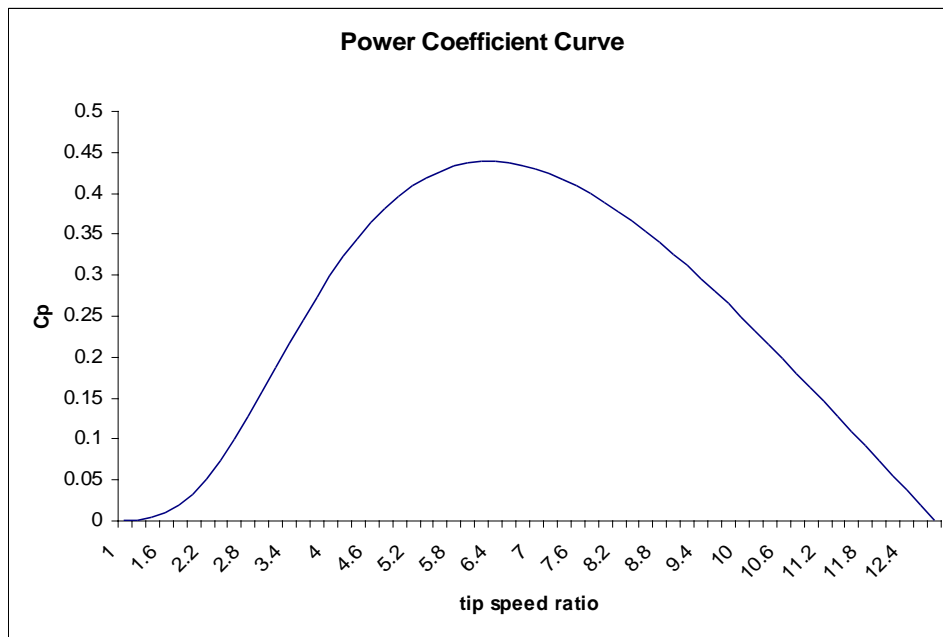


Figure 41: Tip speed ratio for a wind turbine with a fixed pitch of 0 degrees

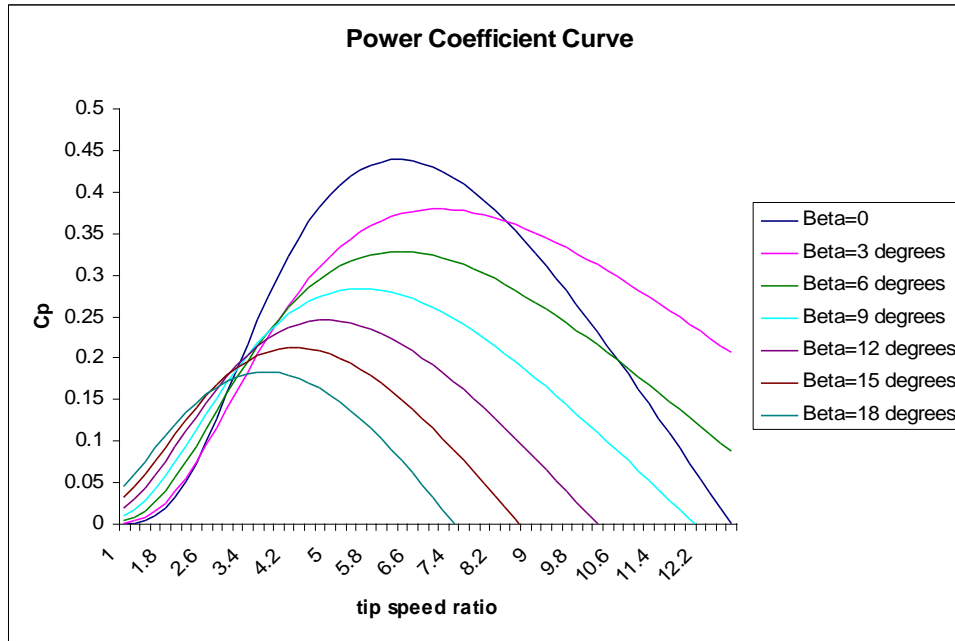


Figure 42: Tip speed ratio for a wind turbine with a variable pitch angle

8.3.2.4 Hub Height Correction

Wind speed data is unlikely to be for the exact hub height of the turbine under simulation; hence, it must be normalized using knowledge of the local terrain. In some cases, the wind speed is recorded near the hub height and so this is an unnecessary complication. For such cases the block can be turned off.

Initially, wind speed is given as;

$$\bar{u}(z) = \frac{u^*}{k} \ln \frac{z}{z_0} \quad \text{Equation 21}$$

Where;

- u^* =friction velocity [ms^{-1}]
- k = von Kármán constant = 0.4
- z =height [m]

The values of z_0 are dependent on terrain. With regard to smooth sea this will be 2×10^{-4} to 3×10^{-4} . However, clearly there will be roughness from the ship. This may be a value around 1.

Equation 21 can be used for two different heights to produce a logarithmic law to relate to wind speeds.

$$\bar{u}(z_1) = \frac{u^*}{k} \ln \frac{z_1}{z_0}$$

$$\bar{u}(z_2) = \frac{u^*}{k} \ln \frac{z_2}{z_0}$$

$$\frac{\bar{u}(z_1)}{\bar{u}(z_2)} = \frac{\ln \frac{z_1}{z_0}}{\ln \frac{z_2}{z_0}}$$

Which rearranges to;

$$\bar{u}(z_1) = \bar{u}(z_2) \frac{\ln \frac{z_1}{z_0}}{\ln \frac{z_2}{z_0}} \quad \text{Equation 22}$$

Equation 22 is only applicable up to a height of 100m, after which the model diverges from reality. A slight modification keeps it accurate up to 300m.

$$\bar{u}(z_1) = \bar{u}(z_2) \frac{\ln \frac{z_1}{z_0} + \frac{5.75z_1}{h}}{\ln \frac{z_2}{z_0} + \frac{5.75z_2}{h}} \quad \text{Equation 23}$$

Where:

$$h = u^* / 6f$$

$$f = \text{Coriolis parameter} = 2\Omega \sin\phi$$

$$\phi = \text{latitude } [^\circ]$$

$$\Omega = \text{angular velocity of Earth } [\text{rad s}^{-1}]$$

From Equation 23, a block was built to take account of the difference in height between the hub and the weather mast. This block, along with the wind speed data input, were put together in the same block with the option of turning it on or off linked to the data input blocks on the top level.

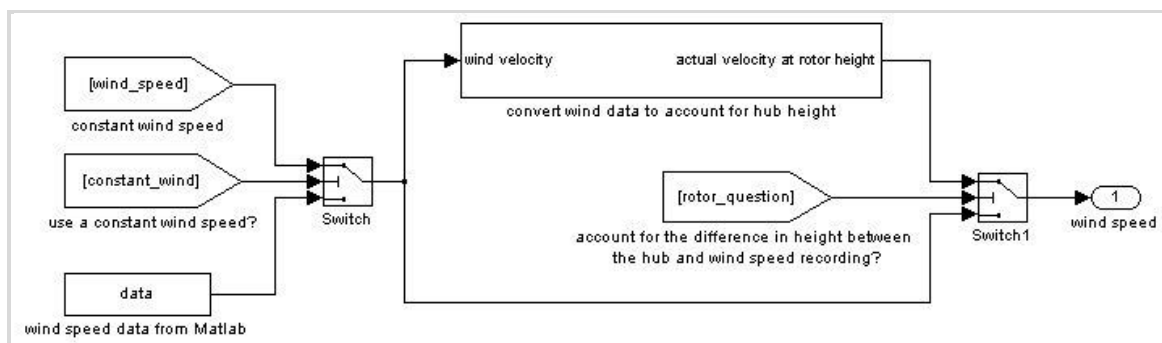


Figure 43: Wind speed and hub height blocks, linked together with switches to allow the blocks to be deactivated when surplus to requirements.

8.3.2.5 Wind Shear and Tower Shadow

So far in this model the wind turbine has effectively been treated as a disk made up of infinite blades in a homogeneous wind, which clearly is not a realistic representation. The number of blades must be considered (in most HAWTs this is three) and also the effect of the tower upon which the turbine is mounted on.

First, consider wind shear. As detailed when looking at corrections due to hub height, the wind will vary with height in a way which is dependent on the roughness of the localized surface. Wind shear is due to the force of the wind on the lower part of the turbine been less so than that at the top, so this inhomogeneity of forces must be dealt with.

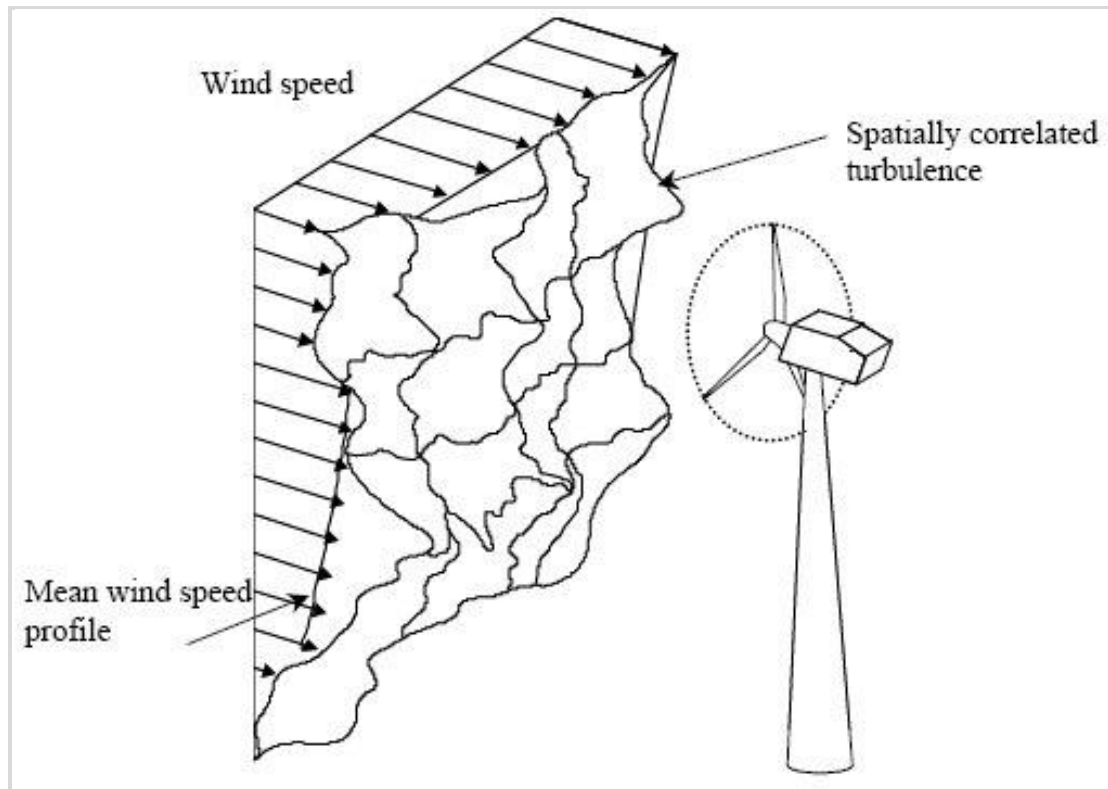


Figure 44.: Wind profile impacting a wind turbine, showing the effects of wind shear

Tower shadow is dependent on the number of blades of the wind turbine. As a blade goes in front of the tower, it will enter a region where the wind is deflected around the tower. This area of reduced incident flow will cause a momentary decrease in the forces acting upon the blade. This is a greater problem for downstream wind turbines than upstream, since with downstream turbines the blade is hidden from the wind behind a tower as opposed to upstream where the blade is in front of the tower. To deal with this, a Simulink block has been developed to incorporate the same methodology used.

$$T_T = T_{mean}1 + A_1\sin(\omega_T t) + A_2\sin(3\omega_T t)$$

Equation 24

Where;

T=mean wind induced torque [Nm]

$A_1=0.2$

$A_2=0.4$

t=time [s]

As with other blocks, the option to turn this section off has been included in a data input block on the top level. This block can be edited for the number of blades to be changed, however, when doing this it is very important to change the moment of inertia by a corresponding amount. As shown in Figure 45, the block was a simple mathematical model.

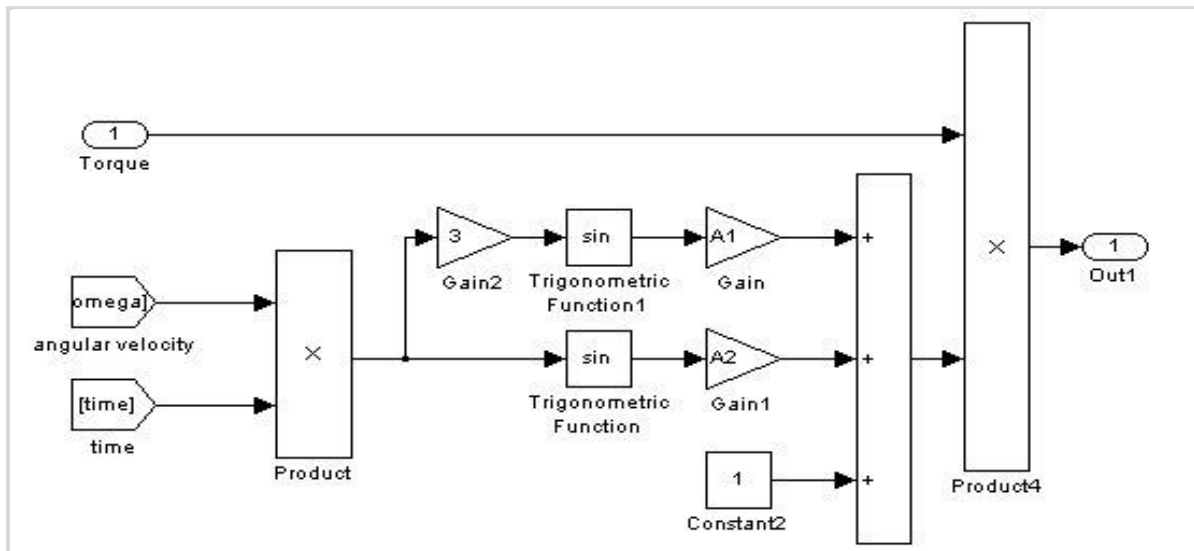


Figure 45: Tower shadow and wind shear block

8.3.3 Gearbox

The gearbox translates the torque from the aerodynamic block to angular velocity for the generator block. This block also feeds back into the aerodynamic model and dictates the blade's angular velocity. For this work, both one-mass and two-mass models have been developed. The full version of the turbine simulator uses a one-mass model, although the two-mass model can be substituted in. Although used throughout the literature, the two-mass model is very simplistic. However, there will be times when there is not sufficient data available for the turbine under simulation to operate the two-mass model. For that reason, a real time one-mass block was also developed within this work. To explain the two-mass model, a description has been adapted.

8.3.3.1 Two-Mass Model

First, consider a rotating disk on a shaft with a moment of inertia J , viscous friction coefficient (damping) D and shaft torsional spring constant (stiffness) K . The torque, T , acting on the disk can be written as;

$$T = J \frac{d^2\theta}{dt^2} + D \frac{d\theta}{dt} + K\theta \quad \text{Equation 25}$$

Next consider a system of two rotating disks linked by a simple gear. This will convert the torque as it passes from one end of the system to the other.

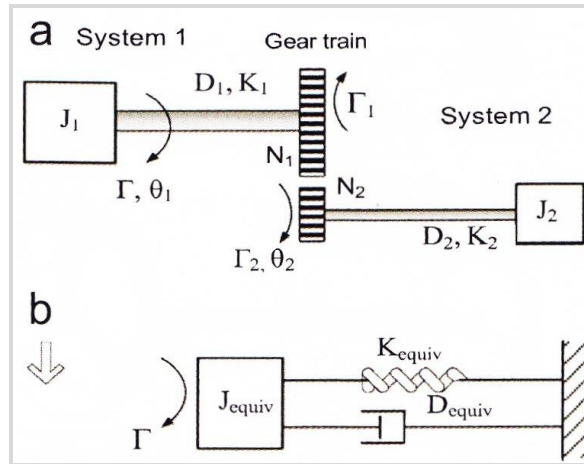


Figure 46: Simplification of two mass model

If an external torque, T , is applied to the disk at system 1, Equation 25 gives;

$$T = J_1 \frac{d^2 \theta_1}{dt^2} + D_1 \frac{d\theta_1}{dt} + K_1 \theta_1 + T_1 \quad \text{Equation 26}$$

Using the same logic, system 2 gives;

$$T_2 = J_2 \frac{d^2 \theta_2}{dt^2} + D_2 \frac{d\theta_2}{dt} + K_2 \theta_2 \quad \text{Equation 27}$$

The two torques, T_1 and T_2 , are related by the gear ratio (ratio of the number of teeth on the two gears in this simplified system, N). Following on from this, logically the angular displacement of the two disks will also be related. Thus, using; $T_1 = NT_2$ and $\theta_1 = N\theta_2$ in Equation 27 provides;

$$\frac{T(t)_1}{N} = J_2 N \frac{d^2 \theta(t)_1}{dt^2} + D_2 N \frac{d\theta(t)_1}{dt} + K_2 N \theta(t)_1 \quad \text{Equation 28}$$

$$T(t)_1 = \left[J_2 N^2 \frac{d^2 \theta(t)_1}{dt^2} + D_2 N^2 \frac{d\theta(t)_1}{dt} + K_2 N^2 \theta(t)_1 \right] \quad \text{Equation 29}$$

This can be rewritten as;

$$T(t)_1 = J_{refl} \frac{d^2 \theta(t)_1}{dt^2} + D_{refl} \frac{d\theta(t)_1}{dt} + K_{refl} \theta(t)_1 \quad \text{Equation 30}$$

So far, the moment of inertia, damping and stiffness have been transferred to the side of the first disk. This can then be substituted into Equation 27 thus;

$$T(t) = J_1 \frac{d^2\theta(t)_1}{dt^2} + D_1 \frac{d\theta(t)_1}{dt} + K_1\theta(t)_1 + J_{refl} \frac{d^2\theta(t)_1}{dt^2} + D_{refl} \frac{d\theta(t)_1}{dt} + K_{refl}\theta(t)_1$$

Equation 31

Therefore;

$$T(t) = J_{equiv} \frac{d^2\theta(t)_1}{dt^2} + D_{equiv} \frac{d\theta(t)_1}{dt} + K_{equiv}\theta(t)_1$$

Equation 32

Where the equivalent moment of inertia, damping and stiffness are defined as;

$$\begin{aligned} J_{equiv} &= J_1 + J_2N^2 = J_1 + J_{refl} & J_{equiv} &= J_1 + J_2N^2 = J_1 + J_{refl} \\ D_{equiv} &= D_1 + D_2N^2 = D_1 + D_{refl} & D_{equiv} &= D_1 + D_2N^2 = D_1 + D_{refl} \\ J_{equiv} &= K_1 + K_2N^2 = K_1 + K_{refl} & JK_{equiv} &= K_1 + K_2N^2 = K_1 + K_{refl} \end{aligned}$$

Equation 33

The above derived a simple model for a torque applied to two disks connected by a simple drive train. Forces can be reflected from one side to the other of the drive train. The next stage is to consider a simple two-mass model of a wind turbine;

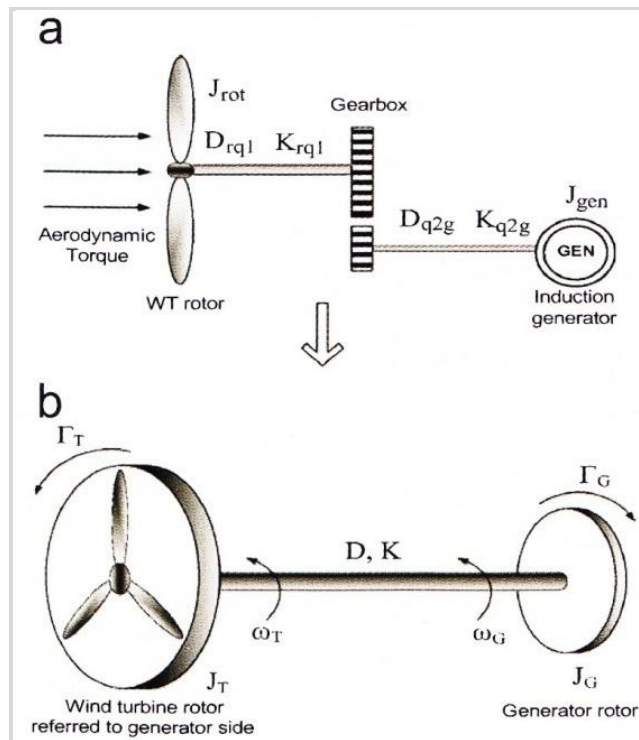


Figure 47: Two mass model of a wind turbine gearbox

In this case, it is necessary to move a torque across from the left to the right hand side. The equations, following the above, can be given as;

$$T(t)_T = J_T \frac{d^2\theta(t)_T}{dt^2} + D \frac{d\theta(t)_T}{dt} - \frac{d\theta(t)_G}{dt} + K\theta(t)_T - \theta(t)_G \quad \text{Equation 34}$$

$$T(t)_G = -J_G \frac{d^2\theta(t)_G}{dt^2} + D \frac{d\theta(t)_T}{dt} - \frac{d\theta(t)_G}{dt} + K\theta(t)_T - \theta(t)_G \quad \text{Equation 35}$$

Which can be written in a slightly more intuitive way;

$$T_T = J_T \ddot{\theta}_T + D\omega_T - \omega_G + K\theta_T - \theta_G \quad \text{Equation 36}$$

$$T_G = -J_G \ddot{\theta}_G + D\omega_T - \omega_G + K\theta_T - \theta_G \quad \text{Equation 37}$$

The equivalent damping and stiffness as used in the above are defined as;

$$J_T = \frac{J_{rot}}{GR^2} \quad \text{Equation 38}$$

$$D = D_{q2g} + \frac{D_{rq1}}{GR^2} \quad \text{Equation 39}$$

$$K = \frac{K_{rq1}}{GR^2} \quad \text{Equation 40}$$

From this, a Simulink model can be made of the gearbox. First consider the requirements of the gearbox model, it is to take the mechanical torque T_T from the aerodynamic block and convert it into an angular velocity for the generator. At the same time, it should produce the angular velocity for the aerodynamic model itself, and be connected to the torque of the generator.

First, rearrange Equation 36 and Equation 37 with respect to the angular acceleration;

$$\ddot{\theta}_T = \frac{T_T - D(\omega_T - \omega_G) - K(\theta_T - \theta_G)}{J_T} \quad \text{Equation 41}$$

$$\ddot{\theta}_G = \frac{-T_G + D(\omega_T - \omega_G) + K(\theta_T - \theta_G)}{J_G} \quad \text{Equation 42}$$

Equation 42 is built up first, using discrete integrator blocks, as continuous ones will not operate correctly in real time;

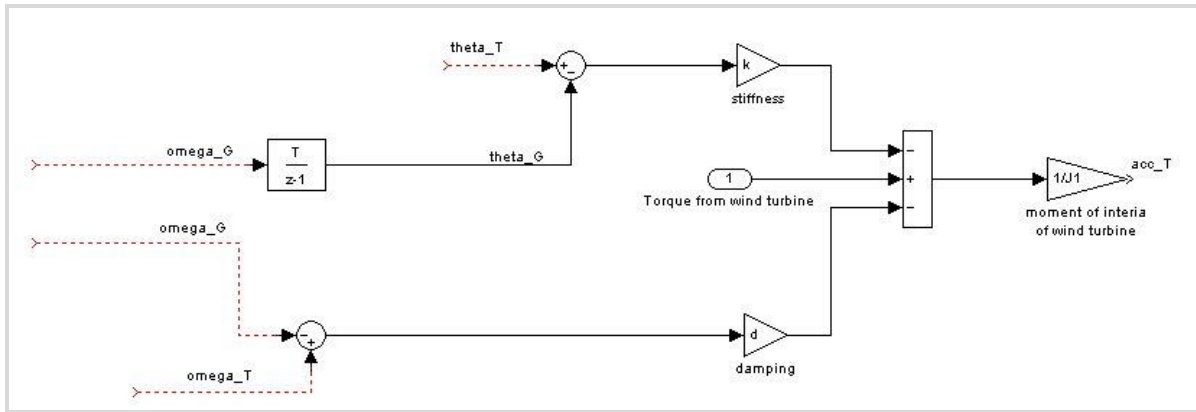


Figure 48: step one of creating a model of Equation 30

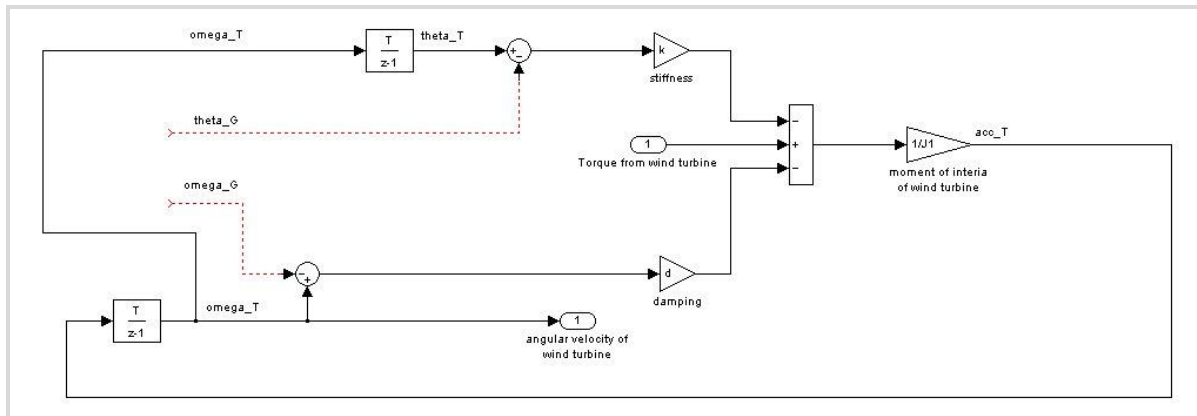


Figure 49: step two of creating a model of Equation 30

Next, loops are introduced relating θ , ω and α .

Equation 42 is added to the block, with the angular velocity of both the blades and generator as outputs.

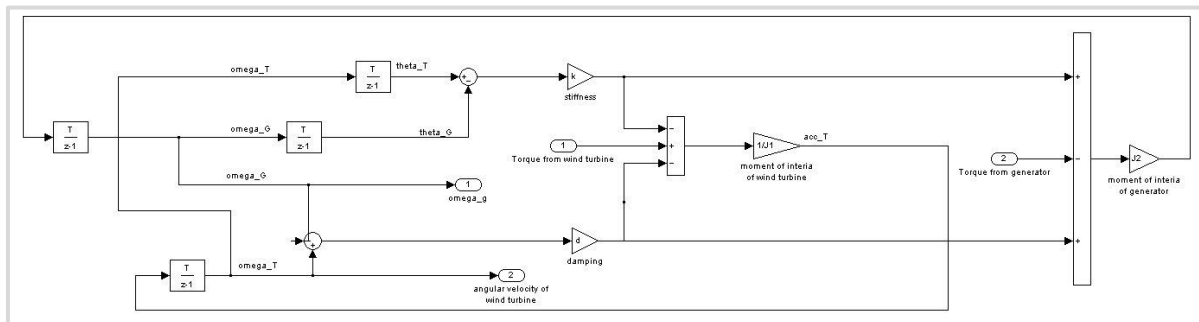


Figure 50: step three of creating a model of Equation 31

Finally, simple mathematical blocks are added to input the values of N , J_{rot} , K_{rq1} , D_{rq1} and D_{q2g} .

8.3.3.2 One-Mass Model

The one-mass model is a further simplification on the above two mass model. Essentially The system is treated as a system such as in Figure 51.

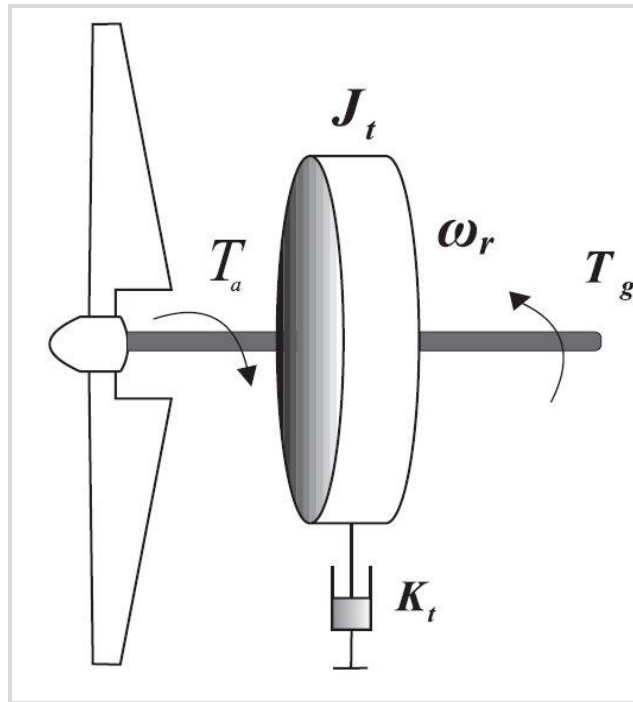


Figure 51: One mass model of a wind turbine.

T_a = aerodynamic torque, J_t = equivalent moment of inertia, K_t = equivalent stiffness, ω_r = generator rotational velocity, T_g = generator moment of inertia.

An equation to calculate the torque transfer this can be derived as follows, the simplest way to describe torque is by;

$$T = J \frac{d\omega}{dt} \quad \text{Equation 43}$$

Thus, for the generator and wind turbine, including the spring constant but no damping constant, it can be shown that;

$$(J_{rot} + N^2 J_G) \omega_T = T_T - K \omega_G - N T_G \quad \text{Equation 44}$$

Where;

$$K = K_T + N^2 K_G \quad \text{Equation 45}$$

The relation between rotational velocity of the wind turbine blades and the generator is given as;

$$\omega_G = N^2 \omega_T \quad \text{Equation 46}$$

This model can be built up as follows;

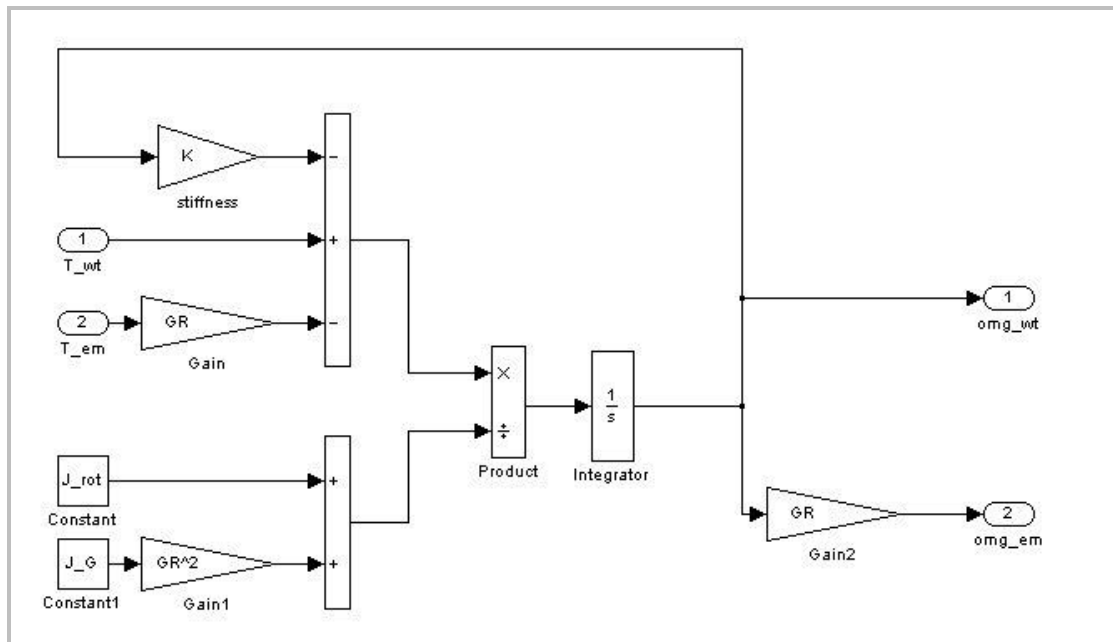


Figure 52: One mass model of gearbox

8.3.4 Moment of Inertia

The gearbox models require the moment of inertia of both the blades and the generator, i.e. the resistance of the blades and generator to changes in their rotational motion. This can be calculated if the dimensions of the blades and rotor are known. To aid with approximations, Equation 47 and Equation 52 were input into a spread sheet, which is supplied in the appendix. Using parallel axis theorem the wind turbine blades can be treated as simple rectangular beams, clearly, this methodology does not supply a high level of precision for aerofoils, but does provide a reasonable approximation. An addition complexity is as the blade pitch angle varies, so too will the moment of inertia, which is not taken into consideration in the gearbox block.

$$J_{rotor} = B^2 L^2 \frac{M_{blade}}{12} N_{blades} \quad \text{Equation 47}$$

Where;

- B=width of blade [m]
- L=length of blade [m]
- M_{blade} =mass of blade [kg]
- N_{blade} =number of blades

The generator is treated as a rotating hollow cylinder around a shaft of greatest thickness at the centre. This is described by;

Hollow cylinder (rotor):

$$J_{rotor} = \frac{M_{rotor}}{2} \left[\frac{D_{outer}^2}{2} + \frac{D_{inner}^2}{2} \right] \quad \text{Equation 48}$$

Where;

- M_{rotor} =mass of rotor [kg]
- D_{outer} =outer diameter of rotor [m]
- D_{inner} =inner diameter of rotor [m]

Left hand end of shaft:

$$J_{\text{shaft LH}} = \frac{M_{\text{shaft LH}}}{2} \left[\frac{D_{\text{shaft LH}}^2}{2} \right] \quad \text{Equation 49}$$

Where;

$M_{\text{shaft LH}}$ =mass of rotor [kg]
 $D_{\text{shaft LH}}$ =outer diameter of rotor [m]
 $D_{\text{shaft LH}}$ =inner diameter of rotor [m]

Centre of shaft:

$$J_{\text{shaft centre}} = \frac{M_{\text{shaft centre}}}{2} \left[\frac{D_{\text{shaft centre}}^2}{2} \right] \quad \text{Equation 50}$$

Where;

$M_{\text{shaftcenter}}$ =Mass of rotor [kg]
 $D_{\text{shaftcenter}}$ =Outer diameter of rotor [m]
 $D_{\text{shaftcenter}}$ =Inner diameter of rotor [m]

Right hand end of shaft:

$$J_{\text{shaft RH}} = \frac{M_{\text{shaft RH}}}{2} \left[\frac{D_{\text{shaft RH}}^2}{2} \right] \quad \text{Equation 51}$$

Where;

$M_{\text{shaft RH}}$ =Mass of rotor [kg]
 $D_{\text{shaft RH}}$ =Outer diameter of rotor [m]
 $D_{\text{shaft RH}}$ =Inner diameter of rotor [m]

Total moment of inertia of generator;

$$J_G = J_{\text{rotor}} + J_{\text{shaft LH}} + J_{\text{shaft centre}} + J_{\text{shaft RH}} \quad \text{Equation 52}$$

8.3.5 Generator

SimPowerSystems Blocks

SimPowerSystems within Simulink 6.0 has models of generators which one would assume could be used for this work. However, these are not designed to be used in real time. A typical generator model is shown in Figure 53 based around the asynchronous machine block (SI version). This was run in both continuous and discrete modes. To run as a fixed step model it was necessary to substitute all continuous integrator blocks which were replaced with discrete time dependent integrator blocks, whilst ensuring the initial values were kept the same. Comparing and contrasting the torque produced by the generator in the two different versions in Figure 54 and 55 clearly shows issues with using blocks in real time which are not designed for such applications. Hence, the pre-designed blocks available with SimPowerSystems could not be used for this work.

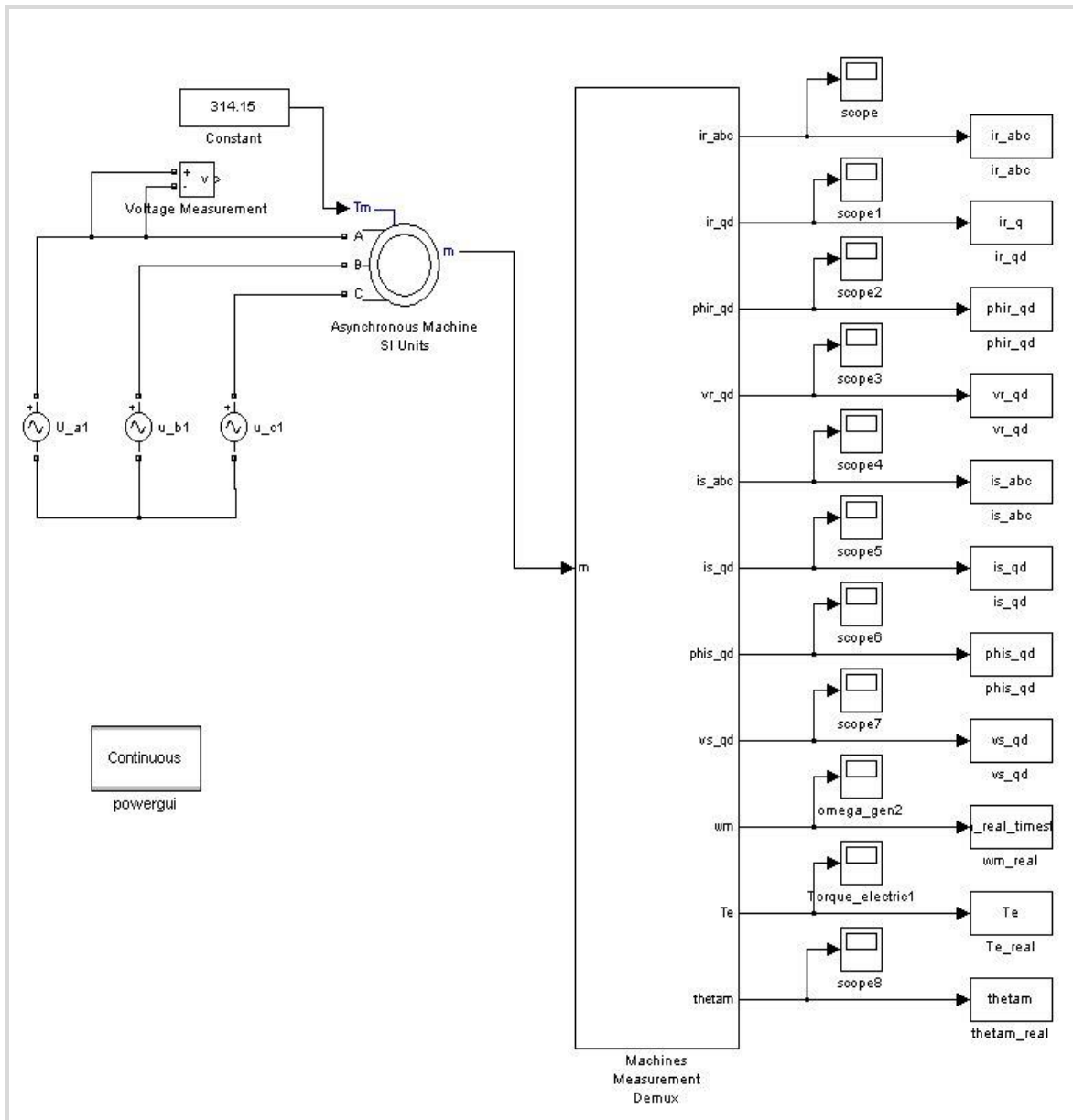


Figure 53: Asynchronous machine with a constant voltage supply

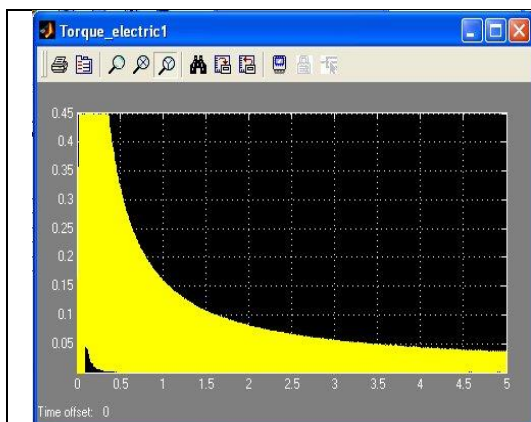


Figure 54: Torque produced by asynchronous machine when used with continuous integration blocks.

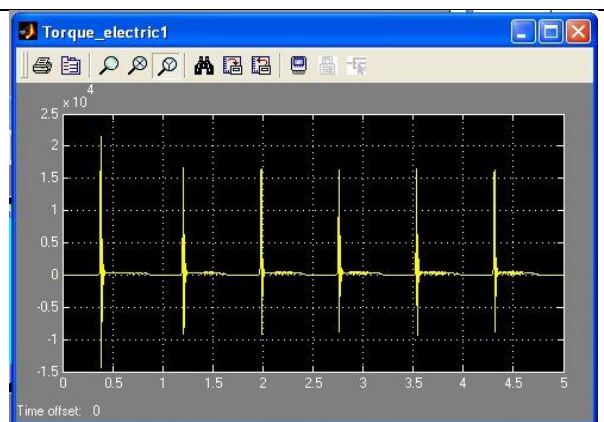


Figure 55: Torque produced by asynchronous machine when used in discrete mode.

8.3.5.1 Voltage and Flux Equations

The real time induction generator was constructed from the Park-Blondel voltage and flux equations in a d-q reference rotating reference frame, in which the q-axis is $\pi/2$ radians ahead of the d axis.

$$u_{ds} = -R_s i_{ds} - \Psi_{qs} + \frac{1}{\omega_b} \frac{d}{dt} \Psi_{ds} \quad \text{Equation 53}$$

$$u_{qs} = -R_s i_{qs} + \Psi_{ds} + \frac{1}{\omega_b} \frac{d}{dt} \Psi_{qs} \quad \text{Equation 54}$$

$$u_{dr} = R_r i_{dr} - s \Psi_{qr} + \frac{1}{\omega_b} \frac{d}{dt} \Psi_{dr} \quad \text{Equation 55}$$

$$u_{qr} = R_r i_{qr} + \Psi_{dr} + \frac{1}{\omega_b} \frac{d}{dt} \Psi_{qr} \quad \text{Equation 56}$$

Where;

U =instantaneous voltage [V]

I=instantaneous current [A]

R=resistance [Ω]

ω =angular velocity of generator [rad s^{-1}]

ψ =instantaneous flux Wb

s=slip = (actual speed – synchronous speed)/synchronous speed

d and q relate to the d and q axis in the rotating frame of reference

The magnetic fluxes are given by;

$$\Psi_{ds} = -(X_s + X_m) i_{ds} + X_m i_{dr} \quad \text{Equation 57}$$

$$\Psi_{qs} = -(X_s + X_m) i_{qs} + X_m i_{qr} \quad \text{Equation 58}$$

$$\Psi_{dr} = -(X_r + X_m) i_{dr} - X_m i_{ds} \quad \text{Equation 59}$$

$$\Psi_{qr} = -(X_r + X_m) i_{qr} - X_m i_{qs} \quad \text{Equation 60}$$

Where;

X_r =rotor inductance [H]

X_s =stator inductance [H]

X_m =magnetizing inductance [H]

To construct the generator block equations, Equation 53 and Equation 56 were rearranged into the following forms;

$$\frac{d}{dt} \Psi_{ds} = \Psi u_{ds} + R_s i_{ds} + \Psi_{qs} \omega_b \quad \text{Equation 61}$$

$$\frac{d}{dt}\Psi_{qs} = \Psi u_{qs} + R_s i_{qs} - \Psi_{ds} \omega_b \tag{Equation 62}$$

$$\frac{d}{dt}\Psi_{dr} = \Psi u_{dr} - R_r i_{dr} + s \Psi_{qr} \omega_b \tag{Equation 63}$$

$$\frac{d}{dt}\Psi_{qr} = \Psi u_{qr} - R_r i_{qr} - \Psi_{dr} \omega_b \tag{Equation 64}$$

Flux Equation 57 to Equation 60 were rearranged as follows;

$$i_{ds} = \frac{\Psi_{ds} - X_m i_{dr}}{-(X_s + X_m)} \tag{Equation 65}$$

$$i_{qs} = \frac{\Psi_{qs} - X_m i_{ds}}{-(X_s + X_m)} \tag{Equation 66}$$

$$i_{dr} = \frac{-\Psi_{dr} + X_m i_{ds}}{(X_r + X_m)} \tag{Equation 67}$$

$$i_{qr} = \frac{\Psi_{qr} + X_m i_{qs}}{(X_r + X_m)} \tag{Equation 68}$$

From the above, the following Simulink block was created;

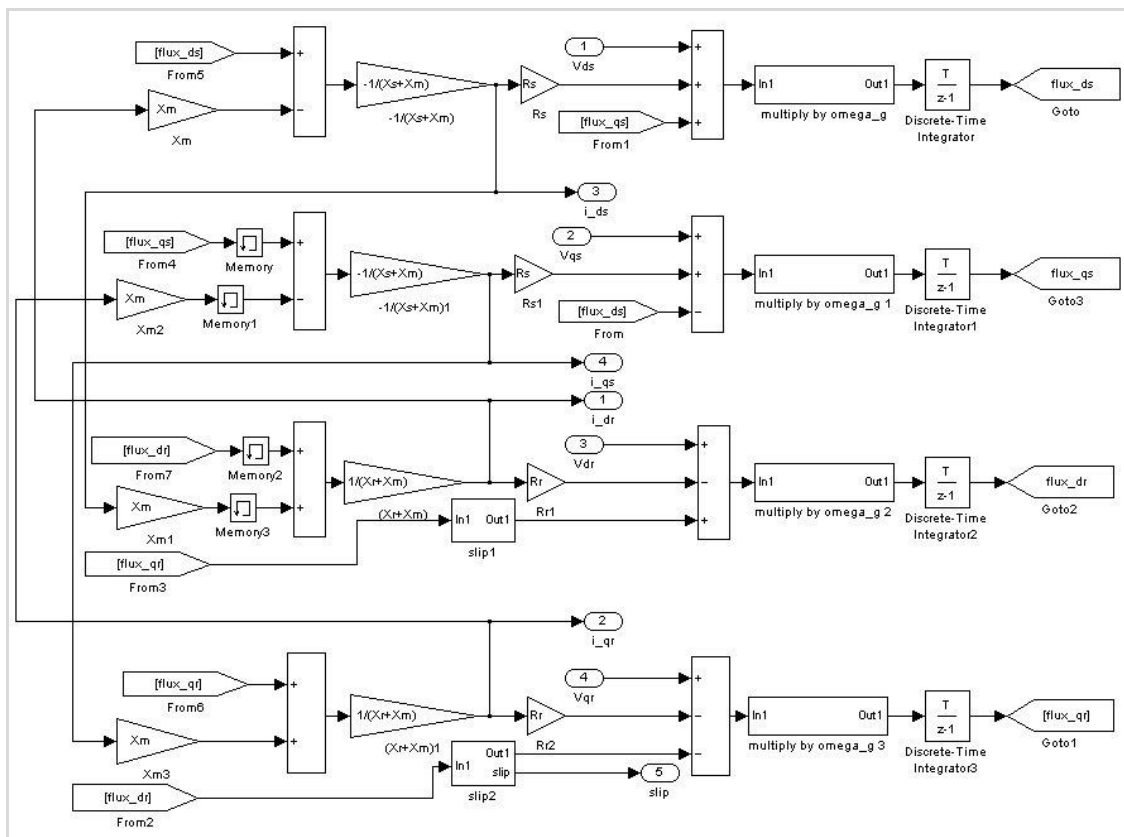


Figure 56: Simulink representation of equations

The model feeds back the current values between the voltage and flux equations, which necessitated inputting memory blocks within Equation 67 and Equation 68 to prevent the entire system initializing simultaneously, as if this occurred various equations would attempt to start without any inputs. The slip equation was added as in Figure 57;

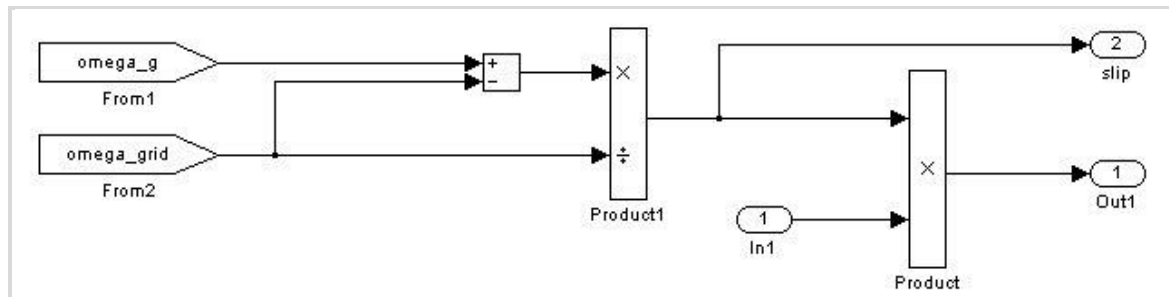


Figure 57: Simulink representation of slip calculation.

With currents in the d-q reference frame calculated, the electrical torque of the system is calculated as;

$$T_e = p \frac{3}{2} L_m (i_{dr} i_{qs} + i_{qr} i_{ds}) \quad \text{Equation 69}$$

Where;

p = number of poles

This could be built up as a very simple mathematical block in Simulink. Real and reactive power from the rotor and stator are calculated as;

$$P_s = u_{ds} i_{ds} + u_{qs} i_{qs} \quad \text{Equation 70}$$

$$Q_s = u_{qs} i_{ds} + u_{ds} i_{qs} \quad \text{Equation 71}$$

$$P_r = -u_{dr} i_{dr} - u_{qr} i_{qr} \quad \text{Equation 72}$$

$$Q_r = -u_{qr} i_{dr} - u_{dr} i_{qr} \quad \text{Equation 73}$$

For the initial generator model a squirrel cage induction machine was simulated, hence

$$u_{dr} = 0, u_{qr} = 0 \quad \text{Equation 74}$$

$$P_r = 0, Q_r = 0$$

It would only take a small change of the voltage inputs to the model to simulate a doubly fed induction generator, and for such purposes the block has been made as general as possible. Within the model used, it has been assumed current flowing from the generator to the network is positive.

8.3.5.2 Control of Generator

Two separate sections are included in the generator controls. The first of these was to ensure the generator does not cut in until the system has reached synchronous speeds. This was done by inserting a switch into the system that outputs a constant of zero until ω_G is greater than the grid connected voltage of 50Hz (314 rad s^{-1}). A ramp block was added to the controller, to provide a level of hysteresis, thus, the generator would not instantly cut out the moment it experienced electrical torque.

8.3.5.3 Pitch controller

In order to control the speed of the turbine, a pitch controller was added to the system. This would alter the angle of the blades to either increase or decrease the efficiency of the turbine, and hence the power extracted from the wind. The variations in the power coefficient against pitch angle are shown in Figure 58;

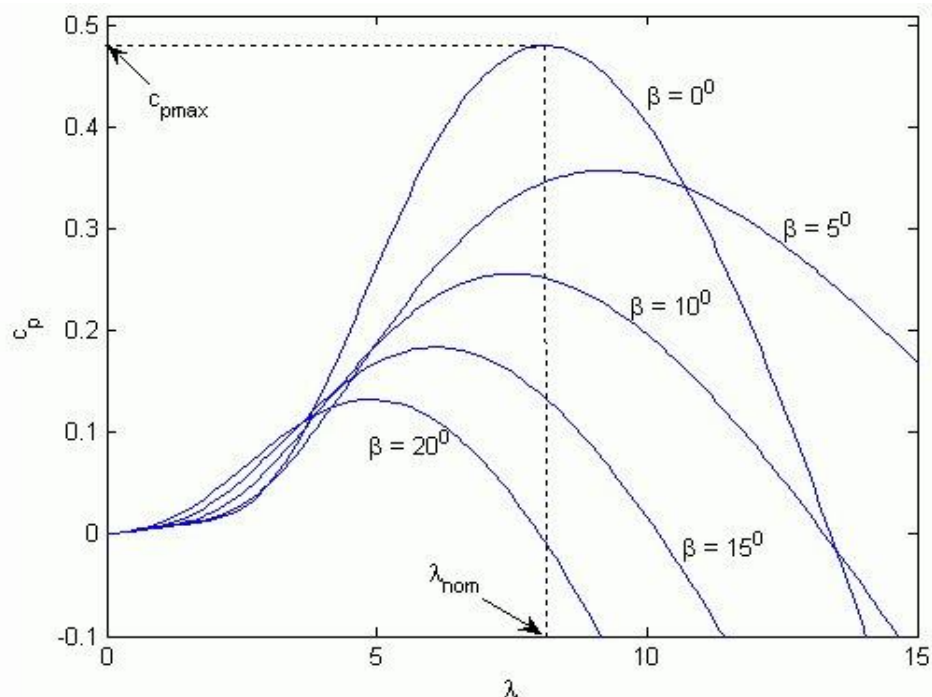


Figure 58: Varying levels of pitch angle alter the position a value of the peak C_p .

The block works using two switches as an equivalent of a nested “if” statement. This first switch is to deal with values of the generator speed which are too high, or exist close to synchronous speed. The second is for values below synchronous speed. The block acts to keep the system running at slightly above synchronous speed. As with other blocks, a help file was written in HTML to allow this block to be used separately. In order to prevent the blades from simply cycling through pitch angles, a saturation block was added to ensure the pitch angle remained between 0 and 90 degrees. It is important to note that high pitch angles lead to negative values of C_p , this is representative of the added drag when the blades are near feathered.

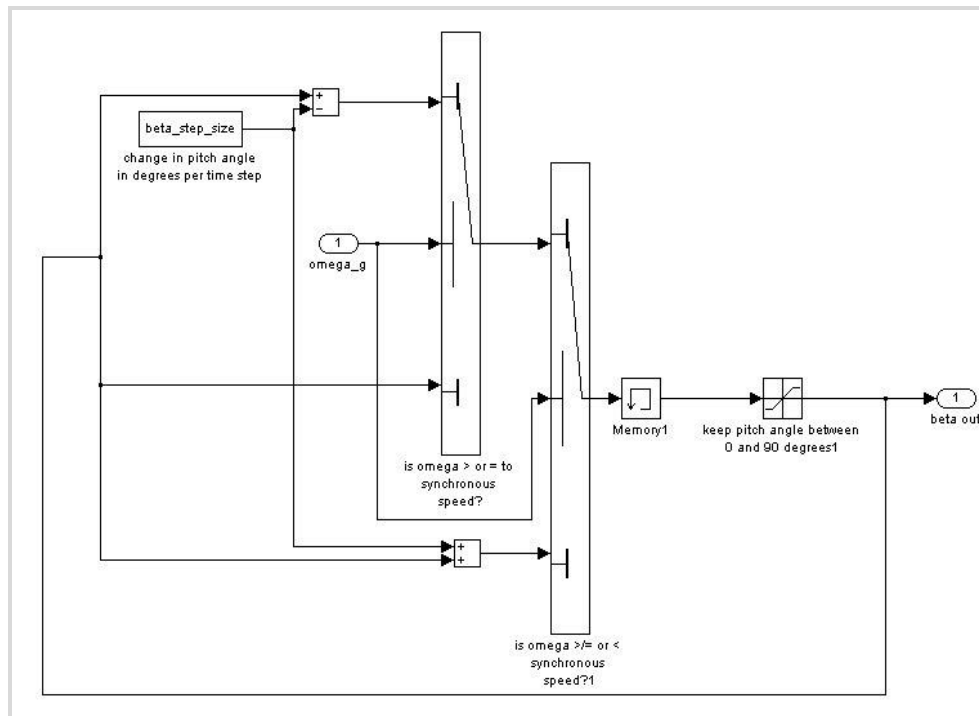


Figure 59: Pitch controller block

This complete model is a real time model of a wind turbine, which can take real wind speed data and convert it into the three-phase output of an induction generator.

8.4 Conclusion

Two models have been created for wind turbines on ships. The first is a basic and quick highly configurable model, which can be used to try out multiple turbines with different power curves very quickly. The second is more detailed, but complex to reconfigure, and can be used for the later stages of the project.

9 DISTRIBUTION

The distribution system facilitates the transport of electrical power from the source(s) to the consumers. For each vessel the distribution system is built up in one or more power levels, examples of power levels for a large power system are:

1. <1kW - (Household components such as PC's, hotel appliances, etc.)
2. <500kW - (Power components such as pumps, compressors, etc.)
3. < xMW - (Propulsion and process components such as thrusters, plant, etc.)

These power levels are mainly because of the short circuit and nominal current limitations of distribution components. It implies also that the voltage is higher for larger power levels.

Furthermore, a clear distinction can be made between AC and DC distribution networks. Today all main distributions are by means of AC, because this voltage is easy to be converted to other voltage levels and protection is much easier to implement. However, today's consumers are using DC voltages and many new sources and buffers operate on DC. A future distribution system is likely to be a mix of AC and DC sub-distributions. The components that allow the addition of future distribution system together are described in this chapter.

9.1 Transformers

Currently, transformers are one of the most important components of distribution networks. They convert AC power into AC power with a lower, higher or similar voltage and the same frequency. It is also possible to create a defined phase shift. Transformers are technically well known and have advantages like:

- Relatively simple technology
- Galvanic separation of two electric grids
- High efficiency
- Parasitic effects cause attenuation of higher (unwanted) harmonics

Besides the advantages, transformers also have disadvantages which are:

- Unsuitable for DC conversion
- Only suitable for transforming the amplitude of the voltage, not the frequency
- For low frequencies (50-60 Hz) a transformer is relatively large

9.1.1 Power Rating

The power rating of transformers ranges from a few VA up to tens of MVA (on-board ships) or even up into the GVA range (in land-based applications).

9.1.2 Power Density

The power density of transformers can vary. A high power density results in higher losses and thus a heating effect which may require dedicated cooling system adaptations. The graph of Figure 60 shows the relationship between the specific power of a transformer, its wild heat and the direct investment costs. The costs for additional air conditioning to handle the wild heat are not included.

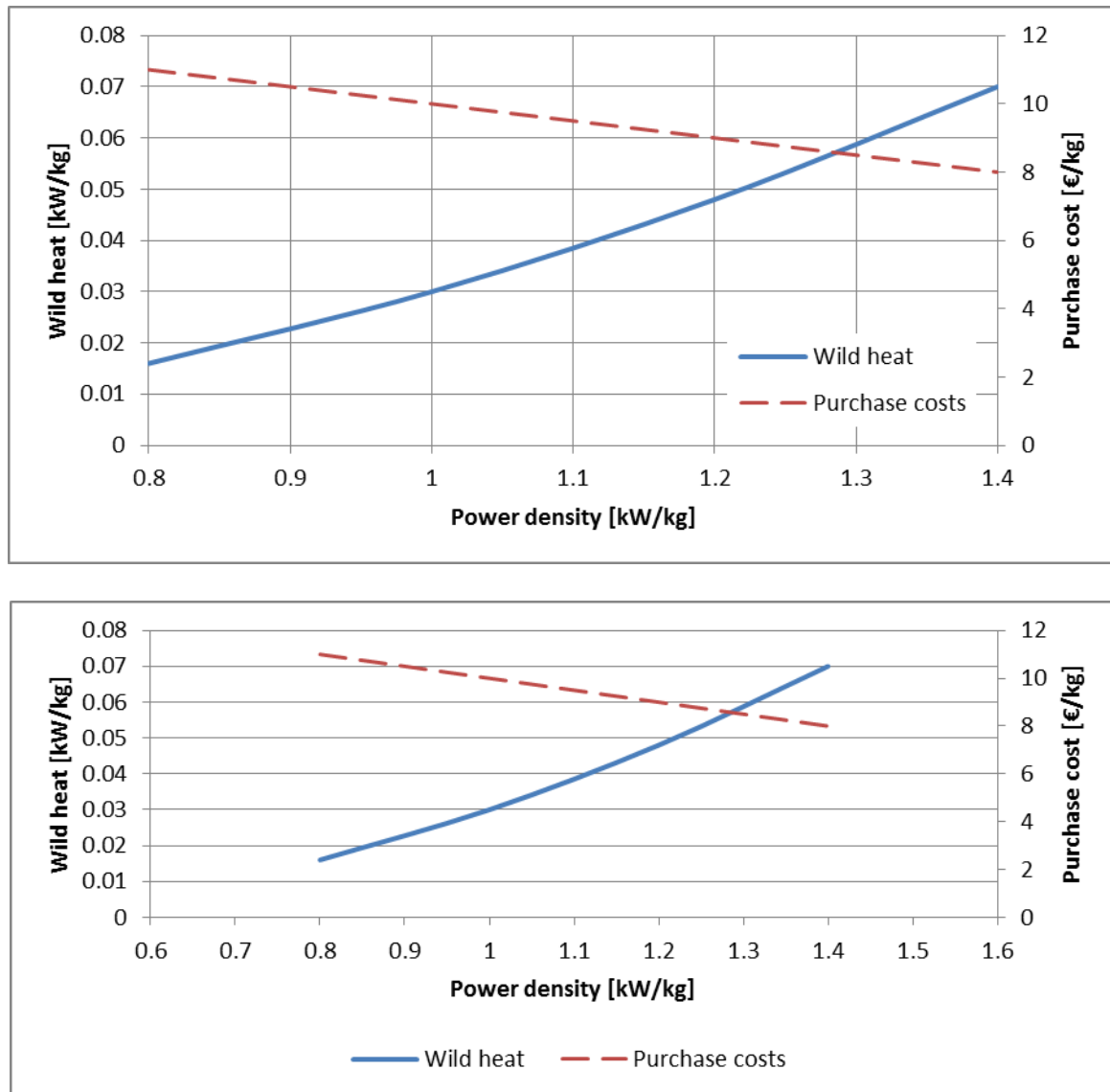


Figure 60: Wild heat and purchase costs for three phase transformers as a function of the power density

9.1.3 Efficiency

Transformers suffer from load losses (P_k) and no-load losses (P_0). Load or winding losses vary directly by the square of the load factor. No-load or core losses are more or less constant with respect to the load factor. The efficiency of a transformer is the output power divided by the sum of the output power and the transformer losses. Equation 75 shows the equation for calculating the efficiency. In this equation S_l equals the transformer load, $\cos \varphi$ equals the power factor, P_0 equals the no-load losses and P_k equals the nominal load losses. The load factor L is defined in Equation 76. Here S_l equals the transformer load and S_r equals the transformer rating.

$$\eta = \frac{S_l \cos \varphi}{S_l \cos \varphi + P_0 + (P_k L^2)} \quad \text{Equation 75}$$

$$L = \frac{S_l}{S_r} \quad \text{Equation 76}$$

Figure 61 shows the efficiency for Siemens dry type transformers for different load factors. From this figure it can be seen that for different load factor transformers, an optimum operating point can be achieved.

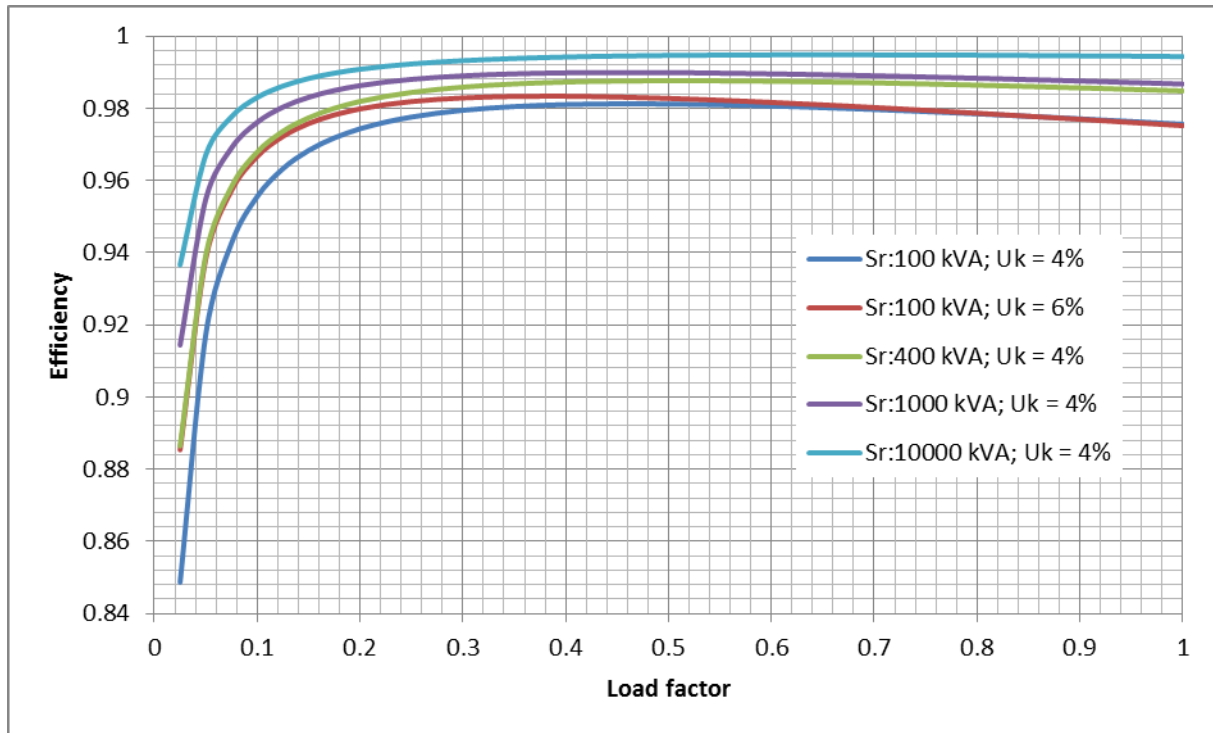


Figure 61: Transformer efficiency for varying load factors.

9.2 Static Converters for Distribution

Static converters are essential for integrating the new type of sources and buffers, such as fuel cells and batteries, into one bi-directional distribution system. Static converters use the same power electronics as the converters used for motor drives with only the control strategy being different.

Basically the converters can be divided into the following broad categories:

- AC to DC
- DC to AC
- DC to DC
- AC to AC

For AC to AC conversion a transformer can be used in case where the frequency doesn't have to be converted. Otherwise the conversion is carried out via an intermediary DC stage by an AC/DC and a DC/AC converter. This conversion category is therefore not described.

9.2.1 AC/DC and DC/AC converters

As indicated above for future distribution bidirectional distribution converters are required. This implies that AC/DC and DC/AC converters are the same components, being a four-quadrant switch-mode inverter (see Figure 62).

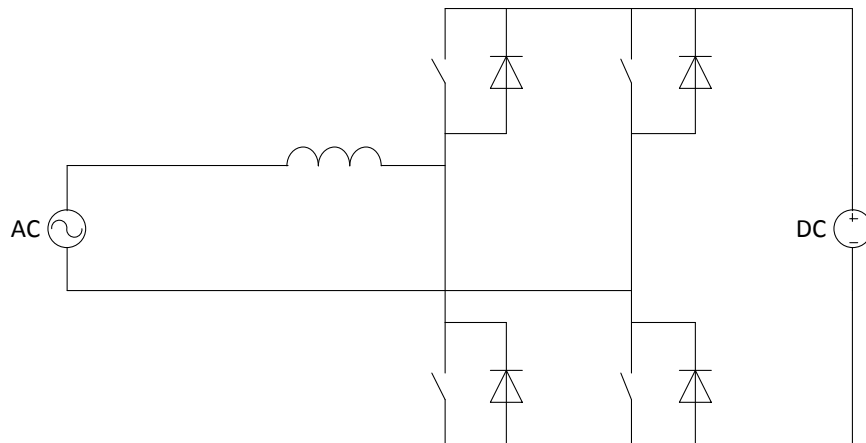


Figure 62: Single phase Switch-mode converter for bidirectional power flow.

The losses of switch-mode converters can be divided into: switching losses, conduction losses and power required for auxiliary systems (e.g. controllers, auxiliary supplies, water cooling pumps). These losses are different for each system, but the losses are generally linear and typically about 3%.

With the present protection systems for short circuits, the converters have to be able to supply overcurrent for about a second to trip the protection. For power electronics the thermal time constant is very short, and is therefore, only able to supply overcurrent for about 1 ms. This means that converters have to be selected with a rating that is about 3 times larger than the nominal current.

The power electronics itself is a relative small part of the complete cabinet, as shown in Figure 63. The majority of the space is for connections, water cooling, control and filtering. The power density for air-cooled switch-mode converters with a 3 time overcurrent capacity is about 125kVA/m³ and 0.2kg/m³ (based on VACON NXC converter sizes)



Figure 63: Example of a motor variable frequency drive with a switch-mode converter. The equipment in the red box is the actual power electronics.

The control of switch-mode converters is in the 1kHz domain, which means that for quasi-static situations the converter is infinitely fast and can easily be modelled by a multiplier that represent the efficiency.

9.2.2 DC/DC Converters (choppers)

A bidirectional DC/DC converter has a similar topology as the AC/DC converter described in the previous chapter. At the moment of writing this document the availability of commercial off-the-shelf DC/DC converters for main power distribution is very limited. An example of a unit is a 120A/650V converter manufactured by MSc electronics Oy.

The efficiency and the power density of this type of converters is similar to the AC/DC converters.

9.3 Cold Ironing

The main objectives of cold ironing, or shore based power connection, are:

- Provide all necessary electrical power, at 50 or 60 Hz, from shore-to-ship while at quayside and thus, reducing harbour ship emissions by not running on-board generators.
- Possible application (if allowed by grid authorities): Load the generators during their on-board testing. During testing of generators, immersed resistors are used and the power produced is wasted. Cold ironing provides the possibility to supply the on-board power generated during testing to the shore. These tests can take about 300 hours for each ship. Cold ironing will participate in improving harbour energy efficiency

According to D1.1, the shore-based substation is typically designed to deliver a ship with a three-phase 6,600V, 50/60Hz power supply, which can be converted on-board to the necessary requirements of the auxiliary systems running at that time.

9.3.1 Model of Cold Ironing

Two types of shore connections can be considered for modelling:

1. Direct connected, connection by an isolation transformer;
2. Shore connection via static converter.

The direct connected shore connection can easily be modelled by three phase supply L/R impedance. This model is valid for quasi-static and dynamic simulations

For the shore supply with static converter the models used for converters can be used

10 GENERAL CONCLUSION

In task 3.1, a comparison was made between the different technical solutions for on-board equipment of a cargo ship, such as energy storage, engines, PV modules, wind power, etc. The review of the different technologies lead to first technical selection of possible systems to be implement and studied as part of this project.

Diesel engines:

- Two stroke 22 MW 95rpm engine for the propulsion (including WHR system).
- Four stroke 14.4 MW 600rpm engine for the power generators.
- Four stroke 3 MW 750rpm engine for the auxiliary generators.

Electrical machines:

- All electrical machines are permanent magnet machines
- One 20MW, 10kV, 2kA, 95rpm for electrical propulsion
- Two 12MW, 10kV, 1.2kA, 600rpm for the power generators
- One 3MW, 10kV, 300A, 750rpm for the auxiliary generators

Storage:

- Lithium batteries of 12MW and 5MWh energy.
- Supercapacitor solutions are heavier than batteries, however, a decision is still to be made on whether this technology is suitable to integrate this technology into a hybrid energy storage system. Further investigation and modelling is required

Fuel cells

- MCFC fuel cell devices for part of the contribution to the energy system will be looked at. These cells will be analysed in combination with a chosen energy storage system.

Solar:

- Polycrystalline silicon PV modules of 100kW peak covering a surface of 1500m².

Wind:

- It is not easy to decide on this subject, but only a horizontal axis wind turbine adapted to a ship environment seems the best option at this stage.

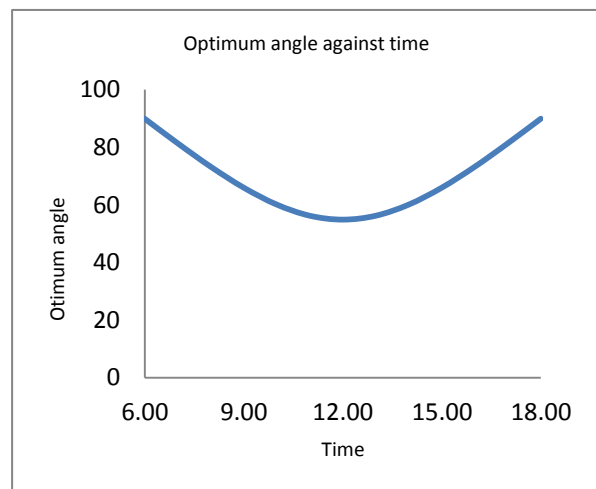
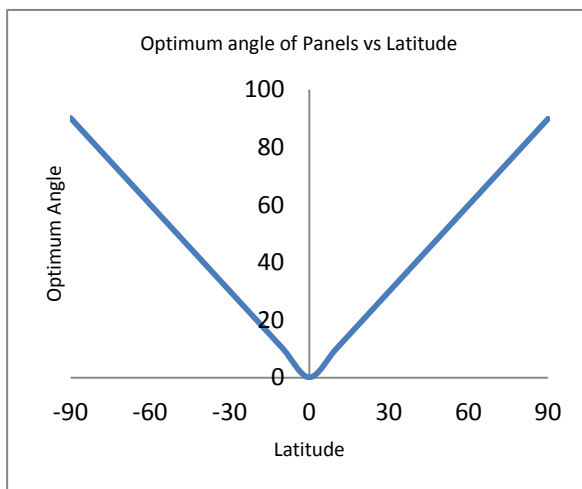
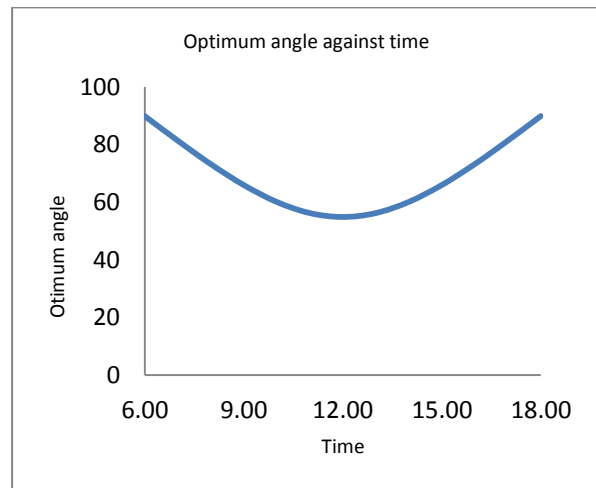
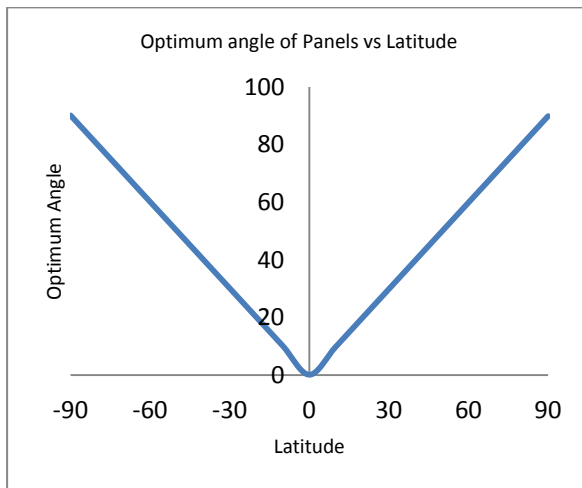
Distribution:

- Based upon described properties of distribution components, D3.3. will result in a detailed topology specifying voltage levels, AC/DC balance and consequent architecture.

APPENDIX A: SOLAR POWER GENERATION

Pitch and Orientation

The levels of irradiance received by the photovoltaic modules will vary with pitch and orientation. As the ship is a constantly moving object, the optimum angle of the panels will be constantly changing. This will alter over the long term with the route of the ship, and over the short term with the pitch and role of the ship. The ideal pitch and orientation will be dependent on the latitude of the system, the time of year and the time of day. The effects of this are shown in A-1 and A-2.

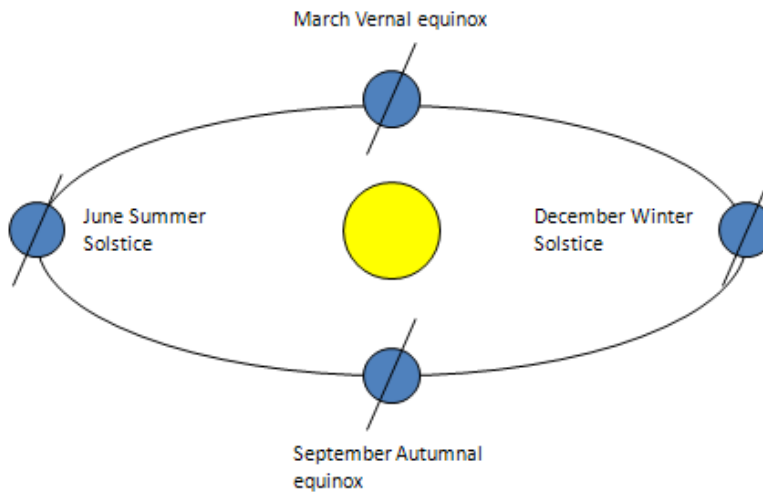


A-1: Varying optimum pitch angle of photovoltaic panels at midday with a declination of zero

A-2: Varying optimum pitch angle at a latitude of 55 degrees with a declination angle of zero

In order to calculate how to vary the pitch and orientation of the modules whilst the ship travels, the following is required.

First, calculate the declination angle; this is due to the changing angle of the Earth's axis of rotation throughout the year. This varies from 23.5 degrees to -23.5 degrees, and is given by;



A-3: varying declination of the Earth throughout the year

$$\delta = 23.5 \sin\left(\frac{360(n + 284)}{365.24}\right)$$

Where;

n = day number (1st of January = 1)

Next, calculate the hour angle, which is due to the angle of the sun's apparent angle from an observer changing by 15 degrees every hour, where midday is taken to be zero degrees, as the sun is overhead.

$$\omega = (12 - t) * 360$$

Where;

t = solar time [hours] (which may not necessarily be the local time)

From the above two equations, the altitude angle of the sun can be calculated. This is the angle between the path of the direct sunlight and the ground.

$$\sin\alpha = \sin\delta\sin\phi + \cos\delta\cos\phi\cos\omega$$

Where;

δ = declination angle [degrees]

ϕ = Latitude [degrees]

ω = hour angle

Therefore α is the optimum pitch for the photovoltaic module, whilst ω due south is the ideal orientation while in the northern hemisphere, and ω due north the ideal orientation when in the southern hemisphere.

For systems which are fixed, the above can be used to calculate the angle of sunlight incident to the module

$$\cos\theta = \sin\delta\sin\phi\cos\beta - \sin\delta\cos\phi\sin\beta\cos\gamma + \cos\delta\cos\phi\cos\beta\cos\omega + \cos\delta\sin\phi\sin\beta\cos\gamma\cos\omega + \cos\delta\sin\beta\sin\gamma\sin\omega$$

Where;

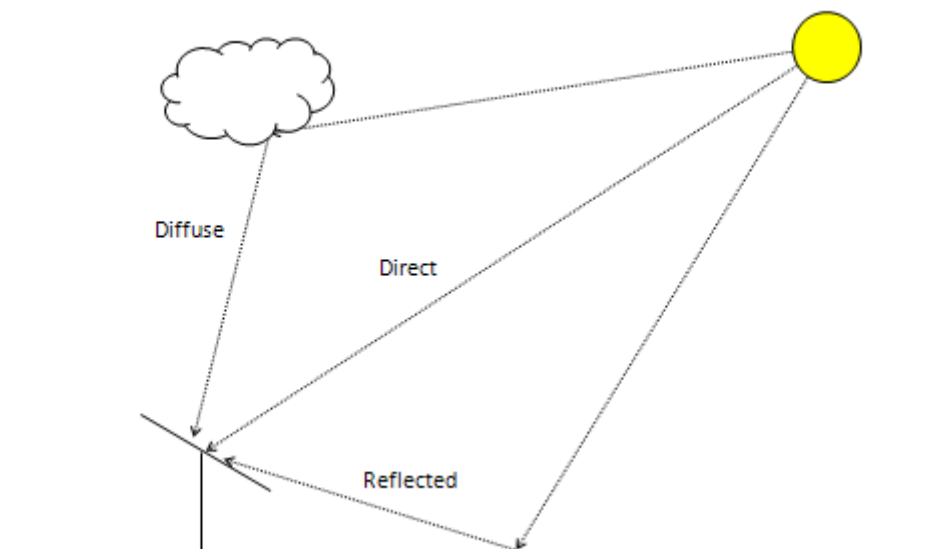
δ = declination angle [degrees]

ϕ = Latitude [degrees]
 β = pitch of panel [degrees]
 γ = orientation [degrees]
 ω = hour angle [degrees]

Types of Irradiance

So far the direct beam radiation has only been considered, however the irradiance received by PV can be divided into three types:

1. Direct beam = light which is coming directly from the sun
2. Diffuse beam = light which has been scattered in the atmosphere due to cloud or particulate cover
3. Reflected beam = light which has reflected off another surface.



A-4: Types of beams

With regard to cargo ships, the majority of their time is spent in transit, and hence there is the possibility of reflection of light from the ocean surface.

The solar gain for a system from these respective sources can be calculated as follows:

$$I_{d,surface} = I_{normal} \cos \theta$$

$$D_{surface} = \frac{1}{2} (1 + \cos \beta)$$

$$R_{surface} = \frac{1}{2} (1 - \cos \beta) \rho D_h$$

Where;

I_{normal} = direct irradiance normal to the surface
 θ = angle of incidence
 β = pitch of system
 ρ = albedo factor
 D_h = diffuse fraction of light

To calculate the diffuse fraction, the following approximation can be used;

$$\frac{D_h}{G} = 1 - 1.13K_T$$

Where;

G = measured global irradiance per unit area on the horizontal surface

K_T = clearness index.

The clearness index is a measure of the attenuation of the solar radiation by the atmosphere and is calculated from

$$K_T = \frac{G}{G_0}$$

$$G_0 = G_{sc} \left(1 + 0.33 \cos \left(\frac{360n}{365} \right) \right) (\sin \delta \sin \phi + \cos \delta \cos \phi \cos \omega)$$

Where;

G₀ = irradiance received by unit horizontal area at the outer edge of the Earth's atmosphere.

G_{sc} = solar constant and the angles are as previously defined.

Therefore, the total irradiance received by a module is given below

$$G_{surface} = I_{d,surface} + D_{surface} + R_{surface}$$

Air Mass

In addition to the geometrical effects of pitch and orientation, the effects of air mass need to be calculated. This is due to the mass of air that the light from the sun passes through, and can be approximated as;

$$AM = \sqrt{(r \cos z)^2 + 2r + 1} - r \cos z$$

Where;

r = radius of the Earth (6371 km) / effective height of the atmosphere (9 km) ≈ 708

z = zenith angle = 90-α

The air mass has an effect on the amount of light from the sun which is scattered, hence will effect both the spectrum and intensity of direct beam irradiance. If the sun is directly overhead, there is a value of 1 for the air mass. However, the majority of photovoltaic systems globally are used at altitudes where the air mass figure is different, hence standard solar conditions for photovoltaic cells are designed using an air mass of 1.5 [IEC Standard 60904-3, Photovoltaic Devices: Measurement principles for terrestrial photovoltaic solar devices]. This equates to a zenith angle of 48.2°.

Sources of Data

In order to calculate the energy yield of PV on cargo ships to be used in simulations of the system, global irradiance data for the whole journey of the cargo ships is needed. Significant levels of irradiance data exists, and is available free of charge. For land areas there are ground measurements, whereas global datasets are taken from satellite measurements.

a. PVGIS

The PVGIS project utilises solar data to create a photovoltaic energy prediction for land locations in Europe and Africa. It is part of the SOLAREC action at the JRC Renewable Energies Unit. This uses several databases, some of which are of interest to the Inomanship project.

- **Original PVGIS Europe**

This database is interpolation of ground station measurements. The ground station measurement data are long-term monthly average of global and diffuse irradiation on a horizontal plane. The data were originally part of the European Solar Radiation Atlas. The time period of data is 10 years, from 1981 to 1990.

- **Original PVGIS Africa**

This database is from satellite-based calculations performed at MINES ParisTech, France, using data from the first generation of the Meteosat series of satellites. These seven satellites in geostationary orbit provided continuous, meteorological observations of earth and the atmosphere every half an hour. The spatial resolution of the original calculation is 15 arc-minutes, or about 28km right below the satellite (at the equator, 0° W). The data cover the period 1985-2004.

- **New CM-SAF - PVGIS database for Europe and Northern Africa**

This data is based on calculations from satellite images performed by CM-SAF. The database represents a total of 12 years of data. From the first generation of Meteosat satellites (Meteosat 5-7), known as MFG, there is data from 1998 to 2005 and from the second-generation Meteosat satellites (known as MSG) there is data from June 2006 to May 2010. The spatial resolution is 1.5 arc-minutes (about 3km right below the satellite at 0° N, 0° W). The coverage extends from 0° N (equator) to 58° N and from 15° W to 35° E.

International Weather for Energy Calculations (IWECC)

This dataset is the result of the ASHRAE (American Society of Heating, Refrigerating and Air-Conditioning) Research Project 1015 by Numerical Logics and Bodycote Materials Testing Canada, which were created for the ASHRAE Technical Committee 4.2 Weather Information. The data is derived from 18 years of DATSAV3 hourly weather data originally archived at the U. S. National Climatic Data Centre. The weather data is supplemented by solar radiation estimated on an hourly basis from earth-sun geometry and hourly weather elements, particularly cloud information. The IWECC CD-ROM is available from ASHRAE.

CM-SAF

One of the largest data sets available is from CM-SAF, as used by CM-SAF PVGIS database detailed above. The full dataset contains from January 1983 to January 2005. This has a temporal resolution of 1 hourly at a spatial resolution of 0.03°². It covers an area of 70S-70N, 70W-70E. As this is a very detailed dataset the full data is approximately 3TB in size.

SeaWiFS Surface Solar Irradiance

SeaWiFS (Sea-viewing Wide Field-of-view Sensor) was an instrument installed on GeoEye's OrbView-2 (AKA SeaStar) satellite, and was a follow-on experiment to the Coastal Zone

Colour Scanner on Nimbus 7. It began collecting data on 18 September 1997 and stopped on 11 December 2010. The primary activity of the satellite was to measure ocean characteristics such as chlorophyll and ocean clarity. However, solar irradiance data is produced from analysing SeaWiFS data against data from the

International Satellite Cloud Climatology Project (ISCCP). This is given at a spatial resolution of 2.5 degrees 2, at a temporal resolution of daily averages, with six hour averages now been processed.

The output data from the irradiance processing are:

The output data fields are:

- Clear sky irradiance
- Total irradiance including clouds
- Photo synthetically active solar irradiance fields

The output fields are available every three hours, and as daily and monthly averages. Daily and monthly averages of the input fields are also produced when adequate.

Orientation

From the above, the importance of orientation can be seen. There are therefore several options for the system:

Horizontally placed photovoltaic modules: These will have the advantage that whichever way the ship is heading there will be some level of irradiation received by the panels, however they will never be optimally inclined

Tilted panels: Panels could be fixed at an angle whereby they will receive on average a higher level of irradiance along a shipping route. However, tilted panels risk facing away from the sun as the ship turns, so there will be periods during the day when the system will generate a minimal amount of energy. Also, with tilted panels will lead to some level of self-shading

Tracking systems: These would track the path of the sun across the sky as the ship moves. This would increase substantially the level of energy generation from the PV. However, there would be additional moving parts which would need to be considered. Another important consideration is the level of hysteresis to be applied to the tracking. The ship will be continuously pitching and rolling in the waves, it is important that this does not affect the tracking systems.

Shading

Shading is a significant issue for PV. Due to the way strings of cells are connected, by shading 10% of a module, energy production can be decreased by ~50%. Self-shading issues will occur with tilted panels, thus meaning the panels will have to be spaced further apart. For example, at latitude of 55 degrees, the panels should be tilted at 40 degrees, and thus typical 1.5 by 1m panels, installed in portrait, would need to have gaps of ~3m between modules.

With regard to this project, the type of ship used will have a high impact on the shaded surface area available for PV.

Wear and Tear

There are various issues for reliability with PV. A good review of these is provided by NREL (2);

Wafer Silicon

- Cracked cells (bonding processes, strain, etc...)
- Solder joint or gridline interface failure (increased series resistance)
- Reduced adhesion leading to corrosion and/ or delamination
- Slow degradation of I_{SC}
- Fatigue of ribbon interconnect
- Junction box failure (poor solder joints, arcing, etc...)
- Busbar adhesion degradation, electrical contact, etc...
- Glass edge damage of frameless modules (though installation, handling, etc...)
- Light-induced cell degradation
- Effect of glass on encapsulant performance
- Front surface soiling
- Mechanical failure of glass-glass laminates
- General issues

Thin Film Silicon

- Electrochemical corrosion of SnO₂:F
- Initial light degradation (a-Si)
- Annealing instabilities (a-Si)
- General issues

CdTe

- Cell layer integrity- back contact stability
- Cell layer integrity- interlayer adhesion and delamination; electrochemical corrosion of SnO₂:F
- Fill-factor loss (increased series resistance and/ or recombination)
- Busbar adhesion degradation, electrical contact, etc...
- Shunt hot spots at scribe lines before and after stress
- Weak diodes, hot spots, no uniformities before and after stress
- General issues

CIS

- Cell layer integrity – contact stability
- Cell layer integrity – interlayer adhesion
- Fill-factor loss (increased series resistance and/or recombination)
- Busbar failure – mechanical (adhesion) and electrical
- Notable sensitivity of TCO to moisture
- Moisture ingress failure of package Cell-to-cell interconnect (discrete cells)
- Notable sensitivity of TCO to moisture; need to pass damp heat test (non-shingle specific)
- Shunt hot spots at scribe lines before and after stress
- Weak diodes, hot spots, no uniformities before and after stress
- Edge shunting
- General issues

OPV

- Delamination of layers
- Photolytic Instability
- Moisture induced degradation
- Moisture ingress failure of package
- O₂ induced degradation
- Thermal instability of donors and acceptors
- General issues

CPV

- Depolymerisation, bubble formation, and yellowing of silicone encapsulants under high flux and high temperature with thermal cycling for long periods of time
- Soiling and delamination of anti-reflective coatings on internal optical components
- Cell damage from thermal runaway (may be caused by solder voids?)
- Loss of efficiency of optics
- Poor solder joints between string ribbons and wires inside junction boxes – arcing
- Potential issues with highly non-uniform illumination
- Defect migration, ... (especially for lattice mismatched)
- Corrosion and diffusion of silver gridlines/contacts
- Electro migration due to high current under high concentration (tunnel junction)
- Inverter reliability (ability to withstand rapid changes in current)
- Module thermal fatigue (including high frequency and amplitude), materials, interconnects, cell attachment, adhesive failure
- Operational integrity of the mechanical parts of the trackers (for high concentration systems)
- High Al content AlInP can be sensitive to oxidation
- General issues

General Issues Across all Technologies

- Corrosion leading to loss of grounding
- Quick connector reliability
- Improper insulation leading to loss of grounding
- Delamination
- Glass fracture
- Bypass diode failure
- Inverter reliability
- Moisture ingress

Photovoltaic modules undergo rigorous accelerated testing under International Electrotechnical Commission (IEC) test standards, which are now the only tests accepted by both module manufacturers and buyers, as well as being incorporated into certification standards such as the UK's Microgeneration Certification Scheme (MCS). These are to ensure that photovoltaic modules can operate efficiently in a wide variety of environments, including maritime tropical, high-temperature, high-irradiance, deserts, and dirty urban rooftops.

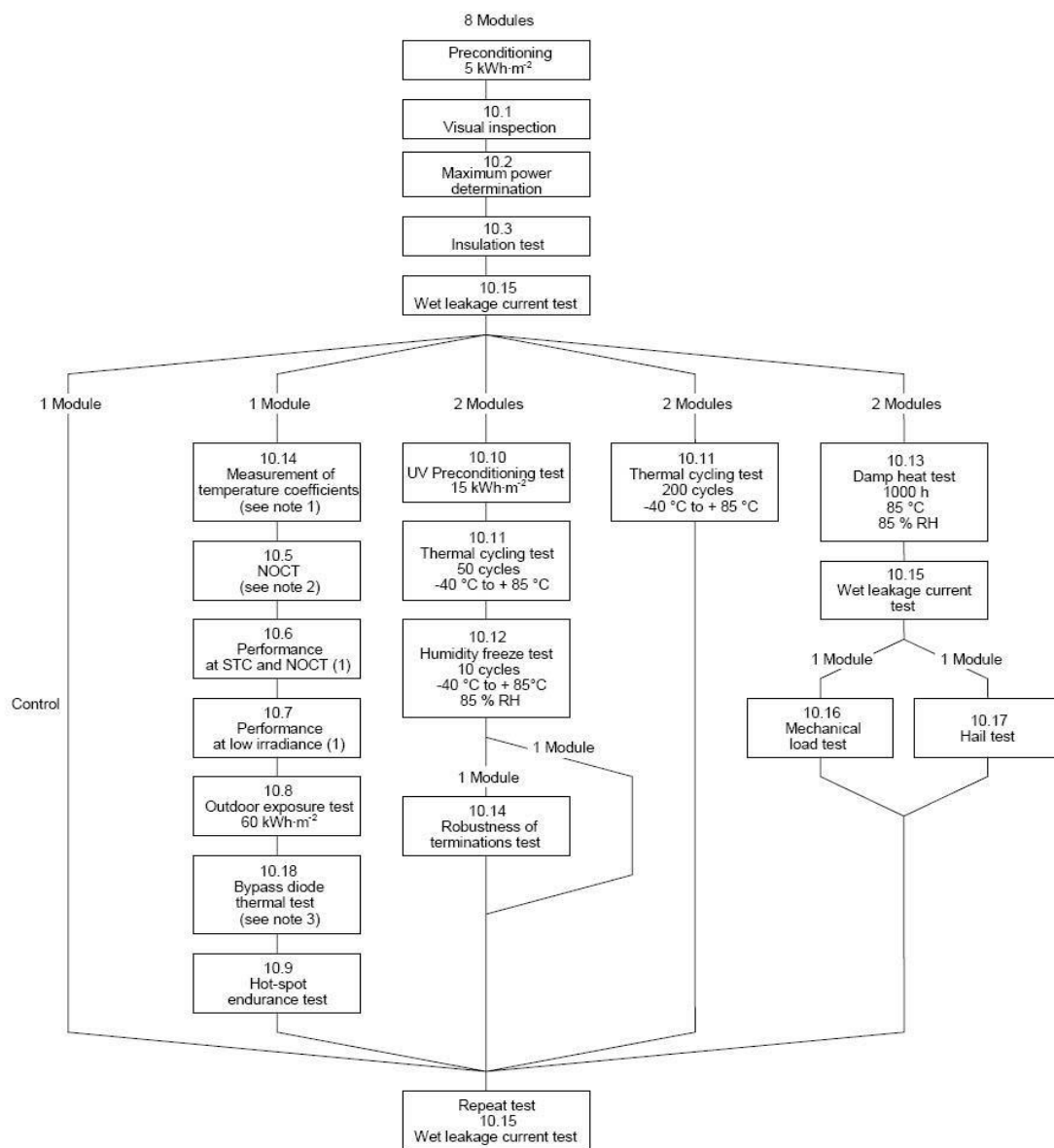
The standards are:

- IEC 61215 (crystalline silicon flat plate modules)
- IEC 61646 (thin film flat plate modules)
- IEC 62108 (concentrator modules/assemblies) DRAFT

Issues which are tested under these standards include:

- Corrosion of materials, especially metals
- Water-vapour intrusion
- Delamination of encapsulated materials, especially polymers
- Physical damage from wind, hail, and installation
- Thermal excursions, including coefficient of thermal expansion mismatches
- Ultraviolet (UV) radiation
- Deterioration of or damage to external components such as junction boxes, wiring, and frames

The full path of testing described in IEC 61215/61646 is shown in B-1.



IEC 584/05

B-1: IEC 61215/61646 testing methodology

With regard to salt corrosion, modules are tested to the voluntary IEC 61701 standard “Salt Mist Corrosion Testing of Photovoltaic (PV) Modules”. The test simulates a real-world environment and is divided into several severity levels, each with progressively longer test

duration. The highest level test, level 6, comprises of eight test cycles. During each cycle, the test module is sprayed for two hours with a 5% solution of sodium chloride (95% water) at an ambient temperature of between 15°C and 35°C. The module is then stored for 22 hours at a temperature of 40°C and a relative humidity of 93%. This procedure is repeated four times in each successive test cycle. The accelerated laboratory corrosion test simulates the effects of salt-laden atmospheres during the entire life of the solar module. Thus for the Level 6 test the process takes 1'280 hours. This should test modules to survive salt laden atmospheres for their entire operational lifetime.

With regard to thin film, it has been found that modules fabricated on tin-oxide glass will experience delamination of the tin-oxide layer from the glass due to sodium accumulation near the interface between the oxide and glass, and from the ingress of moisture at the PV module edges. (3)

Clearly, there are further issues associated with PV on ship, in that the electrical infrastructure for the systems need also to be protected, such as inverters and cabling.

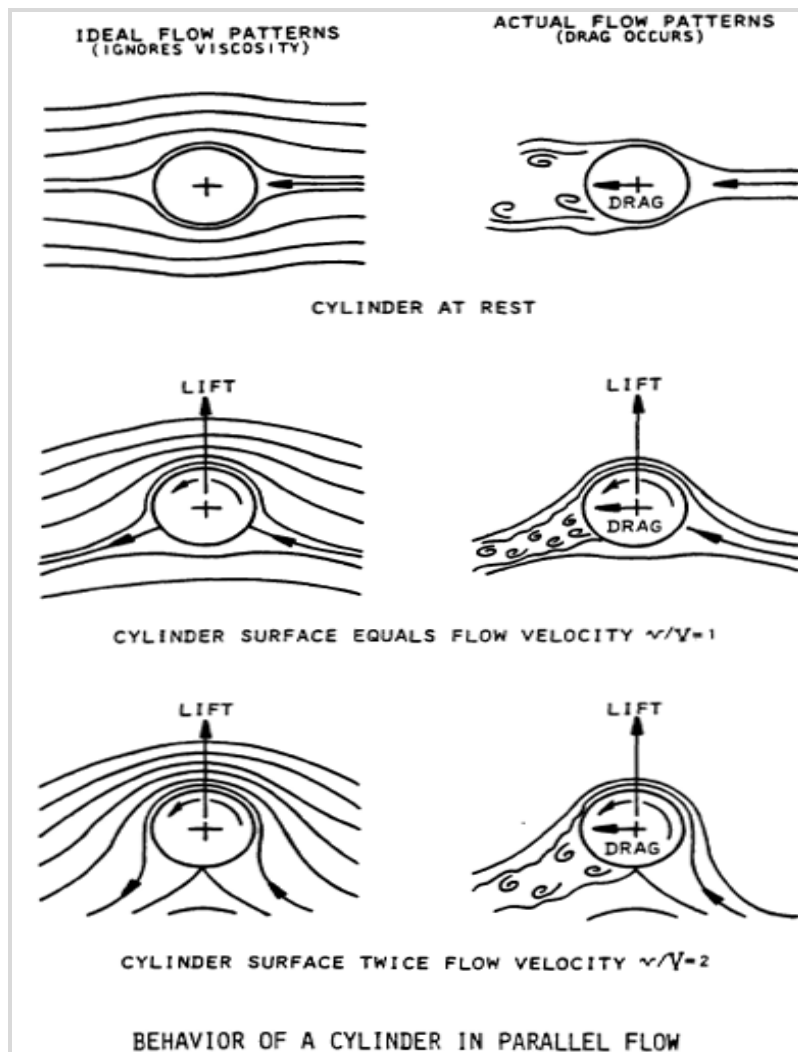
PV modules must be framed with marine grade stainless steel or a non-conducting metal with appropriate seals to prevent water and corrosion damage to the active components of the panel.

Finally, it should be noted that it is not just the photovoltaic modules themselves that need to be tested, but also the electrical systems connected. Work on land based PV (al, 2008) has shown that 69% of photovoltaic failures are due to the inverters, 21% from the system, and only 10% from the modules themselves. It can be presumed that this will be similar for a marine environment.

Fixing Systems

Most standard modules come pre-fitted into aluminium frames so that they can more easily be mounted onto a variety of fixing systems. However, it is also possible to buy frameless laminates or interlocking systems.

APPENDIX B: FLETTNER ROTOR PHYSICS



B-2: Magnus effect diagrams

This section will now explain the basic mathematical model to calculate lift and drag which Flettner Rotors will have. This is mainly taken from (Borg, 1986)

As shown in B-2, when a cylinder experiences an ideal flow, the surface moving in the same direction as the ideal flow will feel a lift in a direction perpendicular to the surface away from the centre of the cylinder. B-2 also shows that the actual flow is more complex with drag to consider, however, this will be calculated further down.

The transverse force L (lift) acting on the cylinder with circulation in a uniform flow may be shown by the equation:

$$L = \rho \Gamma V b \quad \text{Equation 77}$$

Where;

- ρ = mass density of fluid
- $\Gamma = 2\pi c$ = strength of circulation flow
- V = velocity of uniform stream
- c = constant = rv
- b = length of cylinder or span

r = radius vector (drawn from the centre of the cylinder to its surface)

v = velocity at any point which is everywhere normal to radius vector (in this case the surface velocity)

Equation 77 is known as KUTTA-JOUKOWSKI THEOREM OF LIFT, and is one of the great generalizations of mechanics since it applies to all bodies regardless of their shape, the shape factor being contained in the circulation factor " Γ " (S.N.A.M.E., 1967). In dealing with Magnus effect rotors the cylinder may be regarded as the "vortex core".

In an ideal fluid used in inviscid theory, viscosity is ignored; no energy is dissipated into friction and subsequently heat. The energy conversion between pressure energy and kinetic energy involves velocity and pressure changes only.

The expression for the dimensionless lift coefficient, C_L is:

$$C_L = \frac{L}{\frac{1}{2}\rho AV^2} \quad \text{Equation 78} \quad \text{(S.N.A.M.E., 1967)}$$

Where;

A = projected area (in the case of the cylinder $2rb$)

Substituting L for the KUTTA-JOUKOWSKI Equation 70

$$C_L = \frac{\rho\Gamma V b}{\frac{1}{2}\rho AV}$$

Then substituting for Γ and A

$$C_L = \frac{\rho 2\pi r v V b}{\frac{1}{2}\rho 2r b V^2 AV}$$

It is reduced to

$$C_L = 2\pi \frac{v}{V}$$

or the coefficient of lift of a rotating cylinder in an ideal fluid. This theoretical value of the lift coefficient C_L is much higher than has been practically obtained by experiments in real fluids. This is primarily due to viscosity, which is responsible for the large wake often observed and therefore for the associated pressure drag. Since drag cannot be accounted for by a theory based on an ideal fluid concept, the drag coefficient can only be established empirically by measurement. The real lift coefficient may also be obtained by direct measurement.

All this would seem to indicate that theoretical coefficient of lift is of little use in selecting the dimensions of rotors but the results of a majority of experiments tend to fall within an envelope between 50% and 25% of the theoretical C_L . This information can be used in choosing rotor proportions during the preliminary design stage; later tests would confirm the actual values. Approximations within the velocity ratio range of 2 to 5 would approach:

$$C_L = -\frac{v}{V}$$

For high aspect ratio cylinders having generous end plates and be closer to:

$$C_L = -\frac{1}{2}\pi\frac{v}{V}$$

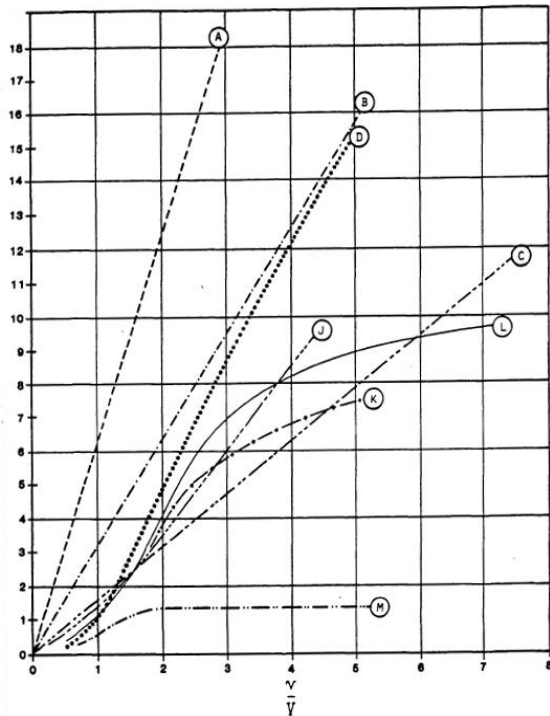
For the stumper designs. There seems to be no convenient engineering recipe for precisely predicting Magnus affect lift for cylinders of untested proportions, but then this is also true of conventional aerofoil sections.

The recommended method for estimating the C_L of an untested rotor is to refer to the family of experimental curves and try to find one of similar proportions. If the aspect ratio and/or end plate diameter are greater, then so too will be the lift coefficient and the opposite will also be true. There have been many Magnus effect investigations since Flettner's time so numerous C_L curves are available for reference.

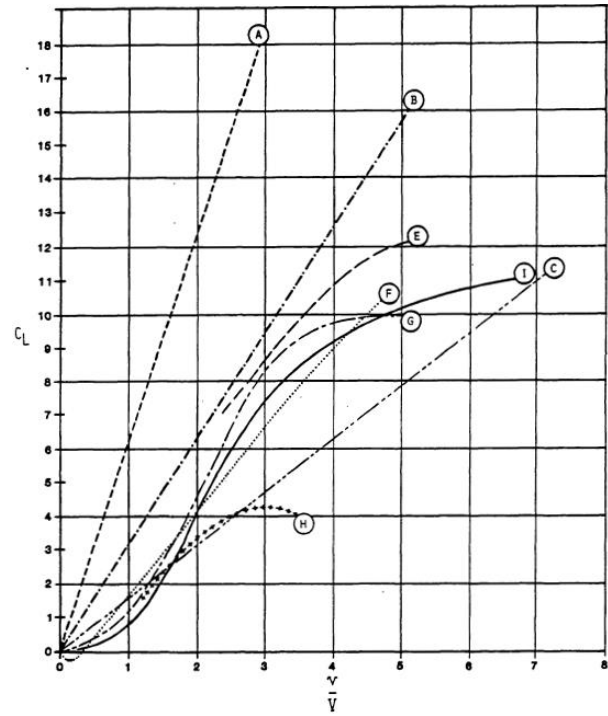
These curves are plotted on a grid whose vertical ordinate is the lift coefficient C_L and whose horizontal ordinate is the ratio of cylinder surface to free stream flow velocities v/V . There is generally little difference in lift values among the curves for v/V ratios of less than **1.5**. The majority of the tests were carried out in wind tunnels but it is reasonably safe to assume that they are also valid for a liquid medium B- 3 and B- 4.

Since there are so many curves, their description is given in tabular form for convenience. They have been plotted on three sheets for easier interpretation.

Curve	Investigator	Reference No.	Aspect Ratio	End plate diameter/ cylinder diameter	Reynold's Number	Remarks
A	Ideal fluid		-	-	-	Inviscid theory
B	50%A		-	-	-	Reference curve
C	25%A		-	-	-	Reference curve
D	Thom	26	12.5 & 26	3	5.3-8.8×10 ³	Approaches curve B
E	Windship	16	6.2	1.58	4.5×10 ⁵	Full size measured at sea
F	Reid	31	13.3	None	3.3-11.6×10 ⁴	C_L equivalent to shorter cylinder with plates
G	Gottengen	32	4.7	1.7	5.2×10 ⁴	Flettner sails
H	Gottengen	32	4.7	None	5.2×10 ⁴	Flettner sails without end plates
I	Borg	Appendix B	4.0	2	11.15×10 ⁴	Tested in fresh water
J	Thom	26	5.7	None	3-9×10 ⁴	Rough surface (sanded)
K	Thom	26	5.7	None	3-9×10 ⁴	Smooth surface
L	Swanson	24	-	None	3.5×10 ⁴ 3×10 ⁴	
M	Swanson	24	2	None	5×10 ⁵	Continuous end sections



B- 3: Magnus effect coefficients of lift – 1



B- 4: Magnus effect coefficients of lift - 2

The family of experimental curves clearly shows how rotors of conventional design fall in the envelope defined by $C_L = \pi v/V$ and $C_L = \frac{1}{2} \pi v/V$ (curves B and C). It also points out the relationship between larger aspect ratios and higher coefficients of lift. The curves G and H compare Flettner rotors with and without endplates, showing a **100%** increase in lift. Curves J and K are of identical cylinders but the rough surface texture of J give it a markedly improved performance.

In order to compute the lifting force developed by a rotor in a particular velocity free stream, one needs to know its lift coefficient (from the C_L curves), its projected area, (length \times diameter) and the mass density of the fluid medium ("ρ"). Values for mass density of a fluid are derived from the expression:

$$\rho = \frac{\text{weight per unit volume}}{\text{acceleration due to gravity}}$$

Or

$$\rho = \frac{\text{pounds per cubic foot}}{g} \quad \text{Equation 79}$$

Obviously the value of ρ is going to vary somewhat due to such factors as temperature, altitude and salinity but for design purposes the following generalizations are acceptable:

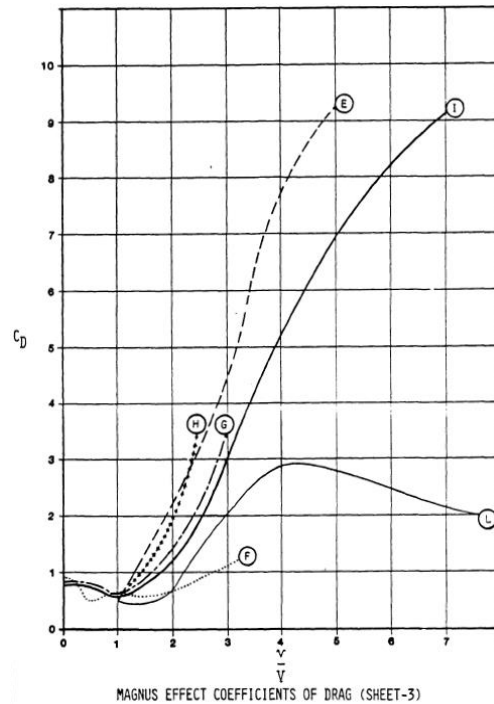
$$\rho: \text{sea water} = \frac{313 \text{ kg m}^{-2}}{9.81 \text{ ms}^{-2}} = 31.906 \text{ kgm}^{-3}$$

$$\rho: \text{fresh water} = \frac{305 \text{ kg m}^{-2}}{9.81 \text{ ms}^{-2}} = 31.091 \text{ kgm}^{-3}$$

$$\rho: \text{air at sea level} = \frac{0.366 \text{ kg m}^{-2}}{9.81 \text{ ms}^{-2}} = 0.03731 \text{ kgm}^{-3}$$

The lifting force of a rotor can be determined from the accompanying curves and solving Equation 84 for L .

$$L = \frac{C_L A \rho V^2}{2} \quad \text{Equation 80}$$



B- 5: Magnus effect coefficients of drag - 3

The drag produced by a rotating cylinder also increases with the surface velocity. This is caused partly by the entrained fluid surrounding the rotor and partly by the wake it generates along its high pressure side.

Drag may be expressed either in terms of a lift to drag ratio or as a coefficient. Although not all of the drag coefficients are available for the experimental curves tabulated in this study, as many as possible have been plotted versus the velocity ratios. They are designated by the same capital letters as their matching C_L curves (E,F,G,H,I,L).

Inspection of the C_D curves quickly reveals that the high aspect ratio cylinders have more favourable drag characteristics than do those of ratios of 6 to 1 or less. These plots also show a typical drop in drag of a rotor near the velocity ratio of 1.

The drag of a rotor can be computed by the equation:

$$D = \frac{C_D A \rho V^2}{2} \quad \text{Equation 81}$$

Which is derived from the relationship:

$$D = \frac{D}{\frac{1}{2}\rho AV^2}, \text{ by solving for } D \text{ (S.N.A.M.E., 1967)}$$

Once the lift and drag forces acting upon a rotor have been computed the only remaining unknown factor is the power needed to overcome surface friction to spin it at the desired rpm. To do this we must first learn the torque. The Reynold's number approach is usually used by scientific investigators.

The Reynold's number for a cylinder is

$$R_N = \frac{\rho V d}{\mu} \quad \text{Equation 82}$$

Where;

d = diameter of cylinder

μ = coefficient of dynamic viscosity

The required Torque would be:

$$T = C \rho n^2 l d^4 \quad \text{Equation 83}$$

(Krasnoperov, 1935)

Where;

C = a torque coefficient, function of Reynolds number

n = rpm of rotor

l = length of rotor

d = diameter of rotor

Some values for C are:

R_N	0.5×10 ⁵	1.0×10 ⁵	1.3×10 ⁵
C	0.065	0.050	0.045

Obviously the Reynolds number method of determining rotor torque is rather ponderous and an accurate coefficient of dynamic viscosity is hard to pin down in the marine environment. Historically this method has resulted in undersized rotor drive systems.

A simpler and more conservative formula is derived from (Attwood, 1954). The cylinder torque:

$$T = f S v^{1.825} r$$

Where;

f = friction factor

$f_{\text{water}} = 0.01$

$f_{\text{air}} = 0.0000121$

S = surface area of cylinder or end plates

v = surface velocity in feet per second

r = effective radius

The rpm is found by using:

$$rpm = \frac{60v}{2\pi r} \quad \text{Equation 84}$$

To find the horsepower use the formula:

$$hp = \frac{\text{torque} \times \text{rpm}}{5252}$$

Equation 85

It is easy to see from the foregoing torque computations that large end plates attached to the cylinder absorb a great amount of power that does not contribute directly to the Magnus effect.

For over a half a century theorists have strived to produce a general equation to account for Magnus effect behaviour. Inspection of the C_L and C_D curves with their great diversity indicates what a difficult project it is. The Kutta-Joukowski equation (Equation 69) is useful in illustrating how lift is generated by rotating bodies, but it is not very helpful to the engineer who is designing a Magnus effect system. The procedures explained in this chapter are to be used for preliminary design guidance only. Until a sufficient number of full-sized applications have been made to provide feedback confirmation, scale model tests should be conducted prior to any prototype construction.

A particularly interesting point brought up in this report is that Flettner rotors, surprisingly, do not have issues in high winds. If the rotors are sped up enough they will deflect with wind around themselves, thus not leading to instability in the ship from high winds. There is still the issue though that they will have lifted the centre of gravity of the ship higher.

APPENDIX C FUEL CELL PAST AND CURRENT PROJECTS

There are a range of fuel cell powered nautical vessels. The majority of these are small scale demonstrators, on-board smaller vessels, but systems are now being installed on larger commercial and naval ships. Up to 2010 the full list was as shown in the figure below (McConnell, 2010). A further search has been carried out by Narec, but no other projects have been found with real demonstration ships.



Figure; ECS Alsterwasser from the Zemships Project. This vessel has a hybrid system of gel cells and lead acid gel batteries.

Key suppliers	Country	Type	Power rating	Date	Vessel name, notes
Non-nuclear submarines					
General Dynamics/Allis-Chalmers	USA	AFC	Unknown	1964	Star 1, 2300 lb (1040 kg), 1-person sub, hydrazine/oxygen
Lockheed Missiles & Space Systems	USA	AFC	30 kW	1967	Deep Quest, 5-person sub using early UTC fuel cell
ThyssenKrupp Marine Systems/HDW	Germany	PEMFC	9 * 34 kW fuel cells (in U31) 2 * 120 kW fuel cells (later subs)	2005	SiNavy PEMFC from Siemens, first contracted for class 212A sub in 1996, U31 and U32 first into service for German Navy, now in service with or ordered by seven countries
UUV/AUV submersibles					
ISE Research Ltd	Canada	AI/02	100 kW	1987	ARCS research AUV, 6.4 m long, hybrid system with Ni/Cad batteries
Perry Technologies/Ballard	USA/Canada	PEMFC	3 kW	1989	PC-14
FFI Norwegian Defence Research Establishment	Norway	AI/hydrogen peroxide	35 * 50 kW	2000	HUGIN, 5.3 m long, rated to 3000 m depth
Atlas Elektronik/ZSW	Germany	PEMFC	160 kW	2002	DeepC, prototype with ZSW fuel cell
Mitsubishi Heavy Industries	Japan	PEMFC	4 kW	2004	Urashima, 317 km long-distance cruise record at 800 m depth, metal hydride storage
Yachts/sailboats					
Yuasa Corporation	Japan	DMFC	30 W	2002	Malt's Mermaid III, 5.8 m long, DMFC as APU on solo Pacific crossing to the US
IESE-EIVD	Switzerland	PEMFC	300 W	2002	Branec III used PEMFC as APU in 6600 km transatlantic Route de Rhum race
MTU CFC Solutions/Ballard	Germany/Canada	PEMFC	4.8 kW	2003	No. 1, 12 m yacht, CoolCell PEMFC in hybrid system with batteries as APU
Max Power	Germany	DMFC	1.2 kW	2004	Mamelie, 15 m long in DaimlerChrysler North Atlantic Challenge race
Voller Energy	UK	PEMFC	5 kW	2007	Emerald Beneteau 411, 12 m long, in 3000 nm ARC transatlantic rally, running on reformed LPG
SFC Smart Fuel Cell	Germany	DMFC	1.6 - 2.2 kW	2009	Pogo 2 using EFOY 2200 second in Transat 6.50 solo transatlantic race (7800 km). Also EFOY 1600 on Nightlife wins class in Atlantic Rally for Cruisers
Research vessels					
Icelandic New Energy/Ballard	Iceland/Canada	PEMFC	10 kW	2009	Elding, 125-tonne whale watching ship with hybrid PEMFC/battery APU, part of Smart H2 Program
MTU Onsite Energy/Wärtsilä	Germany/Norway	MCFC	320 kW	2009	Viking Lady, 5900 metric tonnes, North Sea supply vessel, as APU
Water taxis/ferries					
Etaing GmbH	Germany	AFC	6.9 kW	2000	Hydra, 22 passengers, 9 km/h speed, metal hydride
Duffy Electric Boat Co/Anuvu/Millennium Cell	USA	PEMFC	3 kW	2003	Duffy water taxi for 18 passengers, sodium borohydride Hydrogen on Demand® system
Proton Motor	Germany	PEMFC	6 - 20 kW	2008	ECS Alsterwasser, 100 passengers, Zemships Project, primary propulsion with lead gel battery
Fuel Cell Boat BV	Netherlands	PEMFC	60 - 70 kW	2009	Nemo H2, 22 m long, 82 passenger capacity, hybrid with batteries for main propulsion
Recreational boats					
Hydrocell Oy	Finland	AFC	30 kW	2000	Two different motorboats using HC-100 cylindrical fuel cell with Yamaha electric motor, metal hydride
IESE-EIVD/ZeTek Power	Switzerland/UK	PEMFC	3 kW	2003	Hydroxy 3000 catamaran, two earlier Hydroxy craft
University of Birmingham	UK	PEMFC	5 kW	2007	Ross Barlow waterway maintenance boat, student project, metal hydride

Key suppliers	Country	Type	Power rating	Date	Vessel name, notes
Horizon Fuel Cell/Plug Power	Singapore/USA	PEMFC	300 W	2007	Trolling boat propelled by electric motors
Fronius International/Bitter GmbH	Austria	PEMFC	4 kW	2009	Riviera 600 motor boat (16 m long), H2 in high-pressure cartridges, part of Future Project Hydrogen
IRD Fuel Cell Technology	Denmark	DMFC	500 W	2009	Chaloupe boat (6.4 m long) using DMFC to charge electric motor batteries
Tropical Green Technologies	Greece	PEMFC	1 kW	2009	Testing RFC-1000 unit on motorboat, H2 from reformed LPG
Rensselaer Polytechnic Institute	USA	PEMFC	4.4 kW	2009	New Clermont, 6.7 m Bristol 22 sailboat outfitted as student project with two Plug Power fuel cells

FP7 Projects

There are 115 European research projects which have investigated the use of fuel cells on ships. 35 of which were FP7 projects. The majority of these involve modelling and/or feasibility studies.

List of FP7 projects related to shipping which include an element of fuel cell research

EXTREME			
SEAS	Design for Ship Safety in Extreme Seas	CP-FP	Safety & Security
BESST	Breakthrough in European Ship and Shipbuilding Technologies	CP-IP	Competitiveness
INOMANS ² HIP	INOVative Energy MANagement System for Cargo SHIP	CP-FP	Energy
SUSY	Surfacing System for Ship Recovery	CP-FP	Environment
RISPECT	Risk-Based Expert System for Through Life Ship Structural Inspection and Maintenance and New-Build Ship Structural Design	CP-FP	Competitiveness
SAFEGUARD	Ship evacuation data and scenarios	CP-FP	Safety & Security
POSE2IDON	Power Optimised Ship for Environment with Electric Innovative Designs on Board	CP-IP	Energy
NAXTRONIC	Navigational System for Efficient Maritime Transport	CP-FP	Competitiveness
HORIZON	Research into Effects on Cognitive Performance of Maritime Watch-keepers under Different Watch Patterns, Workloads & Conditions, with Reality Usage of Ships Bridge, Engine & Cargo Control Simulators	CP-FP	Human
RETROFIT	RETROFITting ships with new technologies for improved overall environmental footprint	CP-FP	Environment
SAFEWIN	Safety of Winter Navigation in Dynamic Ice	CP-FP	Safety & Security
GRIP	Green Retrofitting through Improved Propulsion	CP-FP	Energy
REFRESH	Green Retrofitting of Existing Ships	CP-FP	Energy
ThroughLife	Development and proof of new approaches for through-life asset management based on next generation of materials and production technology	CP-FP	Competitiveness
ECO-REFITEC	Eco innovative refitting technologies and processes for shipbuilding industry promoted by European Repair Shipyards	CP-FP	Competitiveness
EU-CARGOXPRESS	Greening of Surface Transport through an Innovative and Competitive CARGO-VESSEL Concept Connecting Marine and Fluvial Intermodal Ports	CP-FP	Competitiveness
DIVEST	Dismantling of Vessels with Enhanced Safety and Technology	CP-FP	Safety & Security
FLOODSTAND	Integrated Flooding Control and Standard for Stability and Crises Management	CP-FP	Safety & Security
ULYSSES	Ultra Slow Ships	CP-FP	Environment
GOALDS	GOAL based Damage Stability	CP-FP	Safety & Security
VISION		CSA-	
OLYMPICS	The next generation products and procedures for vessels and floating structures	SA	Competitiveness
TRIPOD	TRiple Energy Saving by Use of CRP, CLT and PODded Propulsion	CP-FP	Energy
TARGETS	Targeted Advanced Research for Global Efficiency of Transportation Shipping	CP-FP	Energy
STREAMLINE	Strategic Research For Innovative Marine Propulsion Concepts	CP-IP	Competitiveness
SILENV	Ships oriented Innovative soLutions to rEduce Noise & Vibrations	CP-FP	Environment
TULCS	Tools for Ultra Large Container Ships	CP-FP	Competitiveness
KITVES	Airfoil-Based Solution for Vessel on-board Energy Production Destined to Traction and Auxiliary Services	CP-FP	Energy
ARIADNA	Maritime Assisted Volumetric Navigation System	CP-FP	Safety & Security
EXCITING	EXAct geometry simulatioN for optimized desiGn of vehicles and vessels	CP-FP	Energy
DEECON	Innovative After-Treatment System for Marine Diesel Engine Emission Control	CP-FP	Environment
FIREPROOF	Probabilistic Framework for Onboard Fire-Safety	CP-FP	Safety & Security
HERCULES-B	Higher-Efficiency Engine with Ultra - Low Emissions for Ships	CP-IP	Energy
ARGOMARINE	Automatic Oil-Spill Recognition and Geopositioning Integrated in a Marine Monitoring Network	CP-FP	Environment
HYMAR	High Efficiency Hybrid Drive Trains for Small and Medium Sized Marine Craft	CP-FP	Competitiveness
ASIPILOT	Intuitive Operation and Pilot Training when Using Marine Azimuthing Control Devices	CSA-CA	Human

FellowSHIP Project

The most interesting project at the moment using fuel cells is the FellowSHIP project. This project, part funded by the European EUREKA scheme involved Wärtsilä, MTU Onsite Energy and Det Norsk Veritas. The project installed a 330kW Molten Carbonate Fuel Cell (MCFC) on-board an offshore supply vessel, the Viking Lady. The system operated for 18 500 hours until January 2012 without any signs of severe performance degradation. One of the reasons for the choice of MCFC was that the test vessel already used LNG as a fuel, so no extra fuel supplies were needed to be stored on-board the ship. The MCFC was located in a purpose built contained (13 x 5 x 4.4m). Further ancillary equipment to protect the fuel cell from surges, etc... was located in a separate standard 20ft container. The total weight of the fuel cell and infrastructure was 110 tonnes. Including the energy saved through heat recovery, the overall efficiency of the system was on average 55% (Ludvigsen & Ovrum, 2012).

The project has now entered Phase III where the fuel cell will operate as a hybrid system with a battery pack. In addition, to this project, DNV are involved in the PaXell project which will demonstrate a High Temperature Proton Exchange Membrane (HTPEM) system.



Figure; The Viking Lady

APPENDIX D FUEL CELL LEGISLATION

International Electrotechnical Commission (Hydrogen/Fuel Cell Codes and Standards)

- IEC/TS 62282-1 (2010-04) Ed. 2.0 Terminology
- IEC 62282-2 (2012-03) Ed.2 Fuel Cell Modules
- IEC 62282-3-300 (2012-06) Stationary Fuel Cell Power Systems - Installation
- IEC 62282-5-1 (2012-09) Portable Fuel Cell Appliances - Safety
- IEC 62282-6-100 (2012-10) Micro Fuel Cell Power Systems - Safety
- IEC/PAS 62282-6-150 Micro Fuel Cells – Safety - Water reactive (UN Division 4.3) compounds in indirect PEM fuel cells
- IEC 62282-6-200 (2007-11) Micro Fuel Cell Power Systems - Performance
- IEC 62282-6-300 (2012-12) Micro Fuel Cell Power Systems – Interchangeable Fuel Cartridge
- IEC 60079-29-1 Explosive atmospheres – Part 29-1: Gas detectors- Performance requirements of detectors for flammable gases
- IEC 60079-29-2 Explosive atmospheres – Part 29-2: Gas detectors- Selection, installation, use and maintenance of detectors for flammable gases and oxygen

International Organization for Standardization (Hydrogen/Fuel Cell Codes and Standards)

- ISO TR 15916:2004 Basic Considerations for the Safety of Hydrogen Systems
- ISO 22734-1 2008 Hydrogen Generators Using Water Electrolysis Process – Part 1: Industrial and Commercial Applications
- ISO 22734-2 Hydrogen Generators Using Water Electrolysis Process – Part 2: Residential Applications
- ISO 16110-1 Hydrogen Generators Using Fuel Processing Technologies Part 1: Safety
- ISO 16110-2 Hydrogen Generators Using Fuel Processing Technologies Part 2: Test Method for Performance
- ISO 16111 Transportable Gas Storage Devices - Hydrogen Absorbed in Reversible Metal Hydrides

EU Standards (Hydrogen/Fuel Cell Codes and Standards)

- BS EN 50073 Guide for selection, installation, use and maintenance of apparatus for the detection and measurement of combustible gases or oxygen
- BS EN 62282-2:2012 Fuel Cell Modules
- BS EN 62282-3-200:2012 Test Methods for the Performance of Stationary Fuel Cell Power Systems
- BS EN 62282-5-1:2007 Portable Fuel Cell Appliances – Safety
- BS EN 62282-6-100:2010 Micro Fuel Cell Power Systems – Safety
- BS EN 62282-6-200:2008 Micro Fuel Cell Power Systems – Performance
- BS EN 62282-6-300:2009 Micro Fuel Cell Power systems – Interchangeable Fuel Cartridge

EU Directives

- **ATEX 95 (94/9/EC)** supply of equipment in potentially explosive atmospheres
- **ATEX 137 (1999/92/EC)** use of equipment in potentially explosive atmospheres

Specific marine advice

- “Rules for Classification and Construction VI Additional Rules and Guidelines: Guidelines for the Use of Fuel Cell Systems on Board of Ships and Boats”, Germanischer Lloyd Aktiengesellschaft, 2003.

REFERENCES

Imtech;

- B. Blunier (2010). Energies nouvelles et renouvelables, 105p. *UTBM*
- D. Bouquain (2010). Véhicules électriques et hybrides, 442p. *UTBM*
- A. Haupais (1992). Combustion dans les moteurs Diesel, 33p. *Techniques de l'ingénieur – B2700*
- A. Marquet, C. Levillain, A. Davriu, S. Laurent, P. Jaud (1998). Stockage d'électricité dans les systèmes électriques, 29p. *Techniques de l'ingénieur – B2030*
- J. Kouv, J. Bonal, P. Odru (2002). Stockage inertiel de l'énergie, 19p. *Techniques de l'ingénieur – D2030v2*
- H. Gualous, R. Gallay (2007). Applications des supercondensateurs, 12p. *Techniques de l'ingénieur – D3335*
- B. Multon, X. Roboam, B. Dakyo, C. Nichita, O. Gergaud, H. Ben Ahmed (2004). Aéro générateurs électriques, 18p. *Techniques de l'ingénieur – D3960*
- J-L. Noël (2009). Energies éolienne pour la fourniture d'électricité, 16p. *Techniques de l'ingénieur – BE8585*
- B. Blunier (2010). Les éoliennes, 151p. *UTBM*
- J-C. Muller (2007). Electricité photovoltaïque filières et marché, 9p. *Techniques de l'ingénieur – BE8579*
- J-C. Muller (2007). Electricité photovoltaïque principes, 12p. *Techniques de l'ingénieur – BE8578*
- S. Astier (2008). Conversion photovoltaïque : du rayonnement solaire à la cellule, 20p. *Techniques de l'ingénieur – D3935*
- S. Astier (2008). Conversion photovoltaïque : de la cellule aux systèmes, 22p. *Techniques de l'ingénieur – D3936*
- A. Ricaud (2005). Modules photovoltaïque : Filières technologiques, 16p. *Techniques de l'ingénieur – D3940*
- A. Ricaud (2005). Modules photovoltaïque : Aspects technico-économiques, 12p. *Techniques de l'ingénieur – D3941*
- A. Ferrière (2008). Centrales solaires thermodynamiques, 20p. *Techniques de l'ingénieur – BE8903*
- G. Filliau, A. Bondu, L. Mazodier (2000). Le navire tout électrique : Propulsion et production d'énergie, 13p. *Techniques de l'ingénieur – D5610*
- G. Filliau, A. Bondu, L. Mazodier (2001). Le navire tout électrique : Etat de l'art des composants, 15p. *Techniques de l'ingénieur – D5615*

G. Filliau, A. Bondu, L. Mazodier (2001). Le navire tout électrique : Evolutions et systèmes de conduite, 10p. *Techniques de l'ingénieur – D5620*

NAREC;

1 February 2010 - Press Release - Cash Rewards for Low Carbon Electricity and Heating. (2010).

Retrieved April 1, 2010, from DECC:

http://www.decc.gov.uk/en/content/cms/news/pn10_010/pn10_010.aspx

Bosco, N.(n.d.). *Reliability Concerns Associated with PV Technologies*. National Renewable Energy Laboratory.

D. E. Carlson, R. R.-J. (2003). Corrosion Effects in Thin-Film Photovoltaic Modules. *Prog. Photovolt: Res. Appl.*, 11:377–386.

Pablo Kaluza, A.K. (2010). The complex network of global cargo ship movements. *J. Royal Society: Interface*.

(2004). *NASA Surface meteorology and Solar Energy*. NASA.

1 February 2010 - Press Release - Cash Rewards for Low Carbon Electricity and Heating. (2010).

Retrieved April 1, 2010, from DECC:

http://www.decc.gov.uk/en/content/cms/news/pn10_010/pn10_010.aspx

(2012). *Fuel Cell Industry Review 2012*. Fuel Cell Today.

al, M. e. (2008). Progress in Photovoltaics: Research and Applications. 16 (3), 249-259.

Alexander, L., Allen, S., Bindoff, N. L., & Bréon, F.-M. (2013). *Working Group I Contribution to the IPCC Fifth Assessment Report Climate Change 2013: The Physical Science Basis Summary for Policymakers*. Intergovernmental Panel on Climate Change.

Attwood, E. (1954). Theoretical Naval Architecture,. In *Longmans*, (pp. 293-294). London: Longmans, Green and Co.

Barbir, F. (2012). *PEM Fuel Cells: Theory and Practice*. Academic Press.

Behling, N. H. (2013). *Fuel Cells: Current Technology Challenges and Future Research Needs*. Newnes.

Borg, J. (1986). *Magnus Effect - An overview of its past and future practical applications*. NAVSEA.

Bosco, N. (n.d.). *Reliability Concerns Associated with PV Technologies*. National Renewable Energy Laboratory.

D. E. Carlson, R. R.-J. (2003). Corrosion Effects in Thin-Film Photovoltaic Modules. *Prog. Photovolt: Res. Appl.*, 11:377–386.

Hydrogen/Fuel Cell Codes and Standards. (n.d.). Retrieved 10 01, 2013, from <http://www.fuelcellstandards.com/home.html>

INVESTIRE Thematic Network. (2002). *WP ST5 - Electrolyser, hydrogen storage and Fuel Cell - Investigation on Storage Technologies for Intermittent Renewable Energies: Evaluation and*

recommended R&D strategy. EU 5th Framework Programme.

Krasnoperov, Y. V. (1935). Experimental Aerodynamics. *Izdvo aviatsionnoy literatury*, Part II.L.

Krewitt, K. (2007). The use of scenarios in NEEDS – implications for RS1a.

Ludvigsen, K. B., & Ovrum, E. (2012). *Fuel cells for ships*. DNV.

McConnell, V. P. (2010). Now, voyager? The increasing marine use of fuel cells. *Fuel Cells Bulletin*(5), 12-17.

New Energy Externalities Developments for Sustainability. (2008). *Final report on technical data, costs and life cycle inventories of fuel cells*. Sixth Framework Programme.

Pablo Kaluza, A. K. (2010). The complex network of global cargo ship movements. *J. Royal Society: Interface*.

S.N.A.M.E. (1967). Principles of Naval Architecture (Revised).

T. J. Craft, H. I. (n.d.). Dynamic performance of Flettner Rotors with and without Thom Disks.

US Department of Energy. (2011). *Comparison of Fuel Cell Technologies*. US Government.

TNO;

GES modelisations

WARTSILA;

Engines specifications - *Wartsila-O-E-RT-flex68-D-MIM - Wartsila-O-E-RT-WHR - Wartsila-O-E-W-46F-PG - Wartsila-O-E-W-32-PG*